



**Politecnico  
di Torino**

**ScuDo**

Scuola di Dottorato - Doctoral School  
WHAT YOU ARE, TAKES YOU FAR

Doctoral Dissertation  
Doctoral Program in Electrical, Electronics and Communications Engineering  
(35<sup>th</sup> cycle)

# **Single Frequency Network Terrestrial Broadcasting with 5G New Radio**

By

**Majid Mosavat**

\*\*\*\*\*

**Supervisor(s):**

Prof. Guido Montorsi

**Doctoral Examination Committee:**

Prof. David Gomez-Barquero, Universitat Politècnica de València

Prof. Jordi Joan Giménez, Universitat Politècnica de València

Prof. Giulio Colavolpe, L'Università degli Studi di Parma

Prof. Roberto Garelo, Politecnico di Torino

Dr. Assunta De Vita, Centro Ricerche Innovazione Tecnologica RAI

Politecnico di Torino

2023

## **Declaration**

I hereby declare that, the contents and organization of this dissertation constitute my own original work and does not compromise in any way the rights of third parties, including those relating to the security of personal data.

Majid Mosavat  
2023

\* This dissertation is presented in partial fulfillment of the requirements for **Ph.D. degree** in the Graduate School of Politecnico di Torino (ScuDo).

*I dedicate this dissertation to my loving parents, who have always supported me in my academic and personal pursuits. Their unwavering love and encouragement has been a constant source of strength throughout my journey. I would also like to thank my wife, Naeima, for her constant love and support. And my little daughter, Sofia for giving me a reason to strive for a better future. I would also like to extend my deepest gratitude to my supervisor Guido Montorsi for their guidance, support and encouragement throughout the research and writing of this dissertation. Without their expert knowledge and invaluable advice, this work would not have been possible.*

## **Acknowledgements**

I would like to acknowledge the assistance and support provided by Assunta de Vita and Vittoria Mignone in Rai Centre for Research Technological Innovation and Experimentation (CRITS). Their expertise and encouragement were invaluable resources and their friendship and support is greatly appreciated. I am deeply grateful to them for their contributions to this work.

## Abstract

A Single Frequency Network (SFN) refers to a network configuration in which multiple transmitters simultaneously broadcast the same content using the same time and frequency channel. In an SFN, the transmitters are geographically distributed, often with overlapping coverage areas [1]. CP-OFDM or Cyclic Prefix-Orthogonal Frequency Division Multiplexing is the cutting-edge method used to implement SFN in the physical layer. It offers numerous benefits that render it highly suitable for SFN broadcasting. CP-OFDM effectively handles multi-path propagation by incorporating a cyclic prefix, which mitigates signal self-interference and distortion. This capability significantly decreases errors in the received signal, making it particularly crucial in SFN broadcasting scenarios where multiple transmitters' signals may interfere with one another.

5G-NR (5G New Radio) refers to the air interface standard utilized in 5G wireless networks. It plays a vital role in enhancing performance and capabilities compared to previous cellular network generations. Release 15 of 5G-NR, as defined by the 3GPP (Third Generation Partnership Project) [2], primarily focuses on uni-cast transmission and provides a wide range of services through its physical layer. However, the numerologies employed in Release 15, which include a short cyclic prefix, are not suitable for establishing a SFN broadcast network with large inter-site distances. In response to the need for broadcasting and multi-casting capabilities, particularly through LTE-based 5G broadcast, Release 17 was introduced [3]. Nonetheless, the numerologies used in LTE-based 5G broadcast differ from those in 5G-NR, and only a 15 kHz common numerology is available.

Consequently, it is currently not feasible to utilize the numerologies employed in 5G-NR for SFN broadcasting with significant inter-site distances using a traditional receiver structure.

This thesis presents an innovative approach to enable SFN broadcasting over long distances using the 5G-NR. Instead of introducing new numerology options, the thesis focuses on employing advanced receiver techniques.

The first receiver implementation involves the use of optimal channel shortening techniques to equalize the OFDM symbols affected by strong inter-symbol interference (ISI) and inter-carrier interference (ICI). By utilizing this method, SFN broadcasting can be achieved over large inter-site distances, comparable to high-power, high-tower transmission networks, while adhering to the standard 5G numerologies. Through the investigation, it was discovered that a linear channel shortening filter, specifically the 2D-MMSE (Minimum Mean Square Error), can provide near maximum mutual information, assuming a static channel that is known by the receiver.

The second receiver implementation introduces a novel approach to achieving high performance in SFN Terrestrial Broadcasting using 5G-NR. This method utilizes a Recurrent Neural Network (RNN)-based receiver, eliminating the assumption of a static and well-known channel, which was made in the first receiver design. Additionally, a technique of superimposing the pilot signal with the data signal is employed, allocating 100% of the resources to data transmission, thereby enhancing spectral efficiency. The receiver receives a sequence of demodulated OFDM symbols and performs joint channel equalization, channel estimation, and log-likelihood ratio (LLR) computation. The LLR output is then utilized by the channel Low-Density Parity-Check (LDPC) decoder to recover the transmitted data. Simulation results demonstrate that the proposed system can achieve performance similar to classical systems specifically designed for rooftop reception and various mobility scenarios.

Furthermore, the proposed system exhibits high flexibility as it is trained under fixed signal-to-noise ratio (SNR) and speed conditions, yet it demonstrates excellent performance in unseen conditions according to the simulations. Although the RNN-based receiver was initially designed for SFN terrestrial broadcasting systems with mobility, the techniques employed in the design can be applied to any OFDM-based system experiencing strong ISI and ICI. This proposed approach has the potential to simplify the design and deployment of 5G-NR SFN broadcasting, reducing the requirement for additional hardware or software modifications.

While the research yields promising results, there are still several areas that warrant further investigation for future studies. One important aspect to consider is the complexity of the proposed systems and other factors that can impact SFN

networks, such as synchronization. Additionally, it is worth noting that the research conducted was limited to link-level simulations, and further validation at the system level is necessary to comprehensively evaluate the performance of the proposed methods.

# Contents

<b>List of Figures</b>	<b>xii</b>
<b>List of Tables</b>	<b>xiv</b>
<b>List of Acronyms</b>	<b>xvi</b>
<b>1 Introduction</b>	<b>1</b>
1.1 Problem overview . . . . .	1
1.2 Thesis Objectives . . . . .	6
1.3 Organisation of dissertation . . . . .	8
<b>2 Background on SFN Terrestrial Broadcasting</b>	<b>10</b>
2.1 Single Frequency Network overview . . . . .	10
2.2 Transmitter Blocks in SFN broadcasting based on OFDM . . . . .	12
2.2.1 Channel encoder . . . . .	13
2.2.2 Interleaver . . . . .	14
2.2.3 Modulator . . . . .	15
2.2.4 CP-OFDM Modulator with Pilot Insertion . . . . .	16
2.3 Channel Modeling in SFN . . . . .	17
2.3.1 Doubly selective channel in mobile SFN scenarios . . . . .	17
2.3.2 Delay Spread and Doppler spread . . . . .	18



---

2.3.3	Modeling a SFN with Tapped Delay Line . . . . .	19
2.4	The reference "Classical" OFDM receiver . . . . .	21
2.4.1	Synchronization and CP-OFDM demodulator . . . . .	22
2.4.2	Channel estimation . . . . .	23
2.4.3	"Single tap" Equalization . . . . .	28
2.4.4	Soft-Demodulator . . . . .	28
2.4.5	Deinterleaver and decoder . . . . .	29
2.5	Limits of the classical receiver approach . . . . .	30
2.5.1	Minimum system overhead . . . . .	31
2.6	Conclusion . . . . .	32
<b>3</b>	<b>Standards for SFN</b>	<b>34</b>
3.1	Digital Video broadcasting-Terrestrial . . . . .	34
3.1.1	Input Processing and physical layer pipes . . . . .	35
3.1.2	Coding, Interleaving, Modulation . . . . .	36
3.1.3	Frame Builder . . . . .	38
3.1.4	OFDM generation . . . . .	39
3.1.5	Signaling . . . . .	40
3.1.6	Scattered pilot patterns . . . . .	40
3.1.7	Configuration Options . . . . .	42
3.2	Advanced Television System Committee . . . . .	42
3.2.1	Input Formatting . . . . .	44
3.2.2	Coding, interleaving and modulation . . . . .	44
3.2.3	Layered Division Multiplexing . . . . .	45
3.2.4	Interleaver and Framing . . . . .	45
3.2.5	Waveform generation . . . . .	46
3.2.6	Bootstrap . . . . .	49

3.2.7	Preamble . . . . .	49
3.2.8	Channel bonding and MIMO . . . . .	50
3.2.9	DVB-T2 and ATSC 3.0 in a 6 MHz Channel . . . . .	51
3.3	Multimedia Broadcast Multi-cast System . . . . .	51
3.3.1	eMBMS-enhancement . . . . .	52
3.3.2	LTE-based 5G Terrestrial Broadcast . . . . .	53
3.4	Comparison of different standard . . . . .	57
<b>4</b>	<b>5G New Radio</b>	<b>61</b>
4.1	Frame structure . . . . .	61
4.2	Possible Extension for Terrestrial Broadcast . . . . .	64
<b>5</b>	<b>Advanced Receiver for OFDM system</b>	<b>67</b>
5.1	Channel estimation with insufficient CP length . . . . .	68
5.2	Data Detection and Equalization . . . . .	70
5.3	Iterative reception . . . . .	73
5.4	Conclusion . . . . .	75
<b>6</b>	<b>5G-NR SFN broadcasting with channel shortening</b>	<b>77</b>
<b>Appendix A 5G-NR terrestrial broadcasting with channel shortening</b>		<b>81</b>
<b>7</b>	<b>An introduction to Deep learning</b>	<b>88</b>
7.1	Neural network . . . . .	89
7.2	Activation functions . . . . .	91
7.3	Loss Functions . . . . .	93
7.4	Training Neural Network . . . . .	94
7.4.1	Optimization of gradient . . . . .	97
7.4.2	Preprocessing data and hyperparameters . . . . .	100

---

7.4.3	Regularisation techniques . . . . .	101
7.5	Environment and Hardware for Neural Network Training . . . . .	102
7.6	Convolutional Neural Network . . . . .	103
7.7	Recurrent Neural Network . . . . .	105
7.7.1	Tranining RNN and vanishing gradient problem . . . . .	106
7.7.2	Long Short-Term Memory . . . . .	107
7.7.3	Bi-directional Long Short Term Mermory . . . . .	109
7.8	Neural Networks improves OFDM systems . . . . .	111
7.8.1	Channel estimation with neural network . . . . .	113
7.8.2	Data Detection with neural network . . . . .	115
7.8.3	Hybrid model . . . . .	116
7.8.4	Insufficient CP and mobility . . . . .	117
<b>8</b>	<b>5G-NR broadcasting with bi-directional Long Short Term Memory Neural Network</b>	<b>119</b>
<b>Appendix B</b>	<b>Single-Frequency Network Terrestrial Broadcasting with 5G-NR Numerology Using Recurrent Neural Network</b>	<b>122</b>
<b>9</b>	<b>Conclusion and future works</b>	<b>138</b>
	<b>References</b>	<b>141</b>

# List of Figures

1.1	Block Error Rate performance of broadcasting over a Single Frequency Network with 15 kHz carrier spacing. . . . .	4
2.1	Single Frequency Network, utilizing four transmitter antennas and a moving receiver located within the overlapping coverage area. . . .	11
2.2	The blocks of a typical transmitter in an OFDM-based SFN system.	13
2.3	Figure 2.3: Tapped delay line channel model for broadcasting. The model includes M taps, with $h_n[i]$ representing the frequency and time-varying channel. The output is given by $y[n]$ . . . . .	20
2.4	The main blocks of a classical OFDM receiver in an SFN system. .	22
2.5	two-dimensional grid of reference pilot signals in the frequency-time domain, with $d_t = 2$ and $d_f = 2$ , spaced according to the Nyquist sampling theorem for proper channel estimation in the presence of echoes and severe fading in SFN. . . . .	24
2.6	Minimum Pilot Signal Overhead Percentage as a Function of Speed for OFDM Systems. . . . .	24
2.7	The minimum overhead with $k_1=0.1$ and $k_2=0.1$ . . . . .	33
3.1	The architecture of the DVB-T2 system. . . . .	37
3.2	PP3 Pilot Pattern in DVB-T2 . . . . .	41
3.3	LTE based 5G broadcasting simulation platform . . . . .	54
3.4	Staggered RS pattern with $d_f=3$ and $d_t=4$ . . . . .	56

---

4.1	The framing structure of NR, for numerologies $\mu=0$ and $\mu = 1$ . . .	62
4.2	Integration of mini-slots into 5G negative numerology framing. . .	66
5.1	iterative joint estimation procedure algorithm . . . . .	69
5.2	High-performance single input single output (SISO) receiver with parallel data processing stages and maximal ratio combining (MRC) for interference cancellation and channel estimation. The early decoder assists with channel estimation and FD interference mitigation, while the main decoder utilizes more recent and accurate channel estimates for Viterbi detection. . . . .	74
7.1	An illustration of a neuron, the basic building block of a neural network, which receives input, applies a weighted sum, and outputs an activation signal. . . . .	90
7.2	An illustration of a Feed-forward neural network with one hidden layer consisting of three neurons. The input layer receives the input data with two features, $x_1$ and $x_2$ , and the output layer produces a single output. . . . .	91
7.3	Convolutional Neural Network . . . . .	103
7.4	Graphical representation of an RNN cell. . . . .	106
7.5	Unrolled view of the same RNN. The weight matrices $U$ , $V$ , and $W$ are shared across all time steps. . . . .	106
7.6	A diagram of the Long Short-Term Memory (LSTM) cell. . . . .	108
7.7	An illustration of an end-to-end deep learning receiver for an OFDM system. The received OFDM signal is directly fed into a neural network that performs all the functions of the OFDM receiver, including demodulation, channel estimation, channel equalization, demodulation providing soft information, and channel decoding, resulting in bits. . . . .	111

# List of Tables

2.1	Variation in Delay Spread among SFN networks and its representation in TDL-E (Line of Sight) and TDL-A (Non-Line of Sight) channel models. [4, 5]	21
3.1	Comparison of Scattered Pilot Patterns, results from [6]	41
3.2	DVB-T2 physical layer parameters	43
3.3	Capacity Example, results from [7]	43
3.4	Scattered pilot and overhead in ATSC 3.0	47
3.5	Cyclic prefix in ATSC 3.0	49
3.6	Comparing ATSC 3.0 and DVB-T2 in a 6 MHz Channel, results from [8]	52
3.7	Numerologies in release 14 (enhancement of eMBMS)	53
3.8	New numerologies in release 16	54
3.9	Parameters for link-level simulation	55
3.10	Spectral Efficiency of Different RS Tone Combinations for LPLT scenario, results from [9]	55
3.11	RS Tone Separation and Spectral Efficiency for Different Combinations-Rooftop Reception, results from [9]	56
3.12	5G Broadcast PMCH Capacity with 2.5 kHz Sub-carrier Spacing, results from [10]	58
3.13	5G Broadcast PMCH Capacity with 0.370 kHz Subcarrier Spacing, results from [10]	59

---

3.14	Comparison of Physical Layer Specifications for DVB-T2, ATSC 3.0, and enhancement of eMBMS . . . . .	60
4.1	5G numerology for FR1 and FR2 frequency ranges . . . . .	63
4.2	Maximum inter side distance with 5G-NR numerology . . . . .	64
4.3	Negative numerology . . . . .	64

# List of Acronyms

5G-NR 5G New Radio

ATSC Advanced Television Systems Committee

CP Cyclic Prefix

DVB Digital Video Broadcasting

ICI Inter carrier interference

ISD Inter Site Distance

ISI Inter symbol interference

LDPC Low Density Parity Check

LSTM Long Short Term Memory

MBMS Multimedia Broadcast Multicast Service

OFDM Orthogonal Frequency Division Multiplexing

RNN Recurrent Neural Network

SCS Sub-Carrier Spacing

SFN Single Frequency Network

TDL Tapped Delay Line



# Chapter 1

## Introduction

### 1.1 Problem overview

Orthogonal Frequency Division Multiplexing (OFDM) is a modulation technique widely used in terrestrial broadcasting to effectively address channel challenges, particularly multi-path propagation. Unlike a single fast wide-band modulator, OFDM employs multiple low-bandwidth modulators. A key feature of OFDM is the insertion of a guard interval, known as the Cyclic Prefix, between symbols. This guard interval plays a crucial role in eliminating inter-symbol interference (ISI) [11].

OFDM offers several advantages in receiver design. It simplifies the process by using a single frequency-selective filter to receive the entire signal. After receiving the signal, it can be separated into sub-carriers using fast Fourier transform (FFT). However, despite its widespread usage, OFDM has limitations, especially when it comes to mobility. One limitation is its susceptibility to carrier frequency offset (CFO) and sampling frequency offset (SFO), which can result in inter-carrier interference (ICI). The presence of mobility-induced Doppler spread can exacerbate this issue, introducing additional ICI and reducing the channel coherence time, thereby further impacting OFDM's performance.

In an OFDM system designed for time and frequency selective channels, two critical design parameters are the length of the cyclic prefix (CP) and the sub-carrier spacing. The cyclic prefix acts as a guard interval that is copied and appended to the start of an OFDM symbol. Its purpose is to prevent ISI from previous symbols and maintain the orthogonality of sub-carriers. It is important for the length of the

cyclic prefix to be greater than the channel's delay spread, which represents the time difference between the arrival of the first and last significant multi-path components of a signal.

To enable broadcasting over a SFN, OFDM systems must select a CP length that can accommodate both the delay spread introduced by the scattering environment and the long "artificial" delay spread introduced by the SFN infrastructure with multiple transmitters. The distance between two transmitters in an SFN, known as the Inter Site Distance (ISD), affects the delay spread of the channel and thus influences the selection of CP length. To minimize system overhead, the OFDM symbol duration, which is inversely proportional to the sub-carrier spacing, should be significantly greater than the CP.

Designing OFDM systems for mobility scenarios introduces new challenges due to the time selectivity of the channel. In such scenarios, sub-carrier orthogonality can be lost if the channel changes during the transmission of an OFDM symbol. Therefore, the channel coherence time must be much greater than the symbol duration to preserve orthogonality. However, this constraint on the symbol duration puts a limit on the system overhead, which can become significant in challenging SFN scenarios with large ISD and mobility. In simpler terms, we can summarize the key points as follows:

1. To achieve good performance in SFN setups, it is necessary to use a longer CP.
2. A longer duration for OFDM symbols is needed to reduce system overhead.
3. However, increasing the symbol duration negatively impacts the system's ability to handle Doppler effects, so the overall system must be optimized accordingly.

5G NR (New Radio) is a new radio access technology (RAT) developed by 3GPP for the 5G (fifth generation) mobile network [12]. It is designed to provide faster data rates, lower latency, and increased capacity compared to its predecessor, 4G LTE. 5G-NR operates on a wide range of frequency bands, including sub-6 GHz and mmWave frequencies.

5G-NR incorporates several new technologies and features, such as massive MIMO, beamforming, and advanced coding and modulation schemes. Additionally, 5G-NR supports various use cases, including enhanced mobile broadband (eMBB),

ultra-reliable and low-latency communications (URLLC), and massive machine-type communications (mMTC) [13].

5G-NR offers the flexibility to adapt to various deployment scenarios and use cases by adjusting the sub-carrier spacing (SCS) associated with different "numerologies". The SCS is defined by a parameter  $\mu$  that can take integer values from 0 to 4. The sub-carrier spacing is then given by  $\Delta f = 15 \times 2^\mu$  kHz, resulting in SCS values ranging from 15 to 240 kHz. The choice of  $\mu$  depends on several factors such as bandwidth, latency, and mobility requirements. A larger  $\mu$  value is typically used in mobile environments to provide lower latency, but this requires more precise synchronization and channel estimation. In addition, the choice of  $\mu$  affects the system's resilience to delay spread since the CP length is a fixed fraction of the symbol duration (approximately 1/14 with Normal CP). A lower SCS is typically used for large delay spreads to ensure robustness to inter-symbol interference caused by multi-path propagation.

The 5G-NR numerologies, optimized for cellular communication systems, may not be optimal for SFN terrestrial broadcasting due to the the larger artificial delay spread introduced by the infrastructure. In SFN broadcasting scenarios, the maximum ISD sing 5G-NR can be calculated based on the CP length and the speed of light. The equation is:

$$ISD \leq T_{cp} \cdot c = \frac{c}{14} \cdot \frac{1}{15 \times 10^3 \times 2^\mu}, \quad (1.1)$$

where  $T_{cp}$  is the CP length, and  $c$  is the speed of light. For instance, with  $\mu = 0$  and a normal CP length of  $4.7 \mu\text{s}$ , the maximum ISD is calculated to be 1.4 kilometers. However, in typical high-power, high-tower (HPHT) broadcasting scenarios, the ISD can be significantly larger, on the order of dozens of kilometers.

Figure 1.1 illustrates the 0.1% Block Error Rate (BLER) performance of broadcasting over a SFN using a carrier spacing of 5G-NR (15 kHz,  $\mu=0$ ) with a normal cyclic prefix. The graph presents the correlation between Signal-to-Noise Ratio (SNR) values (in dB) on the x-axis and the corresponding block error rates on the y-axis.

In the system setup, a 16QAM modulation scheme with a bandwidth of 5 MHz is used. The carrier frequency is set at 700 MHz. The code rate employed is 0.48 (LDPC channel coding), and it is assumed that ideal channel estimation is in place. To improve signal reception, the simulation includes the use of two receiver antennas.

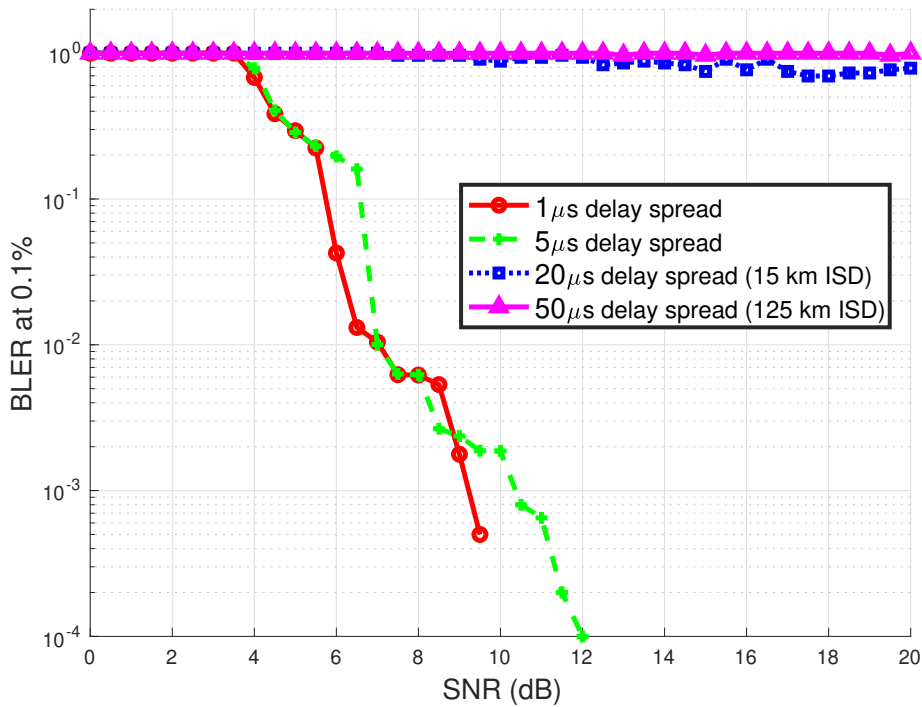


Fig. 1.1 Block Error Rate performance of broadcasting over a Single Frequency Network with 15 kHz carrier spacing.

The channel model utilized is TDL-A. It should be noted that the receiver's speed is set to 30 km/h.

In addition, it is possible to scale the TDL channel model using the root mean square delay spread, which allows us to obtain different single frequency networks. Figure 1.1 illustrates this relationship. By scaling TDL-A with a delay spread of 20  $\mu$ s, we can achieve a low-power, low-tower configuration. Conversely, scaling TDL-A with a delay spread of 50  $\mu$ s results in a high-power, high-tower setup. For further details on the TDL channel model and SFN configuration, refer to section 2.3.3.

It becomes apparent that when utilizing the normal cyclic prefix with a 15 kHz carrier spacing, the system can effectively mitigate ISI caused by multi-path propagation for delay spread values of 1  $\mu$ s and 5  $\mu$ s. However, when implementing LPLT and HPHT SFNs with larger ISDs, the ISI extends beyond the cyclic prefix, resulting in increased block error rates.

Adapting the 5G-NR air interface to meet the requirements of terrestrial broadcasting channels would require several modifications, including:

- **Adjusting cyclic prefix length:** The cyclic prefix length in 5G-NR is optimized for the channel characteristics of cellular networks, but broadcasting channels typically exhibit much larger artificial delay spread. To optimize classical receiver performance, a longer cyclic prefix is required.
- **Narrower sub-carrier spacing:** To reduce the overhead associated with a longer cyclic prefix, a narrower sub-carrier spacing is needed.

The previous design constraints on OFDM parameters, such as the cyclic prefix length and symbol duration, are essential for classical reference OFDM symbol-by-symbol receivers that require orthogonality of the received symbols to perform effectively. However, in challenging SFN scenarios with large ISD and mobility requirements, these constraints can lead to unacceptable system overhead. In such cases, advanced receiver techniques can be employed, which include:

- **Linear equalization techniques:** This includes multidimensional (frequency and time) MMSE (adaptive) equalization and channel shortening.
- **Nonlinear equalization techniques:** This includes interference cancellation and Decision Feedback equalization.
- **Maximum Likelihood Sequence Estimation techniques.**
- **Iterative receivers:** When a powerful channel decoder is present, straightforward application of linear or nonlinear equalization may fail to provide acceptable performance. The use of updated, more reliable information about the transmitted symbols provided by the channel decoder can provide significant gains. This more complex approach requires iteration between detector and decoder.
- **Neural networks:** The use of neural networks has been considered as a substitute for classical blocks in digital baseband receivers in recent years. Despite their complexity, they can provide impressive performance gains and show significant flexibility, especially when facing unknown and/or mismatched channel scenarios.

These advanced receiver techniques can help overcome the limitations of classical OFDM symbol-by-symbol receivers in challenging SFN scenarios.

While these techniques have been widely investigated in the literature [14–19], there is a surprising lack of research on their application specifically to the SFN scenario. This is likely due to the fact that existing broadcasting standards, such as DVB [7] and ATSC [8], are designed to ensure orthogonality at the receiver, at least in the use scenarios they consider. However, the use of 5G-NR numerologies in conjunction with existing SFN broadcasting infrastructure offers significant benefits to broadcasters, as it allows them to deliver broadcasting services using widely available 5G-NR. This also opens up the possibility of delivering broadcasting services in the most challenging SFN use cases associated with large ISD and user mobility, while potentially leveraging advanced receiver techniques to further enhance system performance.

## 1.2 Thesis Objectives

The goal of this thesis is to examine the feasibility of implementing SFN Terrestrial Broadcasting utilizing the existing 5G-NR numerology alongside advanced receiver technologies. Two novel approaches will be developed and evaluated: a 2D-MMSE equalizer and a receiver employing recurrent neural networks.

The objective of the 2D-MMSE equalizer is to address the challenge of strong Inter-Symbol Interference (ISI) and Inter-Carrier Interference (ICI) in SFN Terrestrial Broadcasting with the existing 5G-NR numerology. This equalizer employs channel shortening techniques to equalize the frequency-domain demodulated OFDM symbols affected by ISI and ICI, which may extend beyond a full OFDM symbol duration.

The 2D-MMSE equalizer operates by estimating the transmitted symbols based on the received symbols and the channel response. It takes into account both the temporal (ISI) and frequency (ICI) interference components. By applying the Minimum Mean Squared Error (MMSE) criterion, the equalizer minimizes the mean squared error between the estimated symbols and the true transmitted symbols.

An interesting extension of the 2D-MMSE equalizer is the possibility of incorporating trellis structures. By introducing a parameter, denoted as  $\nu$ , greater than zero,

trellis structures can be employed within the equalizer. Trellis-based equalization allows for capturing the temporal dependencies of the transmitted symbols and the interference components, resulting in improved equalization performance.

The trellis structures within the 2D-MMSE equalizer facilitate the exploration of different paths or sequences of transmitted symbols that are consistent with the received symbols and the estimated channel response. By searching and evaluating these paths using trellis algorithms, such as the Viterbi algorithm, the equalizer can make more accurate symbol estimates, effectively reducing the impact of ISI and ICI.

Through the evaluation and comparison of the 2D-MMSE equalizer with traditional equalization techniques, this research seeks to demonstrate the advantages and disadvantages of employing advanced equalization methods, including trellis structures, in SFN terrestrial broadcasting with 5G-NR numerology. The objective is to explore the feasibility of utilizing the 2D-MMSE equalizer, with the potential extension to trellis-based equalization, to enhance the performance of broadcasting systems by mitigating the effects of ISI and ICI.

The objective of the receiver based on recurrent neural networks (RNN) is to explore the feasibility of utilizing advanced receiver technologies for SFN Terrestrial Broadcasting with the existing 5G-NR numerology. This receiver will provide joint equalization and channel estimation while also generating soft decisions for input into the channel decoder, without requiring prior knowledge of the channel characteristics.

By employing RNN-based techniques, we aim to address the challenges posed by dynamic channel conditions, such as mobility and channel estimation uncertainties, which can significantly impact the performance of the receiver. The RNN will be designed to capture and leverage the temporal dependencies of the received OFDM symbols affected by ISI and ICI, enabling effective equalization and data detection.

The RNN-based receiver will utilize its recurrent structure, such as the bidirectional long short-term memory (Bi-LSTM) neural network, to model and learn the complex temporal relationships within the received OFDM symbol sequence. This will enable the RNN to estimate the channel, perform equalization, and generate soft decisions for subsequent decoding, all within a unified framework. The RNN will learn to adapt to varying channel conditions, including scenarios with high mobility and strong ISI, thus improving the robustness of broadcasting over SFN with 5G-NR.

Furthermore, the RNN-based receiver can offer additional advantages beyond traditional equalization methods. For example, the receiver can be trained using deep learning techniques on a large dataset, allowing it to capture and exploit intricate patterns in the received signals. Additionally, the RNN can operate without the need for dedicated pilot signals by superimposing the data with the pilot signal, thereby improving spectral efficiency and reducing overhead.

Through the evaluation and comparison of the RNN-based receiver with traditional equalization techniques, this research seeks to demonstrate the advantages and disadvantages of employing advanced neural network approaches in SFN terrestrial broadcasting with 5G-NR numerology. The objective is to explore the feasibility of utilizing RNN-based receivers to overcome the limitations of traditional equalization methods and enhance the performance of broadcasting systems in challenging scenarios.

Through the evaluation of the proposed methods, this study seeks to demonstrate the potential of 5G-NR for SFN terrestrial broadcasting without the need to modify the existing standard numerologies. The outcome of this study will be instrumental in advancing the development of more effective and robust broadcasting systems and provide insights into the potential of 5G-NR for future terrestrial broadcasting.

### **1.3 Organisation of dissertation**

This dissertation is divided into nine chapters, each focusing on different aspects of the research topic.

In Chapter 2, we delve into the traditional transmitter and receiver blocks used in SFN based on Orthogonal Frequency-Division Multiplexing (OFDM). We provide a detailed description of the wireless channel model considered, particularly in the context of SFN. We demonstrate how SFN can be modeled using the Tapped Delay Line channel model. We also discuss the main parameters that should be considered in OFDM receiver design to enable the traditional symbol-by-symbol scheme to function effectively, even in the presence of mobility and long inter-site distances.

In Chapter 3, we review relevant SFN broadcasting standards, such as Digital Video Broadcasting (DVB) and Advanced Television Systems Committee (ATSC). In Chapter 4, we assess the suitability of broadcasting for 5G-NR by examining the



5G New Radio (NR) physical layer. Chapter five is dedicated to exploring advanced techniques for OFDM systems when the cyclic prefix length is insufficient.

Chapter 6 provides an introductory overview of the first paper enclosed in Appendix A, titled "Single Frequency Network Broadcasting with 5G-NR Numerology." This paper, presented at the 2021 IEEE Latin-American Conference on Communications (LATINCOM), explores the feasibility of SFN broadcasting with 5G-NR numerology. To enhance clarity, the paper is included in Appendix A, immediately following Chapter 6.

In chapter seven, we discuss the potential of deep learning and various neural networks for OFDM systems, as well as reviewing research papers that examine the use of neural networks to handle insufficient cyclic prefix length and time-varying channels.

Chapter 8 serves as an introduction to the second paper provided in Appendix B titled "Single-Frequency Network Terrestrial Broadcasting with 5G-NR Numerology Using Recurrent Neural Network." This paper, published in Electronics in 2022, discusses the development of an advanced receiver based on recurrent neural networks for SFN terrestrial broadcasting with 5G-NR numerology. The paper itself is included in Appendix B, following Chapter 8, eliminating the need to duplicate the material in the introductory chapter.

Considering the fact that the technical content of our contribution is primarily contained within the two annexed papers, which can be regarded as the most crucial part of the thesis, Appendix A and Appendix B are positioned immediately following Chapter 6 and Chapter 8, respectively, to emphasize their significance within the overall thesis.

Chapter 9 concludes the dissertation, summarizing the key findings and contributions of the research. It also outlines future research directions.

# Chapter 2

## Background on SFN Terrestrial Broadcasting

### 2.1 Single Frequency Network overview

Single Frequency Networks (SFNs) rely on the utilization of Cyclic Prefix Orthogonal Frequency Division Multiplexing (CP-OFDM) to mitigate interference. Figure 2.1 illustrates a SFN, which comprises four transmitter antennas and a mobile receiver located within the overlapping coverage area. The signals transmitted by these antennas reach the receiver at different times due to propagation delays.

Propagation delays can lead to inter-symbol interference (ISI), where adjacent sub-carriers' symbols overlap, degrading the received signal's quality. The objective of this configuration is to ensure uninterrupted reception, even in the presence of scattered signals from nearby buildings. By employing OFDM, SFNs can effectively minimize the interference caused by propagation delays. This enables the receiver to accurately receive and decode signals from multiple transmitters, even in the presence of scattered signals from nearby buildings or other obstacles.

The advantages of a SFN include:[1, 20, 21]

- **Spectrum Efficiency:** SFNs offer high spectrum efficiency compared to traditional multi-frequency networks (MFNs). They can accommodate a larger number of programs or services using the same frequency spectrum, making efficient use of limited or high-demand spectrum resources.

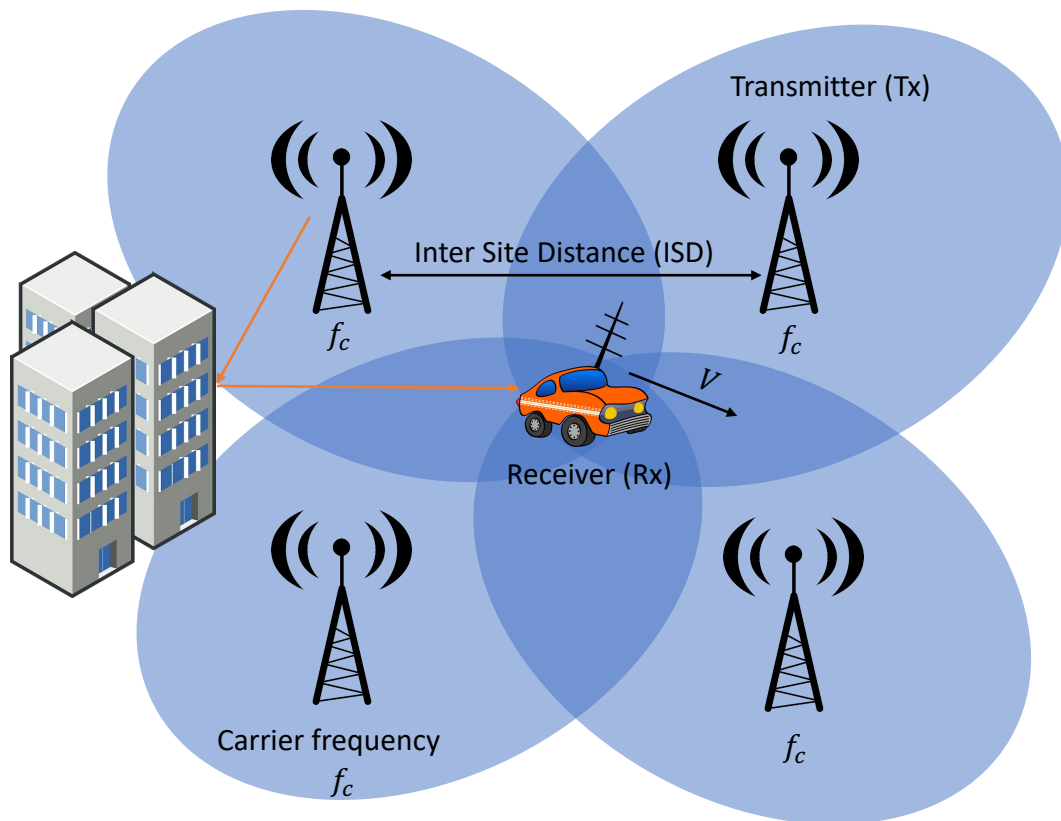


Fig. 2.1 Single Frequency Network, utilizing four transmitter antennas and a moving receiver located within the overlapping coverage area.

- **Coverage and Frequency Economy:** SFNs provide better coverage and frequency economy compared to MFNs. By utilizing a single frequency for all transmitters within a coverage area, SFNs can achieve larger coverage areas without the need for additional frequencies. This results in cost savings and efficient resource utilization.
- **Network Gain or Diversity Gain:** SFNs provide network gain or diversity gain by reducing signal variations or fluctuations at the receiver. The received signal is a combination of signals from multiple transmitters, allowing for reception even if one transmitter is shadowed or affected by interference. This improves signal quality and increases the probability of reception.
- **Homogeneous Field Strength Distribution:** SFNs offer a more consistent distribution of field strength across the service area. This means that the re-

ceived signal strength is more uniform throughout the coverage area, reducing variations in signal quality or coverage gaps.

- **Gap-Filling Capability:** SFNs allow for the easy setup of gap-filling transmitters to improve reception quality in areas with poor signal quality, without requiring additional frequencies. This flexibility enables broadcasters to address specific regions where signal quality may be compromised.
- **Robustness and Redundancy:** SFNs provide increased robustness and redundancy in the network. In dense SFNs, the failure of a single transmitter does not result in a coverage outage for the entire network. This redundancy ensures continuity of service and reduces the risk of complete signal loss.

While SFNs have several advantages, there are also a few disadvantages [21] to consider:

- **Network Splitting:** SFNs do not support network splitting. In other words, it is not possible to divide the network into separate sections or regions with different content. All transmitters within an SFN broadcast the same digital information simultaneously at the same frequency. This limitation can be a drawback if there is a need for localized or region-specific content.
- **Time Synchronization:** SFNs require precise time synchronization among the transmitters. The signal emissions from each transmitter must occur at the same time or with precisely controlled delays.
- **Frequency Synchronization:** SFNs also require precise frequency synchronization both at the transmitter and receiver. Any errors in frequency synchronization can result in frequency orthogonality losses for the received signals.

## **2.2 Transmitter Blocks in SFN broadcasting based on OFDM**

To ensure efficient data delivery in modern wireless systems, particularly in SFN, a well-designed transmitter is essential. Figure 2.2 illustrates the transmitter blocks found in a typical standard for SFN systems based on OFDM.

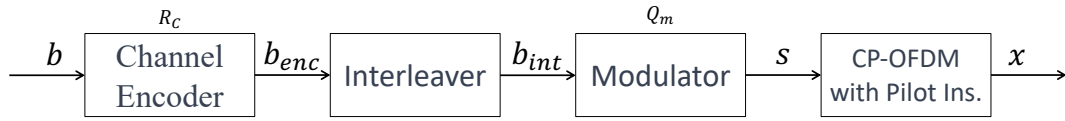


Fig. 2.2 The blocks of a typical transmitter in an OFDM-based SFN system.

Starting from the left-hand side of the figure, the first block is the Channel Encoder with rate  $R_c$ . It takes a Bit Sequence  $b$  as its input and outputs an Encoded Bit Sequence  $b_{enc}$ . The channel encoder adds redundant information to the input bit sequence, which helps protect the data against channel impairments. Next is the Interleaver block. It takes the Encoded Bit Sequence  $b_{enc}$  as its input and outputs an Interleaved Bit Sequence  $b_{int}$ . The interleaver's role is to rearrange the bits in the encoded bit sequence to spread out bursts of errors that may occur during transmission.

The modulator block takes the Interleaved Bit Sequence  $b_{int}$  as input and generates a Modulated Symbol Sequence  $s$  as output. The modulator (or mapper in the following) converts the interleaved bit sequence into a set of modulated symbols, such as conventional Quadrature Amplitude Modulation (QAM) or more advanced non-uniform constellation (NUC) sets.

Following the mapper block, pilot symbols are inserted into the modulated symbol sequence  $s$ . These pilot symbols serve various important functions, including channel estimation and other signal processing tasks at the receiver. By incorporating pilot symbols, the communication system can better estimate variations and distortions introduced by the transmission channel, which helps to correctly estimate the transmitted data.

Finally, the CP-OFDM Modulator takes the Modulated Symbol Sequence  $s$  as its input and outputs an OFDM Symbol Sequence  $x$ . The CP-OFDM modulator computes the transmitted discrete time waveform by inserting a CP and performing the Inverse Fast Fourier Transform (IFFT). In the following sections, we will provide more details on each block.

### 2.2.1 Channel encoder

A channel encoder is a crucial block in a modern digital communication system that is responsible for adding redundancy to the transmitted data to protect against

channel impairments. Channel impairments can be due to various factors such as noise, interference, fading, and other distortions that may occur during transmission. The addition of redundancy through a channel encoder enables the receiver to detect and correct errors in the received data, improving the overall reliability of the communication system. This process is commonly referred to as Forward Error Correction (FEC).

Various types of channel encoders and FEC techniques have been adopted in digital communication standards. The first adopted FEC coding approaches were based on Convolutional Codes [22], Reed-Solomon Codes [23], Bose-Chaudhuri-Hocquenghem (BCH) Codes [24], or concatenation of them. More recently, these encoding schemes have been replaced by "capacity achieving" schemes like Turbo Codes [25] and Low-Density Parity-Check (LDPC) Codes [26]. These classes of codes require an iterative decoder at the receiver to provide the desired performance. Furthermore, the input to the channel decoder must be "soft", typically in the form of Log-Likelihood Ratios (LLR).

The presence and performance of a channel decoder cannot be neglected when designing the inner detector, as it strongly affects the design and performance measures that should be considered for optimizing it. As mentioned, modern channel decoders are capacity-achieving and accept soft information (LLR). The front-end blocks, including synchronization, equalization, and channel estimation, must be able to provide accurate soft information to the following decoder. Performance measures like BER or FER at the detector output are not particularly useful in this sense. On the other hand, information-theoretic measures like cross-entropy or mutual information of delivered soft messages are more useful. Also, the detector output before outer decoding is typically affected by many errors, so classical decision feedback schemes that do not exploit the outer decoder fail to provide satisfactory performance.

### **2.2.2 Interleaver**

Interleaving is a technique that rearranges the sequence of encoded data in a specific order before transmission. Its purpose is to spread out errors that occur during transmission over a large number of data symbols, so that bursts of errors do not affect many consecutive bits belonging to the same codeword. Correlated errors

can considerably reduce the effectiveness of the following channel decoder and potentially nullify it.

Row-column permutation laws are very effective in reducing error correlation. Block interleaving [27] involves dividing the input data into several frames and then rearranging the symbols within each block. The blocks are then transmitted in a different order, resulting in the interleaved output.

On the other hand, convolutional interleaving [28] involves writing the input sequence in a memory in a given order and reading the output sequence from the same memory in a different order. This process does not require segmentation of the input sequence into blocks and requires smaller memory and latency for providing the same spread performance. However, the absence of a block structure is not desirable in discontinuous or multi-user transmissions as the information stream cannot be packetized. For this reason, the convolutional interleaver is seldom adopted in standards.

### 2.2.3 Modulator

The Modulator (or mapper) is responsible for mapping a block of input bits to a block of complex symbols, which for OFDM are then modulated onto sub-carriers in the frequency domain. The modulation efficiency  $m$  specifies the number of bits used to label each complex symbol. The constellation used for mapping can be either uniform or non-uniform.

In QAM [29] "uniform" constellations, all the points are equally spaced in both In-phase and Quadrature dimensions. The QAM constellations are obtained as a cartesian product of a uniform PAM constellation, which simplifies the transmitter and, more importantly, the detector operations. The detector complexity, in fact, grows with the square root of the modulation cardinality.

In Non-Uniform Constellations (NUC) [30], on the other hand, points are not uniformly spaced in the two dimensions. A non-uniform constellation is more complex to encode and decode, and the detector cannot process independently the two dimensions to provide the output LLR. The detector complexity grows, in this case, linearly with the modulation cardinality and thus exponentially with the modulation efficiency  $m$ . The increased degree of freedom in their design, on the other hand, can be used to provide several important advantages, such as increased

mutual information, reduced PAPR, increased robustness to phase noise and other channel impairments.

Commonly used constellations for SFN standard include uniform QAM constellations with up to 256 points. More recently, ATSC standard also adopted some specially designed NUC.

## 2.2.4 CP-OFDM Modulator with Pilot Insertion

Cyclic Prefix Orthogonal Frequency Division Multiplexing (CP-OFDM) is a digital modulation technique widely used in modern wireless communication systems, including SFN systems for TV broadcasting. Unlike traditional single-carrier modulation techniques, OFDM divides the data into multiple parallel streams and modulates each stream onto a separate (sub)carrier frequency. This makes OFDM more flexible and provides several benefits such as resistance against multi-path and time-selective fading. The core flexibility of CP-OFDM is providing a trade-off between symbol duration and carrier spacing. This flexibility can be used to match the signal waveform to the type of selectivity (time or frequency) of the target channel scenario. The available bandwidth ( $B$ ) is partitioned into  $N$  sub-carriers with sub-carrier spacing (SCS)  $\Delta f$ . The CP-OFDM modulator takes the modulated symbol sequence  $s$  as input and generates the OFDM waveform  $x$ . The CP-OFDM modulator implements two key operations: the inverse fast Fourier transform (IFFT) and the insertion of a cyclic prefix (CP).

The IFFT operation can be expressed as:

$$x_{tmp}(m) = \frac{1}{\sqrt{N}} \sum_{n=0}^{N-1} s_n e^{-j\frac{2\pi}{N}mn}, \quad (2.1)$$

where  $x_{tmp}$  is the temporary sequence obtained after IFFT,  $s_n$  is the  $n$ -th element of the modulated symbol sequence  $s$ , and  $m$  is the sub-carrier index.

The CP insertion operation can be expressed as:

$$x = [x_{tmp}(N-L+1), \dots, x_{tmp}(N), x_{tmp}(1), \dots, x_{tmp}(N-L)], \quad (2.2)$$



where  $x$  is the final OFDM symbol sequence, and  $L$  is the length of the cyclic prefix. The CP is inserted by replicating  $L$  samples from the end of the IFFT output to the beginning of the sequence.

Accurately estimating channel state information (CSI) is critical for successful communication in CP-OFDM systems. Known symbols, called pilots, are embedded into the CP-OFDM signal to enable efficient and accurate channel estimation [31]. There are different pilot insertion methods that can be used in CP-OFDM systems, including block-type, comb-type, scattered-type, and hybrid-type pilots. Block-type pilots are inserted in a block at the beginning or end of each OFDM symbol, while comb-type pilots are inserted periodically along each OFDM symbol. Scattered-type pilots are randomly inserted across the OFDM symbols, making them particularly suitable for SFN systems.

## 2.3 Channel Modeling in SFN

Wireless communication systems are subject to limitations in their performance, mainly due to the effects of the radio channel. This presents unique challenges compared to fixed wired channels, as the channel on top of frequency selectivity, is time-varying and unpredictable. The transmission and analysis of data become more complex in this scenario. Obstacles, both natural and man-made, can obstruct transmission paths, leading to multiple reflections of the transmitted signal, each with possibly time varying propagation delays. These reflections interact with each other, resulting in constructive or destructive interference, which leads to multi-path time selective fading. In certain situations, such as in single frequency networks, where multiple transmitters work in the same time-frequency, also artificial multi-path fading can occur. Multi-path fading can cause significant and rapidly fluctuating attenuation of the signal, as well as phase shifts, which can make reliable information transfer difficult.

### 2.3.1 Doubly selective channel in mobile SFN scenarios

We have seen that in a static SFN scenario, in addition to the delay spread due to the scattering environment, we must consider the additional artificial delay due to the multiple transmitters from different locations, related to the infrastructure inter-site

distance (ISD). This very large delay spread of SFN makes the equivalent channel strongly frequency selective. The addition of mobility of the receiver adds time variability to the channel impulse response, so SFN with mobility becomes one of the most challenging conceivable channel scenarios.

Mathematically, a doubly selective discrete time channel is modeled with a time-varying impulse response,  $h_n[i]$  with  $M$  channel taps. The received signal,  $y[n]$ , can then be represented as:

$$y[n] = h_n[n] * x(n) + v(n) = \sum_{i=0}^{M-1} h_n[i] \cdot x[n-i] + v[n], \quad (2.3)$$

where  $x[n]$  is the input sample, and  $v[n]$  is additive white Gaussian noise (AWGN). Equivalently, in the frequency domain, we can provide the time-varying transfer function as:

$$H_n(f) = DTFT(h_n(i)) = \sum_i h_n(i) \exp(-j2\pi fi). \quad (2.4)$$

The filter taps  $h_n(i)$ ,  $i = 1, \dots, M$ , are typically modeled by a set of independent complex stationary Gaussian processes and characterized by their power spectral density.

### 2.3.2 Delay Spread and Doppler spread

The maximum delay spread is the difference between the arrival times of the earliest and latest multi-path components. However, this measure may not be very relevant as the amount of interference also depends on the relative power level of different paths.

The root mean square (RMS) delay spread is a more meaningful measure of the time dispersion of a signal due to multi-path propagation. Mathematically, it is the standard deviation of the power delay profile (PDP)  $P(\tau)$ , which is a measure of the distribution of the signal power as a function of the delay:

$$\bar{\tau} = \int_{-\infty}^{\infty} \tau P(\tau) d\tau, \quad (2.5)$$

$$\tau_{rms}^2 = \int_{-\infty}^{\infty} (\tau - \bar{\tau})^2 P(\tau) d\tau. \quad (2.6)$$

A channel with a large RMS delay spread implies a higher degree of frequency-selective fading, which can cause significant distortion and inter-symbol interference in the received signal. A Doppler shift occurs when there is a change in the frequency or wavelength of a wave due to the motion of the source, the receiver, or the scatterer relative to the medium. The Doppler shift associated with a single path component can be evaluated as:

$$f_{D,p} = \cos(\theta_p) f_c \frac{|v|}{c} = \cos(\theta_p) f_D, \quad (2.7)$$

where  $\theta_p$  is the relative speed direction associated with the considered path,  $c$  is the speed of light,  $f_c$  is the carrier frequency, and  $f_D = f_0 \frac{|v|}{c}$  is the maximum Doppler shift. When the number of paths contributing to a given discrete delay  $i$  in  $h_n(i)$  is sufficiently large and uniformly distributed in direction, the sum of all path contributions of  $h_n(i)$  can be modeled as a complex Gaussian process with the classical Jake's power spectral density on both I and Q components:

$$S_h(f) \propto \frac{1}{\sqrt{f_D^2 - f^2}}. \quad (2.8)$$

Furthermore, under further assumptions, the processes modeling the different taps  $h_n(i)$  are also assumed to be independent. The presence of Line of Sight (LoS) propagation paths for some particular delays is modeled in this context by simply assigning a non-zero mean to the Gaussian processes associated with the corresponding taps, leading to a more general Rician model of the first-order statistic.

### 2.3.3 Modeling a SFN with Tapped Delay Line

The Tapped Delay line (TDL) channel model (see Figure 2.3) is a widely adopted mathematical representation of a discrete time communication channel that accounts for the effects of a possibly time-varying multi-path propagation. It assumes that the received discrete time sample is the sum of delayed and attenuated versions of the transmitted signal, where each tap represents the contribution of all paths associated to that particular discrete propagation delay through the channel.

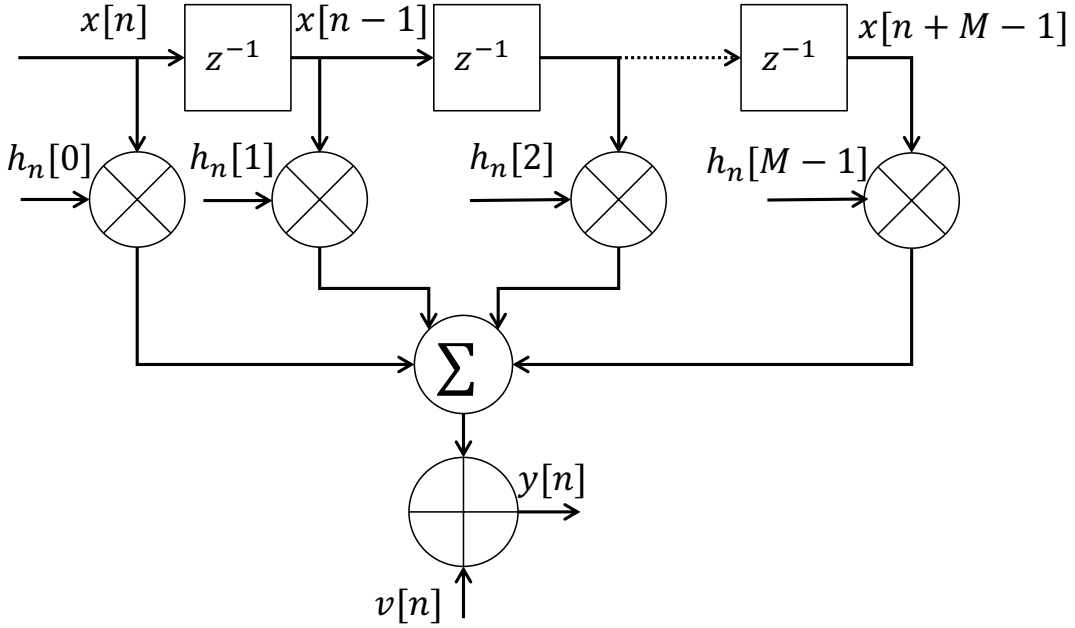


Fig. 2.3 Figure 2.3: Tapped delay line channel model for broadcasting. The model includes  $M$  taps, with  $h_n[i]$  representing the frequency and time-varying channel. The output is given by  $y[n]$ .

The model is fully described by providing the sampling period  $\Delta t$ , the length of the TDL  $M$ , and for each tap  $h_n(i)$ , the corresponding power, Doppler frequency, Doppler spectrum, and the Rician factor.

In [32], a set of TDL channel models have been defined with distinct profile models (TDL-A, TDL-B, TDL-C, TDL-D, and TDL-E) that capture different channel profiles for both Non-Line-of-Sight (NLoS) and Line-of-Sight (LoS) environments. It has also been verified that the same channel models can be utilized to reproduce an SFN scenario by properly tuning the Root Mean Square (RMS) value of the delay spread with the inclusion of the added artificial delay spread of SFN in accordance with the considered Inter-Site Distance (ISD) [4]. By adjusting the delay spread, the TDL channel model can effectively represent various ISDs, thereby enabling the simulation of different SFN networks. Notably, altering the delay spread values in the TDL-E (LoS) and TDL-A (NLoS) channel models can model four unique SFN networks with varying ISDs, which we considered as a reference in our study (see Table 2.1) [4, 5].

The Table 2.1 compares four different SFN networks in terms of their ISD, transmitted power, and delay spread for the TDL-E and TDL-A channel models.

Table 2.1 Variation in Delay Spread among SFN networks and its representation in TDL-E (Line of Sight) and TDL-A (Non-Line of Sight) channel models. [4, 5]

Parameter	LPLT	MPMT	HPH1	HPHT2
ISD [km]	15	50	125	173.2
Transmitted power [dBm]	46	60	70	70
TDL-E Delay Spread(RMS) ( $\mu$ s)	16	35	45	70
TDL-A Delay Spread(RMS) ( $\mu$ s)	20	40	50	75

The SFN networks are classified as Low Power Low Tower (LPLT), Medium Power Medium Tower (MPMT), High Power High Tower 1 (HPHT1), and High Power High Tower 2 (HPHT2), depending on their tower height and power level.

In order to capture the impact of mobility in a TDL channel model that utilizes a typical carrier frequency of 700 MHz for an SFN, incorporating Doppler spread is essential. By calculating the appropriate scale factor based on the relative velocity between the transmitter and receiver, we can determine the maximum Doppler shift in hertz, which can then be incorporated into the TDL channel model.

The choice of the TDL channel model depends on the reception scenario of interest. For portable reception scenarios, where the receiver is moving within an urban or suburban environment with many obstructions, the TDL-A (NLoS) model is more suitable. For rooftop reception scenarios, where the receiver is fixed on a high location with a clear line of sight to the transmitter, the TDL-E (LoS) model is more appropriate.

## 2.4 The reference "Classical" OFDM receiver

The receiver in an OFDM system is responsible for demodulating the received signal and recovering the original data. Figure 2.4 illustrates the main blocks of a classical OFDM receiver in an SFN system. This receiver is considered as the reference when designing the OFDM waveform in standards. In particular, one must ensure by design that the sub-carrier spacing  $\Delta f$  is much smaller than the coherence bandwidth of the channel, and at the same time, the symbol duration  $T_u = 1/\Delta f$  is much smaller than the coherence time of the channel. In the next sections we will provide details on the operations performed by each block.

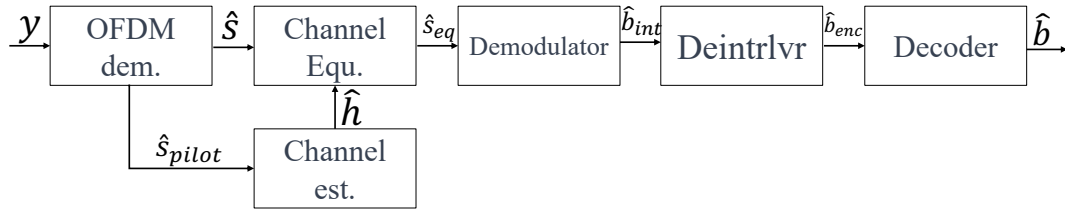


Fig. 2.4 The main blocks of a classical OFDM receiver in an SFN system.

### 2.4.1 Synchronization and CP-OFDM demodulator

The demodulation process in an OFDM receiver involves multiple steps including synchronization [33], cyclic prefix removal, and Fast Fourier Transform (FFT). The first step is time synchronization, which is performed by cross-correlating two samples of the received signal to detect the start of a new symbol period. The cross-correlation is defined as:

$$r(\tau) = \int_{-\infty}^{\infty} y(t)y(t - \tau)dt. \quad (2.9)$$

The receiver detects the start of a new symbol period when the cross-correlation exceeds a threshold value. The second step is secondary synchronization, which is used to determine the best position for the FFT window. Various synchronization strategies can be used, such as synchronizing to the strongest signal or using a sliding FFT window. During the PhD research activity, we assumed ideal synchronization. After the timing synchronization, which is in charge of finding the optimal location of the OFDM symbol, the receiver performs the cyclic prefix removal operation on the received signal. After the cyclic prefix removal, the receiver performs the FFT operation on the received signal to convert it from the time domain to the frequency domain:

$$X[k] = \sum_{n=0}^{N-1} y(n\Delta t)e^{-j2\pi kn/N}, \quad (2.10)$$

where  $k$  is the frequency index,  $N$  is the number of sub-carriers, and  $\Delta t$  is the sampling interval. The result of the FFT,  $X[k]$ , is then demultiplexed into two parts:  $\hat{s}$ , which is the information signal that should be equalized, and  $\hat{s}_{pilot}$ , which are pilot signals for channel estimation.

## 2.4.2 Channel estimation

In OFDM systems, frequency domain channel estimation is the process of determining the possibly time varying frequency response of the communication channel between the transmitter and receiver. The accurate estimation of the channel response is crucial for proper decoding of the transmitted data and to mitigate the impact of echoes generated in SFN which can cause severe fading.

Pilot signals are used to estimate the channel in OFDM. They are inserted into the transmitted signal at specific intervals in both frequency and time domains. The distance between pilot signals in the frequency domain is referred to as  $d_f$  and the distance between pilot signals in the time domain is referred to as  $d_t$ .

The selection of optimal values for  $d_f$  and  $d_t$  for correct channel estimation should be done according to the Nyquist sampling theorem [9]. The two-dimensional Nyquist sampling theorem sets the minimum interval of reference pilot signals in both the frequency and time domains:

$$d_f \leq (4\tau_{\max}\Delta f)^{-1} \text{ and } d_t \leq (4f_D T_s)^{-1}, \quad (2.11)$$

where  $f_D$  is the Doppler shift,  $\tau_{\max}$  is the maximum delay spread,  $\Delta f$  is the sub-carrier spacing, and  $T_s = 1/\Delta f + T_{cp}$  is the total symbol duration.

As an example, Figure 2.5 shows a 2-dimensional grid of reference pilot signals in the frequency-time domain. The horizontal axis represents time, and the vertical axis represents frequency. The reference pilot signals are spaced apart by  $d_t = 2$  in the time domain and  $d_f = 2$  in the frequency domain.

The pilot overhead is defined as  $OH_p \triangleq (d_f d_t)^{-1}$ . To compute the pilot overhead of an OFDM system in a given channel scenario, we can use Equation 2.11, which provides the constraint on  $d_f$  and  $d_t$  based on the maximum delay spread ( $\tau_{\max}$ ), carrier spacing ( $\Delta f$ ), and CP length  $T_{cp}$ . Since we have  $T_{cp} \geq \tau_{\max}$ , we can write:

$$OH_p \geq K \tau_{\max} f_D \Delta f \cdot (1/\Delta f + \tau_{\max}) \quad (2.12)$$

$$\geq K(\tau_{\max} f_D + \tau_{\max}^2 f_D \Delta f). \quad (2.13)$$

To determine  $\tau_{\max}$  in Equation 2.12, we can use the proportionality between  $\tau_{\max}$  and the RMS delay spread provided in Table 2.1. To ensure a cautious estimate, we should multiply the RMS delay spread by a factor of 5. Assuming a sub-carrier

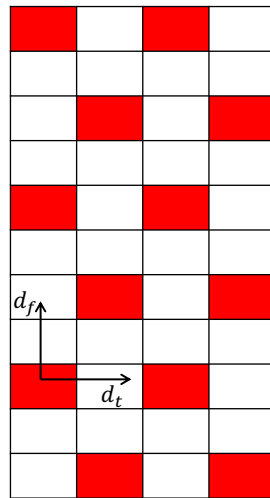


Fig. 2.5 two-dimensional grid of reference pilot signals in the frequency-time domain, with  $d_t = 2$  and  $d_f = 2$ , spaced according to the Nyquist sampling theorem for proper channel estimation in the presence of echoes and severe fading in SFN.

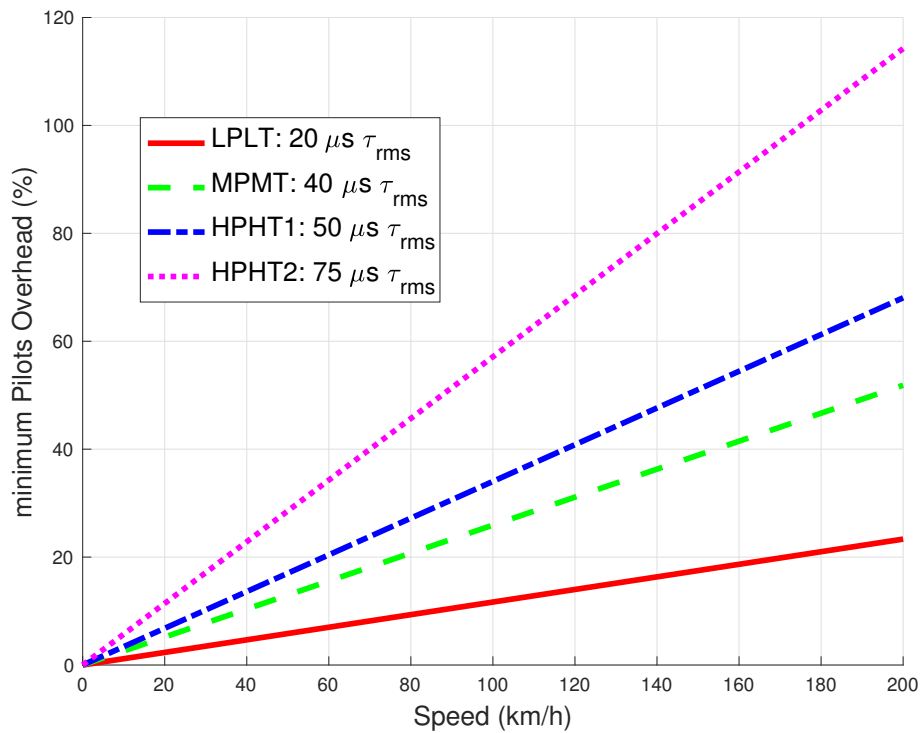


Fig. 2.6 Minimum Pilot Signal Overhead Percentage as a Function of Speed for OFDM Systems.



spacing of  $\Delta f = 1.25$  kHz and carrier spacing 700 MHz, we can then calculate the minimum pilot overhead for various single frequency scenarios and speeds, as shown in Figure 2.6. The pilot overhead and minimum pilot density requirement increase as user speed increases, which may become impractical and infeasible for allocating resources for pilot signals. Alternative advanced channel estimation and tracking methods, such as superimposing [34], may need to be considered in such cases.

For example, in a low-power, low-tower scenario with a root mean square delay spread of  $20 \mu\text{s}$  and a speed of 200 kmph, assigning more than 20 percent of the resources to pilot signals is necessary. However, in a high-power, high-tower scenario with a root mean square delay spread of  $75 \mu\text{s}$ , all available resources must be allocated to pilot signals to comply with the Nyquist theorem for minimum pilot density, as expressed in Equation 2.11.

### Channel estimation algorithms

Least Square [35](LS) and Minimum Mean Squared Error [36] (MMSE) are two common channel estimation algorithms used in OFDM systems to obtain the channel frequency response for each pilot sub-carrier.

To estimate the channel response using LS (Least Squares) estimation, we utilize both the received pilot signal,  $\hat{s}_{pilot}[k]$ , and the transmitted pilot signal,  $x_p[k]$ . The channel response is then determined as the ratio of the received signal to the transmitted signal, which is given by the equation:

$$\hat{h}_{LS}[k] = \frac{\hat{s}_{pilot}[k]}{x_p[k]}, \quad (2.14)$$

where  $\hat{h}_{LS}[k]$  is the estimated channel response and  $k$  is the index of the pilot sub-carrier.

For MMSE estimation, the estimated channel response is calculated as a weighted average of the LS estimate and the prior information about the channel, such as the expected power spectral density (PSD) of the channel. MMSE outperforms simpler LS when the density of pilots is low. The MMSE estimate is given by the equation:

$$\hat{h}_{MMSE}[k] = \sum_{i=0}^{N_p-1} \frac{\hat{s}_{pilot}[i]}{x_p[i]} w_i[k] = \sum_{i=0}^{N_p-1} \hat{h}_{LS}[i] w_i[k], \quad (2.15)$$

where  $w_i[k]$  is the weight associated with the  $i$ -th pilot sub-carrier, and  $k$  represents the index of the pilot sub-carrier. The weights are chosen such that the MMSE estimate is as close as possible to the actual channel response.

### Interpolation

Interpolation is a method of estimating values between known data points. In the context of channel estimation in OFDM systems, it refers to the process of extending the channel response estimates obtained at pilot sub-carrier positions to the whole frame and data sub-carriers.

The Wiener estimator assumes that the channel response is a stationary random process, and it uses the autocorrelation and cross-correlation of the channel response to estimate the channel at non-pilot sub-carriers. The autocorrelation and cross-correlation are estimated based on the known pilot sub-carriers. The Wiener estimator can be expressed as follows:

$$\hat{h}(k) = R(k)^{(-1)} \cdot P(k), \quad (2.16)$$

where  $\hat{h}(k)$  is the estimated channel response at non-pilot sub-carrier  $n$ ,  $R(k)$  is the autocorrelation matrix of the channel response, and  $P(k)$  is the cross-correlation vector between the pilot sub-carriers and the non-pilot subcarrier  $k$ .

The Wiener estimator is computationally efficient and provides optimal linear interpolation performance in OFDM systems. However, the Wiener estimator may not always be used for channel interpolation, since it requires knowledge of the statistical properties of the channel, which may not always be available.

The linear interpolation method is used to estimate the channel response at any arbitrary sub-carrier  $k$ , based on the estimated channel response at the pilot sub-carriers,  $\hat{h}[i]$  for  $i = 0, 1, 2, \dots, N_p - 1$ . The estimation is obtained through the use of interpolation coefficients  $a_i[k]$ , which determine the contribution of each pilot sub-carrier to the estimated channel response at sub-carrier  $k$ . Specifically, the channel response at sub-carrier  $k$  is given by the linear combination of the estimated channel response at the pilot sub-carriers, as follows:

$$\hat{h}[k] = \sum_{i=0}^{N_p-1} a_i[k] \cdot \hat{h}[i]. \quad (2.17)$$

The interpolation coefficients  $a_i[k]$  are selected to create a linear relationship between the estimated channel response at the pilot sub-carriers and the estimated channel response at the arbitrary sub-carrier  $k$ .

It should be noted that while the linear interpolation method is suitable for smooth frequency variations, it may not provide accurate results for severe fading in single-frequency networks. After obtaining the estimates of the pilot sub-carriers, we can apply DFT-based interpolation [37] to estimate the channel impulse response. To achieve this, we first calculate the IDFT of these estimates to obtain the impulse response of the channel.

$$h_p[k] = \frac{1}{N_p} \sum_{i=0}^{N_p-1} \hat{h}[i] \cdot e^{j\frac{2\pi ik}{N_p}}, \quad k = 0, 1, 2, \dots, N_p - 1. \quad (2.18)$$

Here,  $h_p[k]$  is a vector that contains all the channel estimates on the  $N_p$  pilot sub-channels. Typically, the number of pilots,  $N_p$ , is much larger than the channel delay spread,  $L_{ds}$ . For a wireless channel with a delay spread of  $L_{ds}$ , the time-domain channel impulse response,  $h$ , should have non-zero values only in the first  $L_{ds} + 1$  samples. Therefore, a low-pass filter (LPF) is applied to  $h_p$  to reduce estimation noise:

$$h_p = [h_p[0], h_p[1], \dots, h_p[L_{ds}], 0, \dots, 0]_{N_p}, \quad (2.19)$$

where  $L_{ds}$  is the length of the delay spread. The time-domain channel impulse response estimate  $h_p[k]$  is then converted into an  $N$ -sample vector by appending zeros:

$$h_{pN} = [h_p[0], h_p[1], \dots, h_p[L_{ds}], 0, \dots, 0]_N, \quad (2.20)$$

where  $N$  is the FFT size of the OFDM system. Next, the DFT of the impulse response can be calculated to obtain the final interpolated channel estimate:

$$\hat{h}[k] = \sum_{n=0}^{N_p-1} h_{pN}[n] \cdot e^{-j\frac{2\pi kn}{N}}, \quad k = 0, 1, 2, \dots, N - 1, \quad (2.21)$$

where,  $N$  is the total number of sub-carriers in the system.

### 2.4.3 "Single tap" Equalization

When the OFDM waveform satisfies the two conditions mentioned at the beginning of this chapter, received symbols in the frequency-time resource do not interfere with each other, and consequently, "equalization" is not really needed. However, the observed samples on each resource still need to be rescaled by the channel gain before entering the demodulator. This procedure is often referred to as "single-tap" equalization.

In the Zero Forcing (ZF) method, the equalization filter is designed as the inverse of the estimated channel,  $\hat{h}$ , such that:

$$\hat{s}_{eq,ZF}[n] = \frac{\hat{s}[n]}{\hat{h}[n]} = \frac{\hat{h}^*[n]}{|\hat{h}[n]|^2} \hat{s}[n]. \quad (2.22)$$

This method simply cancels the channel effects but does not take into account the presence of noise in the channel estimate. In the more robust MMSE method, the equalization filter is designed to minimize the mean square error between the equalized signal and the transmitted signal. The equalized signal is given by:

$$\hat{s}_{eq,MMSE}[n] = \frac{\hat{h}^*[n]}{|\hat{h}[n]|^2 + \sigma^2} \cdot \hat{s}[n], \quad (2.23)$$

where  $\sigma^2$  is the noise variance.

### 2.4.4 Soft-Demodulator

In the reference receiver, the demodulator computes an estimation of the transmitted coded bits based on the channel-compensated samples  $\hat{s}_{eq}$ . The demodulator's output can be used for either hard decision or soft decision decoding.

In hard decision decoding, the channel-compensated samples  $\hat{s}_{eq}$  are quantized to the nearest point in the signal constellation, denoted as  $s_{ML}$ , and the corresponding binary label is delivered as an estimate of the transmitted coded bit. Specifically, the function  $b_i(s)$  returns the  $i$ -th bit of the binary label of  $s$ , and  $\hat{b}_{int}[i]$  denotes the estimate of the  $i$ -th bit based on the quantized sample  $s_{ML}$ . The quantization and

decoding process can be expressed mathematically as:

$$s_{ML} = \arg \min_{s \in \mathcal{S}} \|\hat{s}_{eq} - s\|^2 \quad (2.24)$$

$$\hat{b}_{int}[i] = b_i(s_{ML}); i \in [1, m], \quad (2.25)$$

where  $\mathcal{S}$  denotes the constellation set of possible symbols in the transmitted signal, and the  $\|\cdot\|^2$  notation represents the squared Euclidean distance between two points in the signal space. The goal is to find the symbol  $s$  in  $\mathcal{S}$  that is closest to the received sample  $\hat{s}_{eq}$ , in terms of Euclidean distance. Once the closest symbol  $s_{ML}$  has been identified, the corresponding bit labels can be obtained using the function  $b_i(s)$  for each bit position.

The soft demodulator computes the likelihood ratio for each bit of the transmitted signal, enabling soft decision decoding. The LLR output for the  $i$ -th bit can be computed mathematically as:

$$b_{int,soft}[i] = \max_{s \in \mathcal{S}: b_i(s)=1}^* \left( -\frac{\|\hat{s}_{eq} - s\|^2}{2\sigma^2} \right) - \max_{s \in \mathcal{S}: b_i(s)=0}^* \left( -\frac{\|\hat{s}_{eq} - s\|^2}{2\sigma^2} \right) \quad i \in [1, m] \quad (2.26)$$

where  $\mathcal{S}$  denotes the set of possible symbols in the transmitted signal,  $b_i(s)$  returns the  $i$ -th bit of the binary label of symbol  $s$ , and  $\sigma^2$  represents the noise variance. The  $\max^*$  operator is the logarithmic-sum-exp operator, which is used to compute the maximum value over a set of real numbers while avoiding numerical overflow or underflow issues.

It is important to note that while the LLR values are real numbers, in practical implementations, they are computed using fixed-point representation with a limited number of bits. This is done to reduce computational complexity and memory requirements.

### 2.4.5 Deinterleaver and decoder

The role of the de-interleaver is to apply the inverse permutation of the time axis introduced by the interleaving process. By doing so, it reduces the burstiness of the error sequence introduced by the channel and makes the following decoder more effective.

The purpose of a channel decoder is to make use of the redundancy introduced by channel coding in order to correct errors that may be present in the received data. To achieve this goal, the decoder takes as input the received data  $\hat{b}_{enc}$  and leverages the known code structure and an algorithm to identify and correct transmission errors that may have occurred during the transmission over a noisy channel. The output of this process is an estimated version of the original data.

In the context of LDPC decoding [38], the decoder uses soft decisions as soft information to perform iterative message-passing decoding. This process involves exchanging messages between variable nodes and check nodes in the code graph, where the messages convey the probability that each bit in the codeword is a 1 or a 0. These probabilities are determined based on the quality of the received signal and the messages received from neighboring nodes in the graph.

At each iteration of decoding, the soft information is used to update the messages exchanged between the nodes. The soft information can guide the decoding process by providing a measure of the reliability of each bit and can help resolve ambiguities in the received signal.

## 2.5 Limits of the classical receiver approach

As previously mentioned, the classical OFDM receiver performs optimally only when the transmitted waveform is such that the resources at the receiver are orthogonal and do not interfere with each other. This is achieved by setting a CP length that is larger than the delay spread, and at the same time making the symbol duration much shorter than the channel coherence time. However, this approach has the limitation that the OFDM parameters, such as the CP length and symbol duration, must be adaptive and matched to the channel scenario. This is the main motivation for introducing tunable numerologies in the 5G-NR standard.

Assuming a carrier frequency of 700 MHz, Mathematically, coherence time can be defined as:

$$T_c = \frac{1}{f_D} \quad (2.27)$$

where  $f_D$  is the maximum Doppler shift in Hz. By plugging in the values of Doppler shift of 2 Hz ( $v= 3$  km/h) and 104 Hz ( $v= 160$  km/h) into Equation 2.27, we can calculate the coherence times to be 500 ms and 8.77 ms, respectively. When using a

15 kHz carrier spacing and normal cyclic prefix length, the duration of an OFDM symbol in 5G-NR is approximately 71  $\mu$ s. This symbol duration is significantly shorter than the coherence time of the channel, indicating that multiple OFDM symbols will experience the same channel characteristics.

Mathematically, coherence bandwidth can be defined as:

$$B_c \approx (1/5) \cdot \tau_{rms} \quad (2.28)$$

where  $\tau_{rms}$  is the root mean square (RMS) delay spread of the channel. By substituting the values of RMS delay spread of 20, 40, 50, and 75  $\mu$ s into Equation 2.28, we can calculate the coherence bandwidths to be 10 kHz, 5 kHz, 4 kHz, and 2.67 kHz, respectively. The sub-carrier spacing of an 5G-NR OFDM system, which is 15 kHz at a minimum, different sub-carriers may experience distinct fading characteristics, leading to inter-carrier interference (ICI) and reduced system performance.

### 2.5.1 Minimum system overhead

We now see that under particularly challenging channel scenarios, such as those associated with SFN with mobility, the introduced overhead may be very large. We define the system overhead as the ratio between the CP length and the useful symbol duration:

$$OH = T_{cp}/T_u = T_{cp}\Delta f. \quad (2.29)$$

We can then consider the two channel-related constraints, where  $T_{cp}$  must be larger than  $\tau_{rms}$  and  $T_u$  must be smaller than the channel coherence time  $T_c \propto 1/f_D$ , and plug them into the equations:

$$T_{cp} = \tau_{rms}/k_1 \quad (2.30)$$

$$T_u = k_2/f_D \quad (2.31)$$

where both constants  $k_1$  and  $k_2$  must be positive and smaller than one. The overhead can be expressed as follows:

$$OH = \frac{\tau_{max}f_D}{k_1k_2} = \frac{\tau_{max}f_c|v|}{ck_1k_2}. \quad (2.32)$$

The equation above demonstrates that the system overhead grows as the product of the channel delay spread and user velocity, which is consistent with our expectations. To obtain the maximum delay spread, we can multiply the root mean square (RMS) delay spread by a factor of 5. As an example, we can consider four different scenarios for a signal frequency network, as summarized in Table 2.1. These scenarios correspond to various RMS delay spreads, ranging from 20 to 75  $\mu s$ , and are based on a carrier frequency of  $f_c = 700$  MHz.

To illustrate the impact of speed on overhead, Figure 2.7 shows how the minimum overhead varies with different speeds for a pair of reasonable values of  $k_1=0.1$  and  $k_2=0.1$  and different signal frequency networks. The results demonstrate that as the speed increases, the minimum overhead value eventually becomes impractically high.

At very low speeds, the minimum overhead is reasonable. However, as the speed increases, the overhead also increases rapidly. For instance, in a high-power high-tower scenario with a 175 km inter-site distance and a speed of 100 km/h, we need to allocate all our resources to the cyclic prefix. In contrast, in a scenario where the inter-site distance is smaller, say 15 km, we can allocate fewer resources, approximately 60% of the total, to the cyclic prefix. This is because the time dispersion due to multi-path propagation is less pronounced, and the delay spread is shorter. However, both of these results are impractical when it comes to assigning a cyclic prefix in an OFDM system.

## 2.6 Conclusion

In this chapter, we have provided an overview of the key characteristics of modern OFDM-based standards that support SFN broadcasting, with further details presented in chapter 3. We have discussed the reference symbol-by-symbol receiver, which is assumed in designing the TX waveform. This receiver has a simple structure and performs optimally when the TX waveform is properly matched to the channel constraints, so that both ISI and ICI are nullified at the receiver by design.

However, this approach may lead to unacceptable overhead in challenging scenarios such as SFN with a large delay spread and mobility with a large Doppler spread. Furthermore, it may not perform well when the channel conditions for a specific user



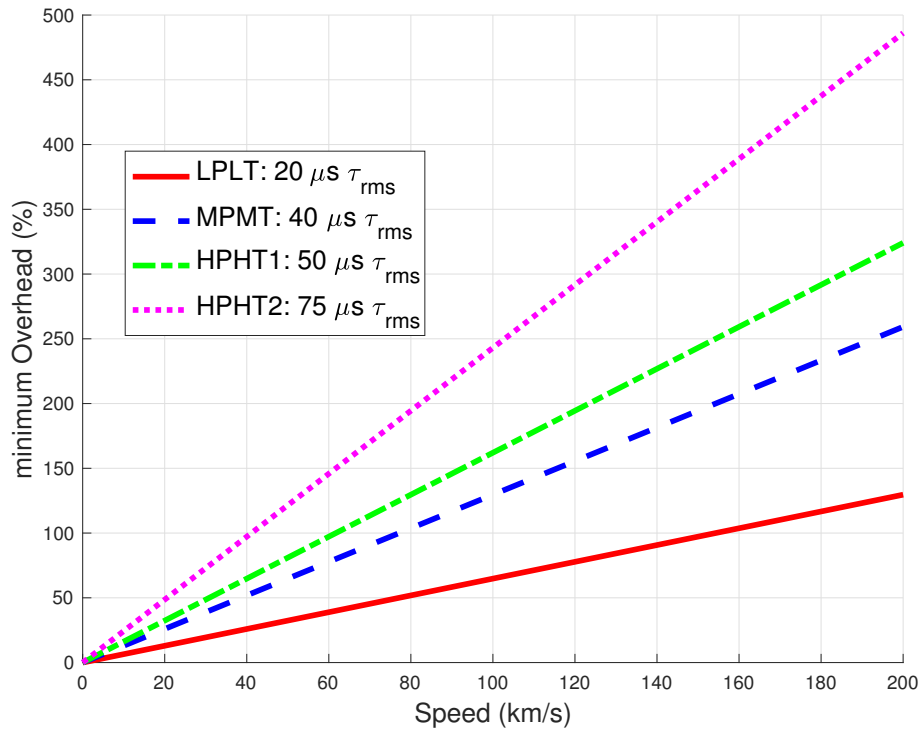


Fig. 2.7 The minimum overhead with  $k_1=0.1$  and  $k_2=0.1$

do not align with the TX waveform constraint. These two limitations, combined with the requirement of using SFN infrastructure with 5G-NR technology, necessitate the exploration of advanced receiver techniques for SFN that can eliminate the need for both ISI and ICI nullification at the receiver.

# Chapter 3

## Standards for SFN

This chapter presents a review of the physical layer of several well-established broadcasting standards, including DVB, ATSC, and MBMS. The essential topics covered in this review include FFT, cyclic prefix, channel coding, modulations, and interleaving. Understanding the similarities and differences between these standards is crucial in identifying their strengths and weaknesses. This knowledge can also be applied to propose solutions and optimizations for future broadcasting systems.

### 3.1 Digital Video broadcasting-Terrestrial

DVB-T [39] and DVB-T2 [6] are two important standards for digital terrestrial television broadcasting. DVB-T stands for Digital Video Broadcasting - Terrestrial, while DVB-T2 stands for Digital Video Broadcasting - Second Generation Terrestrial. DVB-T has been widely used since its introduction in the late 1990s for standard definition and high definition television services in many countries. It employs OFDM modulation with concatenated channel coding and interleaving to transmit compressed digital audio, video and other data in multiplexes. Additionally, DVB-T offers various transmission modes, modulation schemes, cyclic prefixes, and code rates to adapt to different channel conditions and network topologies.

DVB-T2, developed in the late 2000s, is an extension of DVB-T and offers significant benefits in terms of capacity, spectral efficiency, and robustness. DVB-T2 uses many new techniques not previously used in the DVB family of standards, such as physical layer pipes (PLPs), rotated constellations, extended interleaving, multiple

input single output (MISO) transmission, time-frequency slicing (TFS), and future extension frames (FEFs). It is the most up-to-date type of digital signal for terrestrial television and is increasingly being adopted in many countries around the world. DVB-T2 is designed to be backward compatible with DVB-T, which means that DVB-T2 receivers can receive and decode DVB-T transmissions. DVB-T2 also supports SFNs and multiple frequency networks (MFNs), as well as statistical multiplexing. It can carry standard definition, high definition, and ultra-high definition television services, as well as radio and data services.

Compared to DVB-T, DVB-T2 has higher spectral efficiency due to the use of more advanced modulation techniques such as higher-order modulation schemes. It also has significantly lower overhead and improved error-correction coding, allowing for up to nearly 50% increase in capacity for MFN operation and even higher for SFN operation. The extended range of Coded OFDM (COFDM) parameters in DVB-T2 allows for a significant increase in capacity compared to DVB-T, making it more efficient in terms of spectral efficiency and allowing for more data to be transmitted with the same amount of bandwidth.

DVB-T2 also uses more efficient Low-Density Parity-Check (LDPC) and Bose-Chaudhuri-Hocquenghem (BCH) codes for error correction, supports higher code rates, a higher-order 256QAM constellation for higher data throughput, more cyclic prefixes for more efficient use of bandwidth, a wider range of FFT sizes for more flexible use of bandwidth, a smaller percentage of scattered pilots for more efficient use of bandwidth, and a lower percentage of continual pilots for improved signal tracking. Additionally, DVB-T2 provides a higher maximum bandwidth for higher data throughput compared to DVB-T.

### **3.1.1 Input Processing and physical layer pipes**

The diagram in Figure 3.1 illustrates the main processing blocks of the DVB-T2 transmission chain. The DVB-T2 standard supports several input formats, including Transport Stream (TS), which is a stream with constant packet length similar to DVB-T. The standard also allows for the use of Generic Encapsulated Stream (GSE), which supports constant or variable length packets and is intended for broadcasting IP content without the use of TS-MPE (Multi-Protocol Encapsulation). Another format supported by DVB-T2 is the Generic Continuous Stream (GCS), which uses

variable length packets, and where the modulator does not know the actual length. Finally, the Generic Fixed-length Packetized Stream (GFPS) format is included for compatibility with DVB-S2. DVB-T2 introduces Physical Layer Pipes (PLPs) that allow for the configuration of various protection levels, including channel coding parameters, constellation orders, and interleaving depths. A single DVB-T2 signal can support one or more PLPs, enabling the system to be customized for different purposes. However, parameters related to the OFDM symbol configuration, such as FFT size and cyclic prefix, are common to all PLPs.

### 3.1.2 Coding, Interleaving, Modulation

The BICM process, as depicted in Figure 3.1, involves interleaving, coding, and modulation steps for each BBframe of a given PLP. This process begins by coding the input BBframes of a PLP using both an outer encoder (BCH) and an inner encoder (LDPC), following the BICM approach. The use of LDPC [40] is a standard feature of the DVB second-generation standard family (including DVB-S2, DVB-T2, and DVB-C2), and contributes to the increased robustness compared to other systems such as DVB-T. The outer BCH encoder aims to reduce the error floor of the LDPC. There are six defined code rates (CR) or protection levels available, ranging from more to less protected ( $1/2$ ,  $3/5$ ,  $2/3$ ,  $3/4$ ,  $4/5$ , and  $5/6$ ), and two sizes for the LDPC FEC frames (16K and 64K). Short FEC frames, although slightly less robust (by about 0.2 dB [41]), facilitate scheduling, especially for low data rates.

DVB-T2 provides improved encoding compared to the Convolutional and Reed Solomon codes utilized in DVB-T, which is why it introduces the higher-order constellation 256-QAM. This new constellation enhances both spectral efficiency and bit rate. The size of the BBframe, which serves as the input to the FEC frames, is determined by the FEC frame sizes and coding rate in this structure. The DVB-T2 Lite specific profile introduces new code rates of  $1/3$  and  $2/5$ , removes the existing ones of  $4/5$  and  $5/6$ , and only allows for short FEC frames.

After encoding, bit interleaving occurs for the FEC frames before they are mapped to constellations, except in cases where the QPSK constellation is used. In the DVB-T2 standard, the term "cell" refers to the constellation points.

DVB-T2 utilizes a technique called rotated constellations, also known as signal space diversity (SSD), to improve receiver performance in channels with severe

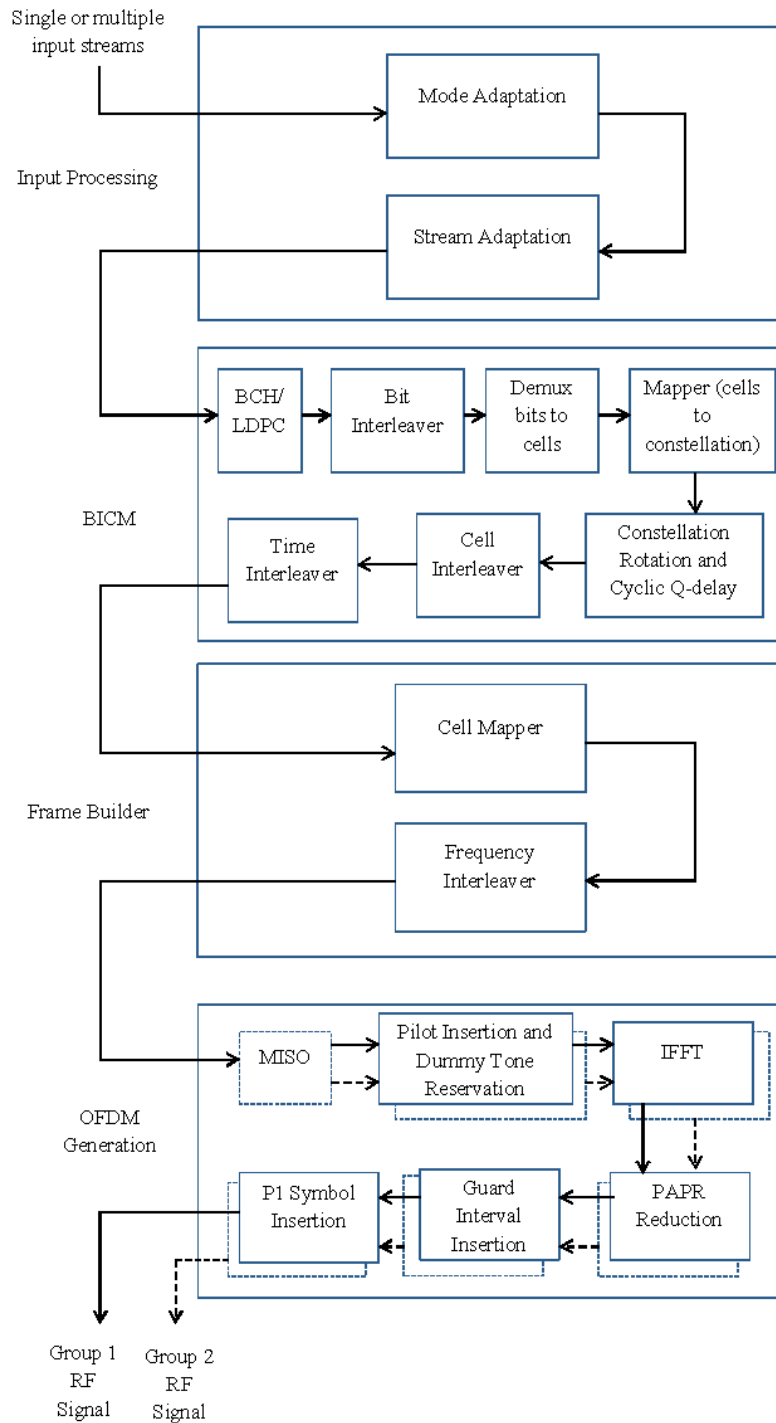


Fig. 3.1 The architecture of the DVB-T2 system.

fading. Rotated constellations introduce redundancy in the coded modulation's

information bits, resulting in additional diversity. In this technique, cells are rotated by a particular angle, which varies based on the constellation used.

The use of rotated constellations in DVB-T2 aims to enhance the receiver's performance, especially in scenarios where deep fading or erasures occur. Simulation results [42] suggest that this technique can provide a gain ranging from 0.2 dB to several dBs compared to conventional QAM constellations, depending on factors such as the constellation order, channel model, and CR. Although there is no capacity penalty associated with this technique, it does increase the complexity of the receiver, particularly for high order constellations.

After performing constellation mapping, the cells within each FEC block undergo a new interleaving process. This process uses a unique sequence for each FEC block, which makes up the time interleaving frame. The penultimate interleaving step is the time interleaving process, which combines cells from different FEC blocks to enhance robustness against low Doppler varying channels. However, it also increases the zapping time. Time interleaving is a compulsory step, and both transmitters and receivers must have sufficient memory, regardless of whether it is employed in the configuration.

Time interleaving is performed at the PLP level, allowing each PLP to have a distinct interleaving sequence and varying final interleaving time. For example, a PLP designed for HD services for rooftop antennas does not require lengthy interleaving times. However, a PLP intended for portable devices requires more protection, and its interleaving time should be extended as much as possible, considering the tradeoff with zapping time. The standard offers three different time interleaving options, depending on the relationship between FEC blocks, TI-blocks, interleaving frames, and T2-frames. The interleaving time depends on the length of the TI-blocks, but it can be increased by dividing TI blocks and assigning them to several consecutive or non-consecutive T2-frames.

### **3.1.3 Frame Builder**

The unit is responsible for assigning cells to data carriers and allocating signaling information within the structure of a T2 frame, which consists of a P1 symbol for synchronization and signaling, followed by P2 symbols and data symbols. PLPs are divided into three types and allocated in a certain order, with common PLPs carrying

shared information and Type 1 PLPs allowing receivers to save battery by only receiving certain slices. Type 2 PLPs are sent in a fixed sequence and spread along the data symbols, increasing time diversity but consuming more battery. Decoding L1 signaling is required to receive any PLP. T2 super-frames consist of FEFs and T2 frames, with FEFs being able to transmit any signal that DVB-T2 receivers can ignore. This system allows for flexibility and new developments.

### 3.1.4 OFDM generation

The final step in the DVB-T2 transmission process involves generating OFDM symbols, which offers a range of options for customization. There are six FFT sizes available (1K, 2K, 4K, 8K, 16K, and 32K), six channel bandwidths (ranging from 1.7 MHz to 10 MHz), and seven cyclic prefix fractions (ranging from 1/128 to 1/4). For FFT sizes of 8K, 16K, and 32K, an extended carrier mode is available, which allows for greater carrier use per symbol and increases data capacity. However, this mode may not be suitable for mobile reception due to limited tolerance for Doppler frequency.

Normal data symbols use pilot cells, data cells, and dummy cells, with scattered pilots used for channel estimation. Less dense pilot patterns result in lower overhead, while denser ones lead to more accurate channel estimation. A special pilot pattern (PP8) is available for use with the CD3 channel estimation algorithm [43], but it should not be combined with time interleaving or multiple PLPs.

To reduce the peak-to-average power ratio (PAPR), the DVB-T2 standard offers two methods: Active Constellation Extension (ACE) and Tone Reservation (TR). However, the use of these methods can result in a reduction in system capacity of approximately 1%.

The Active Constellation Extension (ACE) method is used to reduce the peak power in the OFDM signal by modifying the value of cells using the outermost points of the constellation. However, ACE cannot be used when rotated constellations are present. Unlike Tone Reservation (TR), the use of ACE does not result in a capacity penalty. Lower order constellations provide greater benefits with the ACE method, while higher order constellations provide greater benefits with the TR technique. It is essential to note that the configuration of the OFDM symbol selected will affect all PLPs. Therefore, if different types of services are to be broadcast, a trade-off

must be made to select a configuration that is suitable for all services. An alternative is to use both T2 and T2-Lite in the same RF channel using the FEF feature, which allows for almost completely different configurations.

### 3.1.5 Signaling

DVB-T2 employs two layers of signaling information, namely L1 and L2. L1 is concerned with the physical parameters of the signal and how the information is arranged, while L2 pertains to the data streams. L1 signaling is subdivided into L1-pre and L1-post, and it is transmitted using two special symbols called P1 and P2. The P1 symbol serves as a preamble and enables robust symbol detection and coarse time synchronization. On the other hand, the P2 symbol transmits the remaining L1 signaling and any leftover data. The modulation and coding of L1 in P2 symbols are different from the rest of the system, and this limits the time interleaving possibilities of the L1 signaling, which is considered a weakness for mobile reception. To increase the robustness of L1-post signaling, later versions of the DVB-T2 standard have introduced modifications.

### 3.1.6 Scattered pilot patterns

DVB-T2 offers more flexibility in allocating scattered pilots compared to DVB-T, with options for 1%, 2%, 4%, and 8% of the total cells (carriers). This added flexibility results in less overhead and increased data efficiency. There are 8 different pilot patterns (PP) in DVB-T2, which are used for specific combinations of DFT and cyclic prefix. PP1 provides the highest spectral efficiency but is the least robust, while PP8 provides the highest robustness but the lowest spectral efficiency. In general, the use of Pilot Patterns with a higher number (e.g., PP7, PP8) results in better robustness against fading and interference, while the use of Pilot Patterns with a lower number (e.g., PP1, PP2) results in higher spectral efficiency.

Figure 3.2 shows the PP3 pilot pattern in DVB-T2. It highlights the presence of edge pilots, scattered pilots, and data cells in the signal. Edge pilots are fixed and are used to aid in synchronization and channel estimation at the receiver.

Table 3.1 provides a comparison of different pilot patterns based on their density in time and frequency [6]. The separation of pilot-bearing carriers in time and



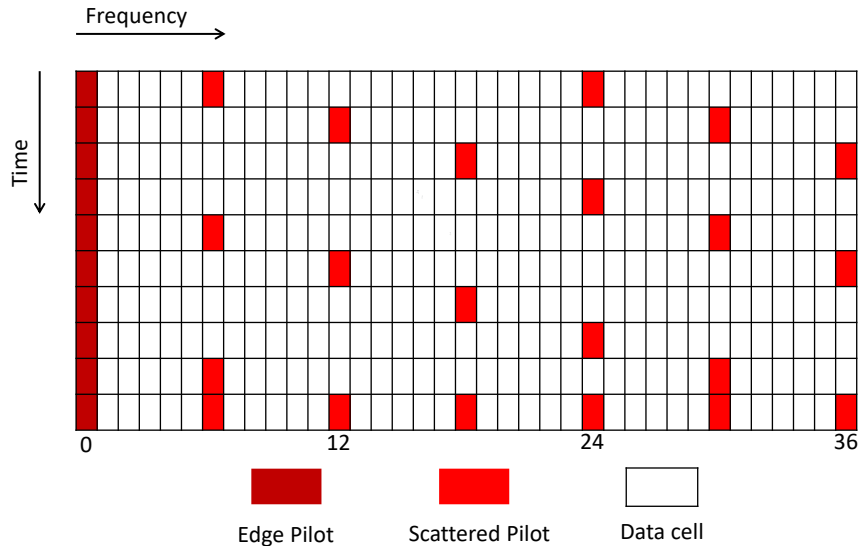


Fig. 3.2 PP3 Pilot Pattern in DVB-T2

frequency is represented by  $d_t$  and  $d_f$ , respectively. The overhead introduced by each pattern is shown in the  $1/d_t d_f$  column.

Table 3.1 Comparison of Scattered Pilot Patterns, results from [6]

Pilot Pattern	$d_f$	$d_t$	$1/d_t d_f$
PP1	3	4	8.33%
PP2	6	2	8.33%
PP3	6	4	4.17%
PP4	12	2	4.17%
PP5	12	4	2.08%
PP6	24	2	2.08%
PP7	24	4	1.04%
PP8	6	16	1.04%

Here are some recommended pilot patterns for typical scenarios [44]:

- **Rooftop Reception:** When using a directional outdoor antenna system on a rooftop, low Doppler environment is often experienced with few reflections. To maximize capacity, it is recommended to use pilot pattern PP7, which has low overhead but is less robust to Doppler.
- **Mobile Reception:** In a fast-changing mobile channel, more pilots are needed for better channel estimation. Temporal resolution is more critical than fre-

quency resolution, so pilot patterns PP2, then PP4, and then PP6 would be the options.

- **Portable Reception:** In a portable reception with slower-changing channel characteristics, fewer (reduced overhead) but stronger pilots are preferred, such as PP3 or PP4.
- **Large Area SFNs:** In networks where large area SFNs are required, a longer cyclic prefix, such as 1/8 or greater, would be necessary. In these cases, only pilot patterns 1, 2, or 3 are available. Pilot pattern 2 may provide the best balance between Doppler performance and cyclic prefix size.

### 3.1.7 Configuration Options

Table 3.2 provides a summary of the available configuration options in DVB-T2 to adjust the system to meet transmission and reception requirements. The DVB-T2 system's capacity is determined by various configuration parameters, and the achievable data rates can range from 3.90 Mbps to 50.32 Mbps for an 8 MHz channel (see Table 3.3), depending on the modulation and coding scheme used. However, certain combinations of FFT size, cyclic prefix, and pilot pattern are restricted. For digital radio transmission with a 1.7 MHz bandwidth, the minimum data rate that can be achieved is 765.77 kbps.

## 3.2 Advanced Television System Committee

The Advanced Television Systems Committee (ATSC) standards are a set of American standards for digital television transmission over terrestrial, cable, and satellite networks. They are mainly used in the United States, Mexico, Canada, and South Korea, and they replace the analog NTSC standard. The ATSC standards have three primary versions: V1.0, V2.0, and V3.0. V1.0 and V2.0 use a single carrier modulation called 8VSB (8-level vestigial side-band), which is patented and requires licensing for devices that use it. ATSC V1.0 supports only MPEG-2/H.262 video coding and Dolby AC3 audio, while ATSC V2.0 allows for MPEG-4/H.264 video coding and additional new features. ATSC V3.0 is the latest version of the standards,

Table 3.2 DVB-T2 physical layer parameters

Parameter	Value
Bandwidth (MHz)	1.7,5,6,7,8,10
FFT size	1k <sup>1</sup> , 2k, 4k, 8k, 16k, 32k <sup>1</sup>
cyclic prefix	1/128, 1/32, 1/16, 19/256, 1/8, 19/128, 1/4
Pilot patterns	PP1, PP2, PP3, PP4, PP5, PP6, PP7, PP8 <sup>1</sup>
Constellations	QPSK, 16-QAM, 64-QAM, 256-QAM
Rotation	Yes <sup>2</sup> /No
L1 modulation	BPSK, QPSK, 16-QAM, 64-QAM
FEC size	16k, 64k <sup>1</sup>
Code rate	1/3 <sup>3</sup> , 2/5 <sup>3</sup> , 1/2, 3/5, 2/3 <sup>2</sup> , 3/4 <sup>2</sup> , 4/5 <sup>1</sup> , 5/6 <sup>1</sup>
Input mode	A (Single PLP), B (Multiple PLP)
Input format	TS, GSE, GCS, GFPS

1-Not allowed in T2-lite mode

2-Not allowed for 256-QAM in T2-Lite

3-Only allowed in T2-Lite

Table 3.3 Capacity Example, results from [7]

Configuration	Data rate
1.7 MHz, 4k FFT, 1/8 CP, PP2 L1 BPSK, L1 repetition, QPSK 1/3	764.7 kbps
8 MHz, 4k FFT, 1/8 CP, PP2 L1 BPSK, L1 repetition, QPSK 1/3	3.90 Mbps
1.7 MHz, 4k FFT, 1/8 CP, PP2 L1 64-QAM, L1 repetition, 256-QAM 5/6	50.32 Mbps

which introduces a new physical layer protocol, a dedicated return channel, an interactive content framework, and enhanced security and service protection features. ATSC V3.0 also supports multiple video and audio codecs, such as HEVC, AC-4, and MPEG-H. ATSC can carry multiple channels of information on a single stream, and it can produce high-definition video formats up to 1920×1080 pixels in size.

The physical layer protocol of ATSC 3.0 provides broadcasters with a range of tools to choose the operating modes that best fit their needs and targeted devices. The protocol is built on OFDM modulation with a suite of LDPC FEC codes and offers a choice of 12 code rates and 3 basic modes of multiplexing. There are also 3 transmission modes of SISO, MISO, and MIMO, and signal protection is provided

by 12 selectable cyclic prefix lengths, 16 scattered pilot patterns, and 3 FFT sizes [45].

### 3.2.1 Input Formatting

ATSC 3.0 uses the Internet Protocol (IP) to deliver various types of data packets. One of the components of ATSC 3.0 is the ATSC Link-Layer Protocol (ALP), which is responsible for encapsulating different input data packets into ALP packets. The ALP packets are then scheduled by a system management function and assigned to physical layer resources. The baseband formatting block performs several operations on the ALP packets, such as constructing baseband packets, adding baseband packet headers, and scrambling the baseband packets. The baseband packet header consists of three parts: a common header, a type-dependent header, and an optional extension header. The baseband packet scrambler ensures proper constellation mapping by randomizing the baseband packet bits before forward error correction encoding. The baseband formatting block can also create multiple Physical Layer Pipes (PLPs) if needed, which are logical channels that can have different transmission parameters and error protection levels.

### 3.2.2 Coding, interleaving and modulation

FEC consists of an inner code and an optional outer code. The input to the FEC block is a baseband packet, and the output is a FEC frame, whose size depends on the LDPC code length. The inner code is an LDPC code with 12 available code rates ranging from  $2/15$  to  $13/15$ . There are two available code lengths, 16200 and 64800 bits, that are used to ensure proper reception of the transmitted baseband packets.

The outer code has three options: the Bose, Ray-Chaudhuri and Hocquenghem (BCH) code, the Cyclic Redundancy Check (CRC), and no outer code. The BCH code provides error detection and correction, which can correct up to 12 bit errors, while the CRC only provides error detection. The length of the parity data per FEC frame is 32 bits for CRC and 168 bits and 192 bits for BCH for 16200 and 64800 bits LDPC, respectively. If no outer code is used, no additional error correction or detection is provided.

The bit interleaver block includes a group-wise interleaver, a parity interleaver, and a block interleaver. It is optimized for channel efficiency performance for each LDPC code rate and constellation order. The modulation scheme used is based on six different modulation orders, including uniform QPSK modulation and five non-uniform constellation (NUC) sizes: 16-NUC, 64-NUC, 256-NUC, 1024-NUC, and 4096-NUC. The 16, 64, and 256 NUC constellations are 2-dimensional, while the 1024 and 4096 constellations are derived from non-uniform 1-dimensional PAM constellations for both in-phase (I) and quadrature (Q) components. Each combination of NUC modulation order and LDPC code rate has a different constellation, except for QPSK, where the same constellation is used for all code rates. However, the constellation does not vary with the LDPC code length.

### 3.2.3 Layered Division Multiplexing

Layered Division Multiplexing (LDM) is a technology that combines two independent data streams with different modulation and coding configurations in one RF channel, with the core layer being more robust than the enhanced layer. LDM offers Unequal Error Protection (UEP) and can provide simultaneous provision of mobile and fixed services in the same RF channel. Compared to traditional TDM or FDM, LDM can potentially offer performance gains. LDM offers 2.7 Mbps capacity for the core layer and 20.5 Mbps capacity for the enhanced layer, while TDM requires different capacity allocations to achieve similar performance levels. [8].

### 3.2.4 Interleaver and Framing

The module responsible for framing and interleaving consists of three components: time interleaving, framing, and frequency interleaving. The framing block outputs OFDM symbols arranged in physical layer frames, and the input to the time interleaving and framing blocks can include multiple PLPs.

When using a single PLP (S-PLP) with LDM or multiple PLPs (M-PLPs) with constant cell rate transmission, a convolutional interleaver (CI) is used to double the time interleaving depth. However, for M-PLPs with variable cell rate transmission, a hybrid interleaver is used, which comprises a cell interleaver, a block interleaver, and

a convolutional interleaver. The hybrid TI operates on a per PLP basis, and different parameters may be applied to each PLP.

The CI offers advantages over a sheer block interleaver, such as doubling the interleaving depth with the same memory size and reducing the average zapping time for the same interleaving depth by approximately 33%. However, these benefits only apply to inter-frame and inter-subframe interleaving when the CI is used.

The time interleaving (TI) module in this system has a memory size of  $2^{19}$  units, which is shared among PLPs in the same group for M-PLP. QPSK modulation allows for an extended interleaving mode that doubles the interleaving depth or service data rate using cell-to-memory-unit mapping and demapping blocks.

PLP multiplexing in ATSC 3.0 can be done using TDM, FDM, and LDM, with LDM offering benefits. A frame in ATSC 3.0 comprises a bootstrap, preamble, and one or more sub-frames, each with fixed FFT size, CP length, scattered pilot pattern, and NoC. Different sub-frames may have different parameters. Frequency interleaving is used on a per OFDM symbol basis throughout the channel bandwidth to separate burst errors, and is always used for preamble symbols but is selectable for sub-frame data symbols in L1 signaling.

### 3.2.5 Waveform generation

The Waveform Generation module in ATSC 3.0 comprises various blocks, including the pilot insertion, MISO pre-distortion, IFFT, optional peak-to-average-power reduction, and cyclic prefix insertion. The frame begins with the prefixed bootstrap signal, and scattered, continual, edge, preamble, and frame closing pilots are employed in ATSC 3.0. These pilots are modulated with reference information, and their transmitted value is known to the receiver. Pilots can be used for various purposes, such as frame synchronization, frequency synchronization, time synchronization, channel estimation, and transmission mode identification, and they can also track phase noise.

Table 3.4 illustrates the sixteen scattered pilot (SP) schemes defined by ATSC 3.0.  $SPa_b$  terminology is used, where  $a = d_f$  represents the separation of pilot bearing carriers in the frequency direction, and  $b = d_t$  denotes the number of symbols forming one scattered pilot sequence in the time direction. The overhead of these schemes varies from 0.78% to 16.6%.

Table 3.4 Scattered pilot and overhead in ATSC 3.0

Pilot Patter	$d_f$	$d_t$	overhead(%) $1/d_f d_t$
$SP_{3,2}$	3	2	16.6
$SP_{3,4}$	3	4	8.33
$SP_{4,2}$	4	2	12.5
$SP_{4,4}$	4	4	6.25
$SP_{6,2}$	6	2	8.33
$SP_{6,4}$	6	4	4.16
$SP_{8,2}$	8	2	6.25
$SP_{8,4}$	8	4	3.12
$SP_{12,2}$	12	2	4.16
$SP_{12,4}$	12	4	2.08
$SP_{16,2}$	16	2	3.12
$SP_{16,4}$	16	4	1.56
$SP_{24,2}$	24	2	2.08
$SP_{24,4}$	24	4	1.04
$SP_{32,2}$	32	2	1.56
$SP_{32,4}$	32	4	0.78

### Multiple-Input Single Output

ATSC 3.0 uses a Transmit Diversity Code Filter Set (TDCFS) technique to minimize destructive interference caused by multiple multi-path echoes received outside the configured cyclic prefix (CP) duration. TDCFS artificially decorrelates signals from multiple transmitters in a SFN by implementing linear frequency domain filters before the IFFT, which allows for compensation in the receiver as part of the equalizer process. The filter design is based on creating all-pass filters with minimized cross-correlation over all filter pairs under the constraints of the number of transmitters and the time domain span of the filters. The effective cyclic prefix length is decreased by the filter time domain span, which should be taken into consideration when choosing a filter set for a particular network topology. TDCFS does not require doubling the pilot density, unlike the Alamouti-based MISO scheme of DVB-T2.

### IFFT

ATSC 3.0 defines different FFT sizes and bandwidths to support various capacity needs and RF environment changes. The system's bandwidth and elementary period

are determined by the bootstrap, which sets the maximum capacity for each FFT size and bandwidth. The bandwidths of 6, 7, and 8 MHz have corresponding elementary periods of  $7/48 \mu\text{s}$ ,  $1/8 \mu\text{s}$ , and  $7/64 \mu\text{s}$ , respectively. To adjust to different RF environment conditions and masks, ATSC 3.0 provides an adjustable NoC. Each FFT size has five NoC values to choose from, separated by equal steps. A reduction coefficient is used to signal the chosen NoC value in L1, based on the maximum NoC value. This ensures maximum capacity is supported under various masks and RF environment changes.

### **Peak-to-Average Power Ratio (PAPR)**

ATSC 3.0 has two PAPR reduction methods: Tone Reservation (TR) and Active Constellation Extension (ACE). TR involves using certain OFDM carriers to insert cells that aim to reduce overall PAPR of the output waveform, while ACE decreases PAPR by altering the transmitted constellation points. The ACE algorithm should not be used with pilot carriers or reserved tones and is not compatible with LDM, MISO, and MIMO. When using ACE, the constellation dimension and the LDPC code rate must also be taken into account. TR cells contain no payload data or signaling information and make up approximately 1% of symbol carriers.

### **Cyclic prefix**

According to Table 3.5, ATSC 3.0 provides a wide range of twelve options for cyclic prefixes with varying durations expressed in both samples and microseconds for different FFT sizes. The available cyclic prefixes are dependent on the FFT size, which is indicated by an '✓' in the respective columns of the table. For a bandwidth of 6 MHz, the cyclic prefix ranges from  $28 \mu\text{s}$  to over  $700 \mu\text{s}$ , with the maximum naturally occurring echo (non-SFN) being around  $104 \mu\text{s}$ . Despite this, broadcasters may opt to select any FFT size beyond this range to safeguard their signals in challenging terrains with many hills and SFN networks.

ATSC 3.0 also offers a time-aligned mode that allows for the insertion of additional samples to make the frame length a multiple of ms, which are distributed to the CPs of the non-preamble OFDM symbols within the frame. In addition, a conventional symbol-aligned mode is also available.



Table 3.5 Cyclic prefix in ATSC 3.0

CP	6 MHz	$d_t$	FFT			#Samples
			8k	16k	32k	
#1	22.78 $\mu$ s	4	✓	✓	✓	192
#2	55.56 $\mu$ s	4	✓	✓	✓	384
#3	74.07 $\mu$ s	3	✓	✓	✓	512
#4	111.11 $\mu$ s	4	✓	✓	✓	768
#5	148.15 $\mu$ s	3	✓	✓	✓	1024
#6	222.22 $\mu$ s	4	✓	✓	✓	1536
#7	296.30 $\mu$ s	3	✓	✓	✓	2048
#8	351.85 $\mu$ s	3	-	✓	✓	2432
#9	444.4 $\mu$ s	4	-	✓	✓	3072
#10	527.78 $\mu$ s	4	-	✓	✓	3648
#11	592.59 $\mu$ s	3	-	✓	✓	4096
#12	703.70 $\mu$ s	3	-	-	✓	4864

### 3.2.6 Bootstrap

The bootstrap in ATSC 3.0 provides a priori information about incoming signals to digital communication receiver devices. It consists of a series of OFDM symbols that are highly robust and can be received even in difficult channel conditions. The bootstrap contains basic information that must be received by all devices and is made up of four symbols. The first symbol is used for synchronization, while the following symbols carry additional information. The first signaled information is the version of the ATSC 3.0 standard, and subsequent symbols carry information about emergency alerts, system bandwidth options, time to the next frame, sampling rate indications, and preamble structure. The bootstrap symbols have a sampling frequency of 6.144 Msymbols/s and an effective bandwidth of 4.5 MHz, and their total length is 2 ms [8].

### 3.2.7 Preamble

The preamble in ATSC 3.0 occurs once per frame, after the bootstrap and before the payload, and is used to convey the L1 signaling necessary to access the payload. The signaling information is divided into L1-Basic and L1-Detail, with L1-Basic carrying a fixed number of signaling bits, and L1-Detail carrying more bits that vary

between 400 and 6312. The signaling components are encoded by LDPC codes that are mapped to constellations ranging from QPSK to 256-NUC, with seven modes available for each component. To mitigate fading and burst errors, a zig-zag interleaver is applied to OFDM data cells corresponding to L1-Detail, and frequency interleaving is applied to all preamble OFDM symbols. The waveform parameters of the preamble OFDM symbols have seventeen available modes for CP/FFT/SP, with denser pilots for robust and speedy channel estimation.

### **3.2.8 Channel bonding and MIMO**

One of the features of the ATSC 3.0 standard is the ability to bond two RF channels together to transmit data from a single Physical Layer Pipe (PLP), enabling data rates beyond the capacity of a single RF channel. The channel bonding feature can also take advantage of frequency diversity between the two RF channels. At the receiver end, the output stream of the channel bonding process is identical to the input stream on the transmitter side. This is achieved by passing all PLP data packets through a common input formatting block where baseband headers are inserted. To ensure proper packet reordering at the receiver side, a baseband header extension counter is used, even in the presence of varying delays on each RF channel. There are two operation modes for channel bonding: plain channel bonding and SNR averaging. In plain channel bonding, the two transmitter chains operate without any interaction after joint input formatting and stream partitioning. In SNR averaging, every second cell of every Binary Phase Shift Keying (BPSK) with Incremental Redundancy (BICM) encoder is sent to the other transmitter signal to provide SNR averaging across the two RF channels. Channel bonding is not compatible with MIMO, but other features such as LDM, MISO, and PAPR are. The MIMO antenna system in ATSC 3.0 is based on a 2x2 antenna system, requiring two antenna aerials at both the transmitter and receiver sides. The MIMO transmission chain reuses many blocks from SISO, such as FEC codes, bit interleavers, time interleavers, frequency interleavers, and constellations. The MIMO precoder is based on Spatial Multiplexing and has three steps: stream combining, IQ polarization interleaving, and phase hopping.

### 3.2.9 DVB-T2 and ATSC 3.0 in a 6 MHz Channel

The technical parameters of two digital broadcasting systems, DVB-T2 and ATSC 3.0, in a 6 MHz channel are compared in a Table 3.6. The table highlights some key differences between the two systems [8]. The differences include the outer code used, with DVB-T2 utilizing BCH outer code and ATSC 3.0 using a combination of BCH, CRC, and none. Additionally, both systems support various LDPC code rates, but DVB-T2 supports a more limited range compared to ATSC 3.0. DVB-T2 employs a uniform constellation for modulation schemes like 16-QAM, whereas ATSC 3.0 utilizes non-uniform constellations for some of its modulation schemes. DVB-T2 optionally uses a rotated constellation, while ATSC 3.0 does not. Both systems use time interleaving, but the type of interleaving employed by ATSC 3.0 differs from DVB-T2. The maximum frame size of ATSC 3.0 is much larger compared to DVB-T2. Moreover, the pilot patterns used by the two systems differ in terms of the number of patterns and overhead. DVB-T2 supports a wider range of FFT sizes compared to ATSC 3.0. ATSC 3.0 supports more CP options compared to DVB-T2, and also allows multiple PLPs per service, while DVB-T2 does not. Finally, the data rate supported by ATSC 3.0 is wider compared to DVB-T2.

## 3.3 Multimedia Broadcast Multi-cast System

Multimedia Broadcast Multi-cast Service (MBMS) is a point-to-multi-point interface specification for existing and upcoming 3GPP cellular networks, which is designed to provide efficient delivery of broadcast and multi-cast services, both within a cell as well as within the core network [46]. Cellular communication was initially designed for point-to-point data transmission, but with the introduction of MBMS in 3GPP release 8, it became possible to broadcast data to multiple devices simultaneously. In 2014, 3GPP release 9 defined MBSFN (Multimedia Broadcast SFN), enabling a CP of up to  $16.7 \mu\text{s}$  (5km), which limits the establishment of larger Single-Frequency Networks.

Table 3.6 Comparing ATSC 3.0 and DVB-T2 in a 6 MHz Channel, results from [8]

Parameters	DVB-T2	ATSC 3.0
Outer code	BCH	BCH, CRC, none
LDPC code rate	1/2,3/5,2/3,3/4,4/5,5/6	[2, 3, 4, 5, 6, 7, 8, 9, 10, 11, 12, 13]/15
Modulation	QPSK, 16-QAM, 64-QAM, 256-QAM	QPSK, 2D-16-NUC, 2D-64-NUC, 2D-256-NUC, 1D-1024-NUC, 1D-4098-NUC
Rotated constellation	Yes(Optional)	No
Time interleaver	Block interleaver	CI(S-PLP) Hybrid BI+CI(M-PLP)
TI size (cells)	$2^{19} + 2^{15}$	$2^{19}$ , QPSK( $2^{20}$ )
Maximum frame size	250 ms	5 s
Pilot Patterns	PP1-PP8 (x8) 1.04%-8.33% overhead	$SP_{32}$ - $SP_{32}$ (x16) 0.78%-16.6% overhead
FFT size	1k, 2k, 4k, 8k, 16k, 32k	8k, 16k, 32k
CP ratio	1/128, 1/32, 1/16, 19/256,	3/512, 3/256, 1/64, 3/128, 1/32, 3/64, 1/16, 19/256, 3/32, 57/512, 3/16, 1/8, 19/128, 1/4 (symbol and time-aligned frame)
Multiple PLPs per service	(No 1 common PLP)	Yes (up to 4)
Min-Max Data Rate 6 MHz	5.6 Mbps, 38 Mbps	1 Mbps, 57 Mbps

### 3.3.1 eMBMS-enhancement

To improve the transmission performance of MBMS, in Release 14, 3GPP approved the enhancement of eMBMS (enhancement of eMBMS) [47]. This involved extending the SFN cyclic prefix length to  $200\mu\text{s}$ , which allowed for a wider SFN range. The enhancement of eMBMS also introduced a cell acquisition subframe (CAS) with a larger interval to reduce synchronization overhead and increase broadcast service capacity. A new sub-frame was designed with almost 100% eMBMS carrier allocation and no unicast control region. Table 3.7 summarizes the frame structure

Table 3.7 Numerologies in release 14 (enhancement of eMBMS)

CP mode	$\Delta f$	Sym. per SF	SCSs pre RB	$T_{CP}$ ( $\mu s$ )	$T_u$	ISD
Extended	15	12	12	16.7	66,7	5
	7.5	6	24	33.3	133.3	10
	1.25	1	144	200	800	60

parameters for enhancement of eMBMS sub-frames with different carrier spacing  $\Delta f$  values, as specified in Rel-14.

The maximum supported inter site distances (ISDs) for the two short CPs are 5 km and 10 km, which are only applicable in low-power-low-tower (LPLT) scenario. The use of new CP extends the ISD up to 60 km which can be used in high-power-high-tower (HPHT) deployments. The structure of enhancement of eMBMS frames is influenced by the selected OFDM parameters, and the enhancement of eMBMS modes have a set of reference signal patterns.

### 3.3.2 LTE-based 5G Terrestrial Broadcast

In Release 14, the frame structure and Cell Acquisition Sub-frames (CAS) structure are not sufficient for meeting the the requirements for broadcasting with of 5G Radio Access Technology, particularly for serving high-mobility users and covering large geographic areas. Release 16 introduces two new CP lengths,  $100\mu s$  and  $300\mu s$ , for car-mounted and rooftop reception, respectively, to provide wider coverage and stronger robustness in high-mobility scenarios [48, 4]. The newly investigated CP length of  $100\mu s$  can support transmission with a maximum speed of 250km/h in car-mounted reception of LPLT scenario. Numerology with CP duration of  $300\mu s$  is adopted by medium power medium tower (MPMT) and HPHT scenarios to support 100 km coverage for rooftop reception. The frame structures corresponding to the new numerologies are presented in Table 3.8. In Release 16, significant extensions were made to the expected ISDs for rooftop and car-mounted receptions in all scenarios.

As a result of the increased CP length, the legacy sub-frame duration has now been extended to 3ms ( $\Delta f=0.37$  kHz). The carrier that is solely dedicated to multimedia broadcast and multi-cast services (MBMS), the common control signaling (CAS) is transmitted every 40ms, while the MBMS single-frequency network (MBSFN)

Table 3.8 New numerologies in release 16

CP mode	$\Delta f$	Sym. per SF	SCSs pre RB	$T_{cp}$ ( $\mu s$ )	$T_u$	ISD
Extended	2.5	2	72	100	400	30
	0.37	1	486	300	2700	100

sub-frames take up the remaining 39ms. Hence, the CAS is broadcasted ahead of 13 MBSFN sub-frames.

### The performance of LTE-based 5G Terrestrial Broadcast

The performance of new numerologies and CAS enhancement schemes are evaluated using system-level simulations (SLSs) and link-level simulations (LLSs) [9]. Figure 3.3 shows that a simulation platform is built to conduct SLSs and LLSs for different scenarios. The SLS process involves generating the network topology, UE

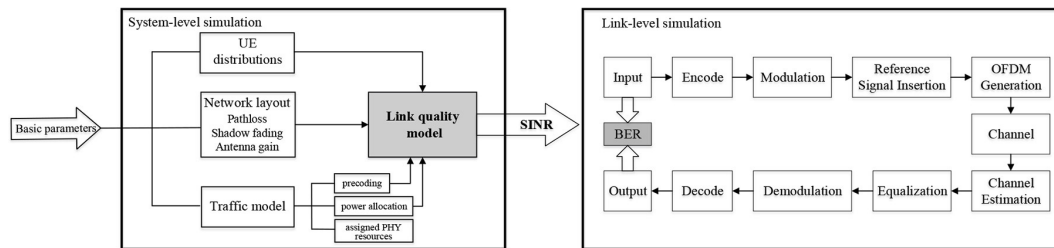


Fig. 3.3 LTE based 5G broadcasting simulation platform

distributions, and channel coefficients, as well as calculating the SINR and CDF of each UE. The SINR threshold given by SLS determines the TBS and MCS for LLS [9]. LLS involves encoding and modulation, reference signal insertion and OFDM generation, channel estimation and equalization, demodulation and decoding, and calculating the BER.

The simulation parameters and assumptions used in [9] are detailed in Table 3.9. The channel model selected is TDL-B, with a Delay Spread of  $20\mu s$ ,  $35\mu s$ , and  $45\mu s$  for LPLT, MPMT, and HPHT-1, respectively. For channel estimation, the UE performs independent one-dimensional linear interpolation in the time and frequency domains, following the recommendation in [49].

For car-mounted reception, the appropriate combination of  $d_t$  and  $d_f$  for the design of RS pattern depends on RS overhead and system performance. From LLS

Table 3.9 Parameters for link-level simulation

Parameter	Value
System Bandwidth	10 Mhz
Carrier Frequency	700 Mhz
Sub-carrier Spacing	2.5 kHz/0.37 kHz
Channel model	TDL-B
Delay Spread	LPLT: $20\mu s$
	MPMT: $35\mu s$
	HPHT-1: $45\mu s$
N. of RX antennas at the UE	2
Turbo Decoding algorithm	Max-Log-MAP/8 iterations

results, the RS pattern with  $d_f = 2$  and  $d_t = 2$  provides the best BER performance. Table 3.10 gives the 95%-tile SINR thresholds and spectral efficiencies in terms of different RS patterns in LPLT scenario, and it can be seen that  $d_f = 2$  has a larger spectral efficiency compared with  $d_f = 3$ . Thus, the RS pattern of  $d_f = 2$  and  $d_t = 2$  is specified for the new numerology of  $T_{cp} = 100 \mu s/T_u = 400 \mu s$  to support mobility of up to 250km/h in Rel-16.

Table 3.10 Spectral Efficiency of Different RS Tone Combinations for LPLT scenario, results from [9]

$d_f, d_t$	Overhead	95%tile SINR (dB)	SE @ 150/250 km/h (bps/Hz)
2,2	25%	9	1.11/0.97
2,4	12,5%	9	0.97/0.78
3,2	16,7%	7.6	0.96/0.85
3,4	8.3%	7.6	0.85/0.68
4,2	12,5%	6.9	0.85/0.85
4,4	6,25%	6.9	0.78/0.68

For MPMT and HPHT-1 scenarios, staggered RS pattern proposed by Qualcomm [50] and rhombic RS patterns proposed by Huawei [51] and Shanghai Jiao Tong University [30] are introduced and analyzed to support larger coverage in rooftop reception. The staggered RS pattern with  $d_f = 3$  and  $d_t = 4$  [52], where the RSs from 4 consecutive symbols are coalesced together, and the rhombic RS pattern with  $d_f = 3$  and  $d_t = 4$  are shown in Figure 3.4.

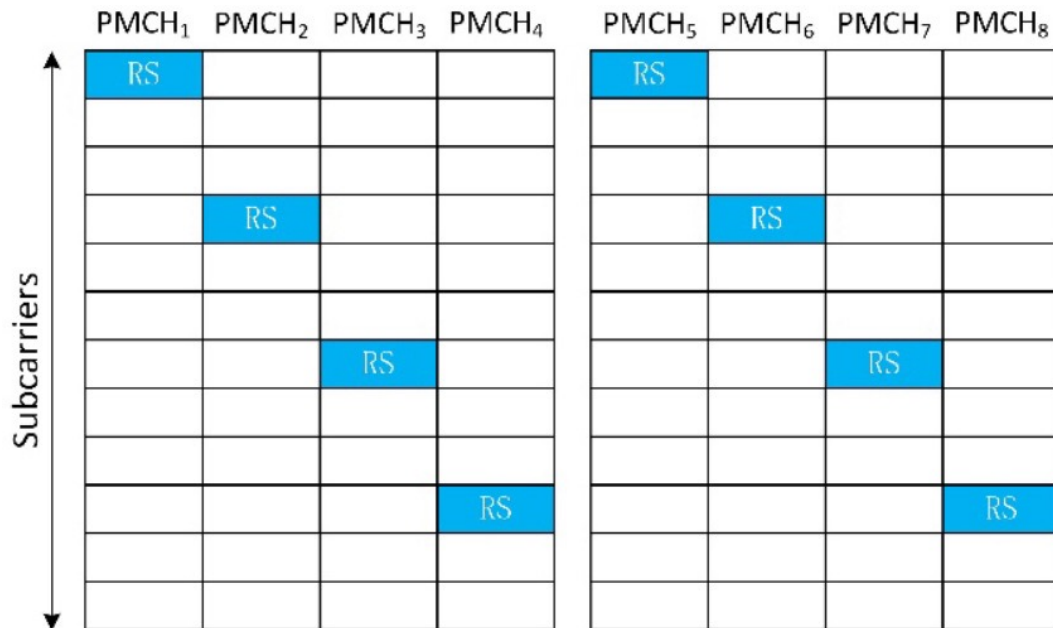


Fig. 3.4 Staggered RS pattern with  $d_f=3$  and  $d_t=4$ .

Table 3.11 RS Tone Separation and Spectral Efficiency for Different Combinations- Rooftop Reception, results from [9]

Network Topology	Pattern	$d_f, d_t$	95%-tile SINR (dB)	SE (bps/Hz)
HPHT-1	Rhombic	3,2	10.9	1.65
HPHT-1	Staggered	3,4	9.4	1.52
MPMT	Rhombic	3,2	18.4	2.75
MPMT	Staggered	3,4	14.9	2.47

Table 3.11 presents a summary of the 95%-tile SINR thresholds and spectral efficiency values for rooftop reception using the rhombic RS pattern and the staggered RS pattern.

The table shows that the rhombic RS pattern with  $d_t = 2$  outperforms the staggered RS pattern in terms of spectral efficiency for both HPHT-1 and MPMT rooftop scenarios. Moreover, simulations conducted in [50] demonstrate that for large transport block size (TBS) values of 71112 bits, the staggered RS pattern with  $d_t = 4$  outperforms those with  $d_t = 1/2/3$ . However, for small TBS values of 45352, the performance difference between the staggered RS pattern with different  $d_t$  values is negligible. Hence, both the staggered RS pattern with  $d_f = 3$  and  $d_t = 4$  and rhombic



RS pattern with  $d_f = 3$  and  $d_t = 2$  are supported in the case of rooftop reception, given a  $T_{CP}$  value of  $100\mu s/T_u = 400\mu s$ .

The PMCH (Physical Multi-cast Channel) throughput for 5G LTE-based terrestrial broadcast was evaluated in a link-level simulation study by [10]. The study considered the PMCH channel with a 10 MHz channel bandwidth and Modulation and Coding Scheme settings were based on [4], and the results were obtained with a Transport Block Error Rate (BLER) of 0.1%.

Table 3.12 shows the PMCH throughput for 5G Broadcast using a 2.5 kHz sub-carrier spacing, 100  $\mu s$  CP duration, and TDL-A channel model (mobile/handheld) with 20  $\mu s$  Delay Spread, and two-antenna receivers. The table displays the values of  $Q_m$ , Code Rate, and Min SNR for each modulation scheme, which represent the modulation order, effective code-rate, and required minimum SNR (in dB) to achieve a Transport Block Error Rate (BLER) of 0.1%. Non-decodable results are indicated by "–".

Table 3.13 presents the results for 5G Broadcast PMCH throughput for a 10 MHz channel bandwidth and 0.37 kHz sub-carrier spacing. The results were obtained using the TDL-E channel model for roof-top reception with a maximum Doppler shift of 1 Hz (1.5 km/h), a delay spread of 45  $\mu s$ , and a single receiver antenna. Non-decodable values are also denoted by "–".

To enable comparison, we also include the results obtained using the TDL-A channel model, which represents mobile/handheld reception conditions using two receiver antennas. In the TDL-A model, the maximum Doppler shift is 2 Hz (3 km/h) with a delay spread of 50  $\mu s$ . Non-decodable values are denoted by "–".

### 3.4 Comparison of different standard

DVB-T2, ATSC 3.0, and LTE-Advanced Pro enhancement of eMBMS are technologies that enable digital broadcasting of audio, video, and data services, with differences in features, capabilities, and areas of application.

DVB-T2 provides higher spectral efficiency than its predecessor, DVB-T, allowing for more TV channels and higher-quality video services. It supports HEVC for Ultra High Definition (UHD) content delivery and DRM for content protection. ATSC 3.0 uses OFDM modulation and provides new features, such as UHD video,

Table 3.12 5G Broadcast PMCH Capacity with 2.5 kHz Sub-carrier Spacing, results from [10]

MCS	Qm	CR	Thr. (Mbps)	SNR 3 km/h	SNR 160 km/h
4	2	0.34	3.5	3.6	3.8
5	2	0.41	4.3	4.6	4.6
6	2	0.48	5.0	5.6	5.8
7	2	0.58	6.0	7.0	7.2
8	2	0.65	6.8	7.8	8.2
9	2	0.75	7.8	9.2	9.6
10	4	0.37	7.8	8.2	8.6
11	4	0.41	8.5	9.0	9.4
12	4	0.46	9.7	10.0	10.4
13	4	0.53	11.2	11.2	11.4
14	4	0.60	12.6	12.4	12.8
15	4	0.66	13.8	13.2	13.8
16	4	0.71	14.9	14.2	14.8
17	6	0.47	14.9	14.4	15.0
18	6	0.51	16.0	15.0	15.6
19	6	0.57	17.9	16.4	17.0
20	6	0.62	19.4	17.4	18.6
21	6	0.66	20.8	18.4	19.8
22	6	0.71	22.3	19.6	21.2
23	6	0.79	24.8	21.6	25.0
24	6	0.85	26.7	26.4	-
25	6	0.88	27.6	28.0	-
26	6	0.95	29.8	-	-
27	6	0.98	30.9	-	-

immersive audio, and interactive services. It supports IP-based content delivery for greater flexibility and interactivity in multimedia service delivery. enhancement of eMBMS enables the broadcast/multicast delivery of multimedia content over LTE networks, complementing uni-cast delivery by efficiently distributing popular multimedia content to multiple users. enhancement of eMBMS is designed for LTE networks and is used for efficient distribution of multimedia content to multiple users simultaneously.

DVB and ATSC are widely used broadcasting standards that use CP-OFDM, with DVB used mainly in Europe, Asia, and Africa, while ATSC is used primarily in

Table 3.13 5G Broadcast PMCH Capacity with 0.370 kHz Subcarrier Spacing, results from [10]

MCS	Qm	CR	Thr. (Mbps)	SNR 1.5 km/h	SNR 3 km/h
4	2	0.34	5.0	3.6	4
7	2	0.41	6.0	4.6	4.8
8	2	0.47	6.7	5.2	5.6
9	2	0.53	7.7	6	6.4
10	2	0.60	8.6	6.8	7.2
13	4	0.38	11.1	8.6	8.8
14	4	0.44	12.8	9.8	9.8
15	4	0.48	13.8	10.2	10.6
16	4	0.51	14.7	10.8	11
17	4	0.55	15.9	11.6	11.8
18	4	0.62	17.9	12.8	13
19	4	0.67	19.3	13.6	13.6
20	4	0.72	20.7	14.6	14.8
21	6	0.48	20.7	15	14.8
22	6	0.52	22.4	15.8	15.6
23	6	0.57	24.8	17.2	16.8
24	6	0.61	26.4	18.2	17.8
25	6	0.64	27.5	19	18.2
26	6	0.68	29.5	20.6	19.4
27	6	0.70	30.5	21.4	19.8

North America. These standards provide high-quality digital video and audio with efficient use of the available spectrum.

MBMS is another broadcasting technology that uses CP-OFDM but has not been widely adopted due to challenges with limited availability of spectrum and lack of widespread adoption. MBMS is designed to deliver multimedia content to mobile devices using a broadcast network. The latest release of this technology is MBMS Rel-17, which is LTE-based 5G Broadcast.

Table 3.14 Comparison of Physical Layer Specifications for DVB-T2, ATSC 3.0, and enhancement of eMBMS

Parameters	DVB-T2	ATSC 3.0	enhancement of eMBMS
Bandwidth (MHz)	1.7, 5, 6, 7, 8, 10	6, 7, 8	1.4, 3, 5, 10, 20
Code rate	1/2, 3/5, 2/3, 3/4, 4/5, 5/6	2/15, ..., 13/15	1/3
FEC	BCH, LDPC	BCH, CRC, none, LDPC,	CRC, Turbo code
MISO	2 × 1 with Alamouti	TDCFS	not defined
FEC frame (bit)	16200, 64800	16200, 64800	6144
Transmission frame duration (ms)	250	5000	10
Modulator	QPSK, 16QAM, 64QAM, 256QAM	QPSK, 2D-16NUC, 2D-64NUC, 2D-256NUC, 1D-1024NUC, 1D-4096NUC	QPSK, 16QAM, 64-QAM, 256-QAM
FFT	1k, 2k, 4k, 8k, 16k, 32k	8k, 16k, 32k	128, 256, 512, 1024, 2048
Carrier spacing (Hz)	279-8929	281,5-1125	1250, 7500, 15000
Symbol Period ( $\mu$ s)	119-4116	909-4084	71-1000
Cyclic prefix( $\mu$ s)	7-532	20.833-527.778	4-200
Pilot Patterns Overhead	(1.04%-8.33%)	(0.78%-16.6%)	(12.5%, 20%)
maximum ISD (km)	160	159	60
Max. Time Interleaving memory	$2^{19} + 2^{15}, 2^{19}$	$2^{20}, 2^{18}$	-
Net Data Rate (Mbit/s)	5.35-50.4 (8 MHz)	1.24-77.2 (8 MHz)	3.5-30.9 ( 10 MHz)

# Chapter 4

## 5G New Radio

The physical layer of 5G-NR (New Radio) handles wireless transmission and reception of data over the air interface. This includes modulation, coding, and frequency assignments necessary for signals between user equipment (UE) and the base station, also known as the gNodeB (gNB).

While the physical layer in Release 15 of 5G-NR primarily focused on uni-cast communication, multi-cast and broadcast modes were needed to facilitate group communication and content delivery. To enable this, two approaches were considered: designing a mixed uni-cast/multi-cast/broadcast mode for 5G-NR, or creating a dedicated Terrestrial Broadcast (TB) mode based on LTE technology, which was discussed in a previous chapter.

The mixed mode approach requires modifying the existing 5G-NR physical layer to support multi-cast/broadcast transmission, including new modulation schemes, coding techniques, and resource allocation schemes.

This chapter examines the physical layer and frame structure of 5G-NR, including its limitations for SFN terrestrial broadcasting. It also explores potential solutions for broadcasting with 5G-NR.

### 4.1 Frame structure

The physical channels for both the down-link and up-link in NR are organized into frames, each lasting 10 ms. Each frame is then subdivided into 10 sub-frames, each

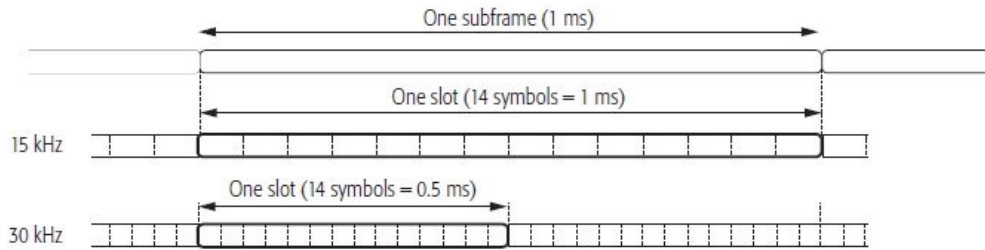


Fig. 4.1 The framing structure of NR, for numerologies  $\mu=0$  and  $\mu=1$

with a fixed duration of 1 ms. The number of OFDM symbols in a sub-frame is determined by the carrier spacing in the frequency domain, which is defined by the numerology parameter  $\mu$  and the type of cyclic prefix used. There are multiple options for numerology, with each defined by a positive integer factor. Slots are used to group the OFDM symbols, and each slot contains 14 OFDM symbols when using normal cyclic prefix. When using extended cyclic prefix, which is only available with numerology  $\mu=2$ , each slot contains 12 OFDM symbols. Figure 4.1 shows an example of the framing structure for numerology  $\mu=0$  and  $\mu=1$ . In a 15 kHz bandwidth with  $\mu=0$ , one slot occupies 1 ms, while in a 30 kHz bandwidth with  $\mu=1$ , one slot occupies 0.5 ms. The 5G-NR system uses OFDM symbols, each consisting of a specific number of sub-carriers in the frequency domain. The number of sub-carriers depends on the selected numerology and the available bandwidth. OFDM symbols can be allocated for either down-link or up-link transmission based on the Slot Format Indicator (SFI), providing flexible resource allocation for both Time Division Duplex (TDD) and Frequency Division Duplex (FDD) modes of operation.

In 5G-NR Release 15, a Resource Element (RE) refers to a single sub-carrier within an OFDM symbol, while a Resource Block (RB) is a set of 12 contiguous REs in the frequency domain. The sub-carrier spacing (SCS) between REs is calculated using the equation:

$$SCS = 2^{\mu} \times 15 \text{ kHz}, \quad (4.1)$$

where  $\mu$  can take values of 0, 1, 2, 3, or 4. 5G-NR can operate in two frequency ranges: FR1 (Sub-6 GHz) and FR2 (millimeter wave range, 24.25 to 52.6 GHz), each with different available bandwidths. FR1, which ranges from 450 MHz to 6 GHz, supports bandwidths from 5 MHz up to 100 MHz, while FR2 offers bandwidths from 50 MHz up to 400 MHz. The sub-carrier spacing for sub-6 GHz 5G-NR is

15/30/60 kHz, while mmWave bands support 120/240 kHz. Additionally, sub-6 GHz supports a maximum bandwidth of 100 MHz, while mmWave ranges support up to 400 MHz. This represents a significant increase compared to LTE, which only supports a maximum bandwidth of 20 MHz. Table 4.1 provides information on the

Table 4.1 5G numerology for FR1 and FR2 frequency ranges

Sub-carrier Spacing (kHz)	15	30	60	120	240
Symbol Duration ( $\mu$ s)	66.7	33.3	16.7	8.33	4.17
Cyclic Prefix Duration ( $\mu$ s)	4.7	2.3	1.2, 4.13	0.59	0.29
Max. BW (MHz)	50	100	100, 200	400	400
FFT Max	4096	4096	4096	4096	4096
Symbols per Slot	14	14	14, 12	14	14
Slots per Sub-Frame	1	2	4	8	16
Slots per Frame	10	20	40	80	160

symbol duration, cyclic prefix duration, maximum bandwidth, and FFT max for each sub-carrier spacing. It also includes the number of symbols per slot, slots per sub-frame, and slots per frame for each sub-carrier spacing.

Significant changes have been made to reference signals in 5G-NR compared to LTE. For instance, there is no longer a Cell Specific Reference Signal (CS-RS), and a new Reference Signal PTRS has been introduced for time/frequency tracking. The Demodulation Reference Signals (DMRS) are now used for channel estimation. In addition, a new channel coding technique based on the channel polarization concept is used for coding control channels. Low-Density Parity Check (LDPC) codes are adopted for user plane data. Channel polarization enables the construction of capacity-achieving codes for binary input symmetric memoryless channels, which outperform the Tail-Biting Convolutional Codes (TBCC) used in LTE control channels.

The maximum inter-site distance (ISD) allowed between transmitters in 5G-NR SFN scenarios is limited by the cyclic prefix length, which is determined by the numerology being used. Table 4.2 shows that if the numerologies from 5G-NR uni-cast are used for SFN broadcasting, only ISDs of up to 1.4 km can be achieved. While this is sufficient for certain scenarios like stadiums, campuses or malls, larger scenarios such as urban and rural areas require higher ISD values that are not supported by 5G-NR numerologies. To address this, various enhancements can be introduced to increase the range in SFN operations.

Table 4.2 Maximum inter side distance with 5G-NR numerology

$\mu$	SCS (kHz)	Type CP	CP ( $\mu s$ )	ISD(km)
0	15	Normal	4.69	1.41
1	30	Normal	2.34	0.70
2	60	Normal	1.17	0.35
2	60	Extended	4.16	1.25
3	120	Normal	0.59	0.18
4	240	Normal	0.29	0.09

## 4.2 Possible Extension for Terrestrial Broadcast

In [47], the authors propose a development framework for a terrestrial broadcast system based on NR. The framework includes new transmission modes that allow for flexible deployment scenarios and considers design principles such as minimizing the footprint for uni-cast transmission and scheduling processes, providing numerology options for diverse scenarios, leveraging 5G-NR bandwidth configuration and spectrum utilization efficiency, and efficiently multiplexing local, regional, and national services for both mobile and fixed reception.

The importance of offering diverse numerologies for terrestrial broadcast operation to accommodate various types of transmission networks is discussed in [53]. Table 4.3 presents a range of numerologies with varying sub-carrier spacing (SCS), overhead, and cyclic prefix (CP) duration. The reference numerology with  $\mu=0$  (A) is

Table 4.3 Negative numerology

	$\mu$	$\Delta f(\text{Hz})$	$T_u(\mu s)$	CP fraction	$T_{CP}\mu s$	$T_s(ms)$	$SC_{RB}$	ISD(km)
A	0	15000	66.67	7%	4.7/5.1	0.07	12	1.4
B	0	15000	66.67	20%	16.67	0.08	12	5
C	-1	7500	133.33	20%	33.33	0.17	24	10
D	-2	3750	266.67	20%	0.33	0.33	48	20
E	-	2500	400	20%	66.67	0.33	72	30
F	-3	1875	533.33	20%	133.3	0.67	96	40
G	-	1250	533.33	20%	200	1.0	144	60

appropriate for single-cell or MFN Terrestrial Broadcast operation, particularly from LPLT networks. Various numerologies can be derived for SFN operation, including those using the concept of NR-MBMS with extended CP by utilizing a negative  $\mu$



factor in Equation 4.1. However, it is impractical to derive numerologies for SFN deployments with large-ISD (e.g., HPHT) that require longer OFDM symbol durations, which may complicate implementation due to leading to non-integer multiples of current NR sub-frames. Moreover, the options are limited to a few modes with 20% CP overhead, following the same principle as in LTE, i.e., targeting mobile reception.

The use of negative numerologies poses a challenge in framing. The 5G standard defines a fixed duration for each sub-frame, with a fixed number of OFDM symbols per slot, and the number and duration of slots are impacted by the numerology. When negative numerologies are employed, the slot duration increases, and slots span over more than one sub-frame in the time domain. This slot expansion requires changes in the framing structure to support negative integer numerologies. As a possible solution to enable the use of negative numerologies, a mini-slot structure has been proposed in [54]. Mini-slots are a small framing unit comprising a group of 2, 4, or 7 OFDM symbols (as opposed to the 14 symbols in a regular frame). They offer greater granularity and flexibility, as well as lower latencies that could be advantageous for specific 5G scenarios [55].

Figure 4.2 illustrates how mini-slots can be integrated into the 5G negative numerology framing, providing a compatible solution. When using numerology  $\mu=-1$  and extended CP, each mini-slot covers two OFDM symbols. Six mini-slots are required to fill the entire slot length. On the other hand, if using  $\mu=-2$ , mini-slots can group up to four OFDM symbols, and three mini-slots are necessary to fill each slot. These options may be helpful in deriving appropriate extended numerologies for LPLT deployments, but options for SFN deployments with large-ISD are limited. Considering larger numerology values would lead to a non-integer number of mini-slots required to fill the slot structure, thereby limiting the feasibility of using negative numerologies to the value of -2. Only numerologies with values of  $\mu = 0$ ,  $\mu = -1$ , and  $\mu = -2$  are deemed compatible with the mini-slot frame structure.

According to Gimenez et al. [47], it is possible to derive different numerologies by redefining the number of sub-carriers per resource block (RB) using:

$$SC_{RB} = 12 \cdot 15\text{kHz} \cdot T_s \cdot (1 - CP). \quad (4.2)$$

This method, originally proposed for LTE, can also be applied to 5G-NR, where the standard numerology is 15 kHz and 25 RBs per 5 MHz carrier (4.5 MHz effective

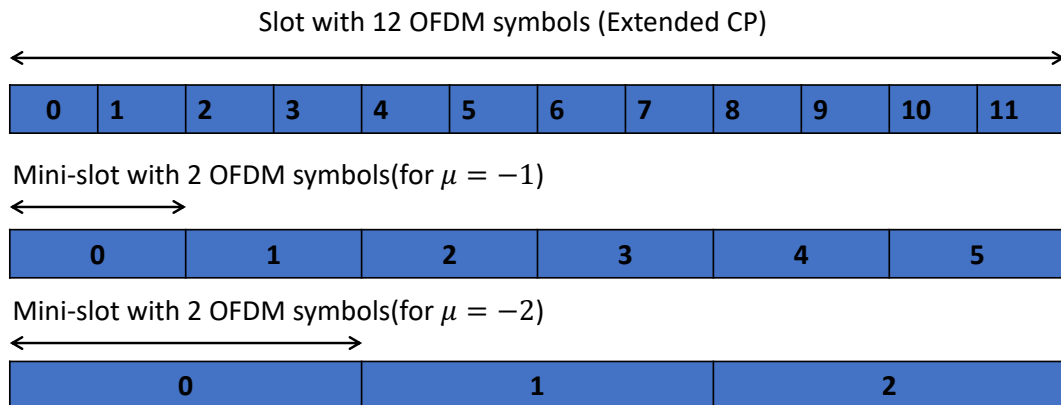


Fig. 4.2 Integration of mini-slots into 5G negative numerology framing.

bandwidth). By selecting an appropriate CP fraction, which makes the number of sub-carriers per RB an integer, multiple combinations of transmission time interval (TTI) and CP duration can be derived.

The selection of numerologies depends on deployment scenarios and receiving environments, taking into account factors such as sub-carrier spacing, cyclic prefix, receiver complexity, and FFT size. Numerology E can be useful for LPLT SFNs, while numerology G corresponds to release 14. The choice of reference signals depends on the deployment type, with uni-cast transmissions using DMRS without modification, while SFN deployments may require new RS and a shared DMRS scrambling sequence. Practical receiver design considerations, such as the impact of increasing FFT size on complexity, must also be taken into account.

These attempts have focused on designing and assigning the appropriate length for cyclic prefix to prevent inter-symbol interference (ISI) and inter-carrier interference (ICI). However, due to the 1 ms limit of sub-frame structure in 5G-NR, achieving this goal has been challenging. In this thesis, we aim to evaluate an alternative approach where we don't need to set the cyclic and OFDM symbol length precisely. Instead, we will use advanced techniques at the receiver side to overcome these challenges. The primary benefit of this approach is that it follows the legacy frame structure of 5G-NR, making it compatible with the current 5G standard. In the next chapter, we will review advanced techniques for OFDM systems to deal with ISI in the absence of sufficient cyclic prefix.

# Chapter 5

## Advanced Receiver for OFDM system

One of the main advantages of orthogonal frequency division multiplexing (OFDM) is its robustness against multi-path fading and inter-symbol interference (ISI). However, this property relies on the assumption that the cyclic prefix (CP) length is longer than the maximum delay spread of the channel. If the CP length is insufficient, then the orthogonality among the sub-carriers is destroyed and ISI and inter-carrier interference (ICI) are introduced. This degrades the performance of the OFDM system and increases the complexity of the receiver.

The challenge for the OFDM receiver in the presence of mobility is even more severe, as the channel becomes time-varying. The Doppler spread caused by the mobility induces additional ICI and also affects the channel estimation and synchronization. Indeed, to preserve orthogonality, the length of the OFDM symbol must be kept much smaller than the channel coherence time, and thus overhead may become large, as we discussed in Chapter 2. To keep a low system overhead in these scenarios, an "advanced" OFDM receiver capable of coping with both ISI and ICI is necessary.

This chapter aims to address these challenges by exploring advanced techniques that can improve the quality and reliability of OFDM transmissions in scenarios where the CP length is insufficient and/or where there is mobility. The two key receiver parts discussed are "channel estimation" and "equalization and data detection". These blocks play a critical role in enhancing the performance of OFDM systems in such scenarios.

In addition, we also investigate iterative reception techniques that can further improve the robustness of OFDM systems. These iterative techniques refine the estimates of the channel and other parameters, thereby improving the performance of the OFDM receiver.

By employing these advanced techniques, it is possible to overcome the challenges associated with insufficient CP length and mobility, leading to high-quality and reliable OFDM transmissions, even in an SFN scenario.

## 5.1 Channel estimation with insufficient CP length

OFDM systems use pilot signals to estimate channels, especially in scenarios where the cyclic prefix is insufficient to accurately estimate the channel while minimizing inter-symbol interference. These pilots consist of a number of OFDM symbols and are referred to as pilot OFDM symbols. The pilot symbols occupy all sub-carriers, and there are various methods for estimating channels using them. These methods have been extensively researched, as cited in [56–65].

With insufficient CP length, there are two approaches to performing channel estimation through the use of pilots. The first method entails creating a pair of pilot OFDM symbols that are consecutive in order to eliminate any inter-symbol or inter-channel interference present in the second symbol. This technique allows channel estimation to be carried out during the second pilot OFDM symbol, as mentioned in [58, 59]. The second method for channel estimation involves using a single symmetric pilot OFDM symbol. There are many references available that discuss this approach, such as [56, 60–62, 66].

To further enhance the accuracy of channel estimation, interference needs to be reduced. One way to achieve this is by using a time-domain symmetric sequence (SS) as a pilot. This approach helps to absorb interference in the first half of the SS, leaving the second half free from interference. By using only the second half, the channel estimate can be calculated more accurately.

In the iterative joint estimation procedure (IJEP) algorithm [66], the interference from the first half of the SS is reduced after the first iteration. This enables the whole SS to be used to enhance the channel estimate from the second iteration onwards. Figure 5.1 illustrates the estimation process of the IJEP algorithm, which

demonstrates how the algorithm utilizes the SS to improve the accuracy of the channel estimation.

The use of a single symmetric pilot OFDM symbol, along with the time-domain symmetric sequence (SS) and the iterative joint estimation procedure (IJEP) algorithm, can significantly improve the accuracy of channel estimation in wireless communication systems.

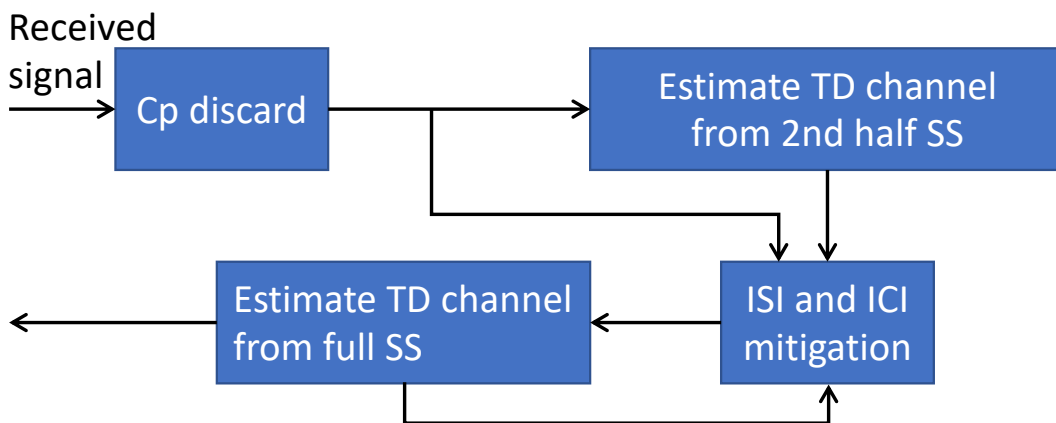


Fig. 5.1 iterative joint estimation procedure algorithm

The SS is obtained with the transmission of the pilot sequence on the even sub-carriers, whereas zeros are used on the odd sub-carriers [56, 61]. This means that a whole OFDM symbol would be used for the pilot. In [57, 63–65], channel estimation algorithms are proposed for a non-symmetric pilot OFDM symbol, while the method proposed in [67] utilizes pilot OFDM symbols with variable CP length to avoid corruption from insufficient CP interference.

While these methods can provide accurate channel estimation, there are practical limitations in mobile systems. This is because major mobile OFDM systems like LTE do not support pilot OFDM symbols. Instead, LTE pilot sub-carriers are mixed with data sub-carriers, making channel estimation significantly more challenging [68]. In addition, due to mobility, the channel needs frequent estimation, requiring frequent pilot transmission. However, since a pilot OFDM symbol consumes a large amount of bandwidth, a significant part of the system bandwidth would be spent on pilots, leading to bandwidth inefficiency, which contradicts the purpose of using insufficient CP to improve bandwidth efficiency.

A blind channel estimation technique for insufficient CP OFDM systems is presented in [69–72], aiming to reduce the bandwidth consumption of pilot signals. This method exploits the redundancy introduced by the CP or unused/virtual sub-carriers to identify the channel. However, this technique is not suitable for mobile systems as it assumes channel invariance over a large number of OFDM symbols. Another method proposed in [73] utilizes scattered pilot sub-carriers and recursive least squares (RLS) channel estimation for insufficient CP single input multiple output (SIMO) OFDM systems. This approach requires a high number of iterations (6 iterations) to achieve a good channel estimate.

There are various channel estimation techniques that employ pilot sub-carriers to estimate the channel affected by Doppler induced ICI, as demonstrated in [74–80]. However, in mobile systems such as LTE, Doppler induced ICI is negligible [78] compared to the significant interference caused by insufficient CP. These techniques do not account for the interference resulting from insufficient CP, which is considerable for high delay spread channels. As of now, there is no high-performing channel estimation technique for OFDM systems with insufficient CP and a limited number of pilot sub-carriers.

## 5.2 Data Detection and Equalization

Numerous methods are available in literature for reducing the impact of insufficient cyclic prefix (CP) induced interference. One equalization approach involves shortening the channel response before demodulation by realizing that interference is caused by the channel delay exceeding the CP length. To achieve this, a finite impulse response (FIR) filter in the form of a shortened impulse response filter (SIRF) is designed as a time-domain equalizer. This ensures that the effective channel, which results from convolving transmit filters, the physical channel, receive filters, and the SIRF, is shorter than or equal to the CP length. A frequency-domain equivalent design of SIRF can be found in references [81, 82]. Despite best efforts, it is not possible to perfectly shorten the channel, and the effective response will still have some energy outside the CP length. Additionally, equalization techniques that use channel shortening are sensitive to parameters like the length of the channel-shortening equalizer and the channel delay, which can change over time for mobile channels as demonstrated in [83].

Channel shortening has been well developed for ADSL (asymmetric digital subscriber line) scenario, which is a wired system that uses twisted-pair copper wires to provide high-speed internet access over telephone lines. ADSL channels typically have long impulse responses due to the multi-path propagation and frequency-selective fading of the wires. Channel shortening can improve the performance and reliability of ADSL systems by reducing the ISI and enhancing the signal-to-noise ratio (SNR).

However, most of these channel shortening techniques for multi-carrier systems do not include mobility, which means they assume that the transmitter and receiver are fixed and do not move relative to each other or to the environment. This assumption may not hold for wireless systems, where mobility is an inherent feature. Therefore, channel shortening techniques that are designed for ADSL scenario may not be directly applicable or effective for wireless systems.

A decision feedback equalizer (DFE) is a technique that can be used to mitigate the effects of ISI and ICI caused by insufficient cyclic prefix (CP) in OFDM systems [16]. A DFE consists of two parts: a feedforward filter (FFF) and a feedback filter (FBF). The FFF compensates for the channel distortion and reduces the noise power at its output. The FBF cancels out the residual ISI by using previous decisions on detected symbols.

Implementing a DFE in OFDM systems with mobility and insufficient cyclic prefix poses several challenges. One challenge is how to estimate the channel state information (CSI) accurately and efficiently, since the channel varies rapidly due to mobility. Another challenge is how to design the feedback filter that does not require knowledge of the channel impulse response or cause error propagation due to incorrect decisions.

Despite these challenges, a DFE can be effectively applied in OFDM systems with mobility and insufficient cyclic prefix in real-time communication systems if some techniques are adopted. For example, one technique is to use pilot symbols [84] or blind algorithms [85] to estimate the CSI adaptively. Another technique is to use sparse linear equalizers or decision-directed algorithms to design the feedback filter without requiring channel knowledge or causing error propagation [86]. A third technique is to use frequency-domain oversampling or time-domain zero-padding to avoid or reduce cyclic ISI [87].

The residual ISI cancellation (RISIC) algorithm [56, 88–91] is a widely used iterative detection technique for OFDM systems. It operates in the time domain (TD) and consists of two steps: tail cancellation and cyclic reconstruction. These steps aim to mitigate the inter-symbol interference (ISI) and inter-carrier interference (ICI) caused by the channel impulse response. The performance of the RISIC algorithm may be limited in accurately estimating data using a one-tap equalizer. This can result in the iterative process failing to converge, particularly when the channel delay spread is significantly longer than the CP length. To address this issue, a variant of the RISIC algorithm has been proposed which includes error control decoding in the iterative detection process [89–91]. However, this approach comes at the cost of significantly increased receiver complexity.

Another significant category of equalization techniques available in the literature are the maximum likelihood based schemes [92]. A maximum likelihood scheme is a detection method that aims to find the most probable transmitted signal given the received signal and the channel state information. In OFDM systems with insufficient cyclic prefix (CP), the effects of ISI and ICI caused by multi-path fading channels degrade the bit error rate (BER) performance significantly. A maximum likelihood scheme can be used to address these effects by jointly detecting a subset of sub-carriers that are most affected by ISI and ICI, while treating the rest of sub-carriers as interference.

The advantages of using a maximum likelihood scheme compared to other equalization techniques, such as single-tap frequency equalization (ST-FEQ), channel shortening and decision feedback equalization (DFE), are that it can achieve better BER performance and higher spectrum efficiency by exploiting the frequency diversity gain from joint detection. The disadvantages are that it requires higher computational complexity and more accurate channel state information than other techniques.

Some reduced-state maximum likelihood (RSML) schemes have been proposed in the literature [93, 94], which can reduce the complexity and improve the robustness of ML detection for OFDM systems with insufficient CP and mobility. The basic idea of RSML schemes is to divide all sub-carriers into several groups and perform joint detection within each group while using pre-detection values for other groups. By doing so, RSML schemes can exploit both time-domain and frequency-domain diversity gains while avoiding exhaustive search over all sub-carriers.



A maximum likelihood scheme can be used to improve the robustness and reliability of OFDM systems in challenging wireless environments with insufficient cyclic prefix and mobility by mitigating ISI and ICI more effectively than other techniques. By finding the most probable transmitted signal given the received signal and channel state information, a maximum likelihood scheme can recover OFDM symbols with high accuracy even when they are severely distorted by dispersive channels. This can enhance the quality of service (QoS) and user experience for wireless communication applications such as 4G LTE, 5G-NR, HDTV broadcasting, or satellite OFDM systems.

### 5.3 Iterative reception

Iterative reception is a highly effective strategy that performs interference mitigation, channel estimation, and channel decoding iteratively to enhance overall receiver performance. [56, 66, 95, 96]. This approach allows for channel estimation and equalization to be carried out in either the time domain (TD) [96] or the frequency domain (FD) [95]. Additionally, receiver operations can be switched between the TD and FD to optimize performance [56, 66, 97]. This is due to the fact that channel estimation is simpler in the TD, where there are fewer independent parameters. For example, a single-tap channel in the TD requires only a single amplitude and phase, whereas its FD equivalent involves  $N$  amplitudes and phases. Figure 5.2 illustrates a high-performance single input single output (SISO) receiver that was proposed in [97]. The receiver has two parallel data processing stages. The main decoder provides the final output, while the early decoder assists with interference cancellation and channel estimation. Both decoders utilize maximal ratio combining (MRC) to combine two adjacent OFDM symbols on a per-subcarrier basis, allowing Viterbi detection on the combined signal. The MRC combiner in the main decoder benefits from more recent and accurate channel estimates. Using the early decoder outputs, FD interference mitigation is performed in the main decoder prior to Viterbi detection.

It is not explicitly explained how interference cancellation is performed in [97], but it is likely similar to the process described in [96]. The cancellation process consists of two steps. Firstly, the interference from the previously detected OFDM symbol and its corresponding channel estimate is estimated to obtain an approxima-

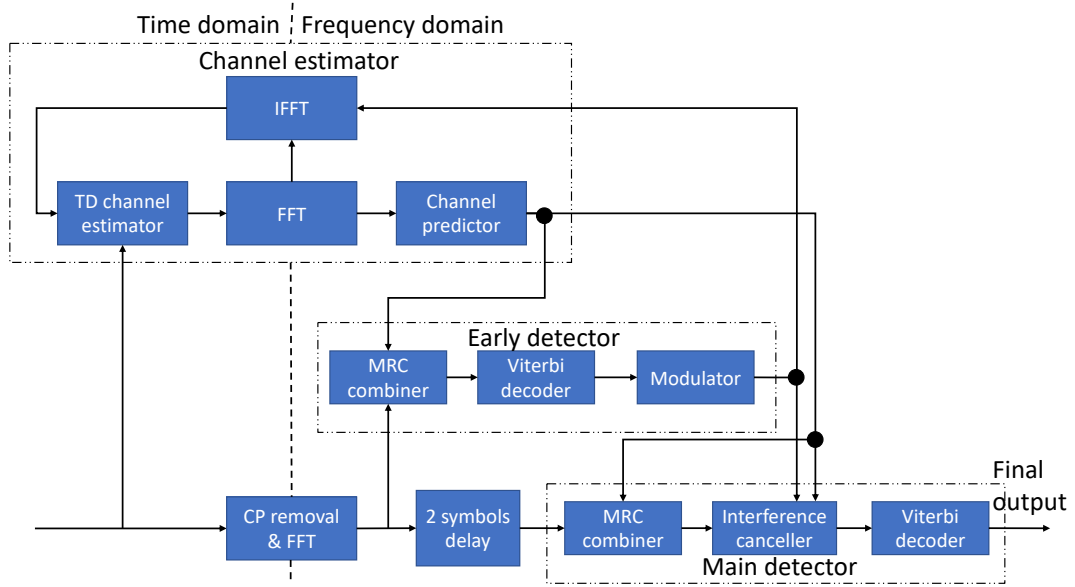


Fig. 5.2 High-performance single input single output (SISO) receiver with parallel data processing stages and maximal ratio combining (MRC) for interference cancellation and channel estimation. The early decoder assists with channel estimation and FD interference mitigation, while the main decoder utilizes more recent and accurate channel estimates for Viterbi detection.

tion of ISI. This ISI cancellation is achieved by subtracting the ISI estimate,  $\hat{R}_{isi,u}(a)$ , from the received signal  $R_u(a)$ , resulting in an intermediate signal  $\check{R}_u(a)$ :

$$\check{R}_u(a) = R_u(a) - \hat{R}_{isi,u}(a). \quad (5.1)$$

The ICI cancellation process is accomplished by subtracting the ICI estimate, from the intermediate signal  $\check{R}_u(a)$ , resulting in the final signal denoted as  $\dot{Y}(a)$ :

$$\dot{Y}(a) = \check{R}_u(a) - \hat{R}_{ici,u}(a), \quad (5.2)$$

where  $\hat{R}_{ici,u}(a)$  is the ICI estimate.

One of the benefits of this design is that it can achieve high detection accuracy with a small number of pilot sub-carriers needed in an OFDM symbol for channel estimation. The receiver processing is done on a per OFDM symbol basis, rather than on a per frame basis, which reduces latency [97]. However, this receiver is tailored for 802.11 OFDM systems, so it has several major drawbacks that make it unsuitable for 5G-NR terrestrial broadcasting systems. First, the receiver depends on the 802.11

preamble, which has a pilot OFDM symbol reserved for obtaining initial channel estimates [98]. However, such preamble does not exist in 5G-NR systems, which use distributed pilot sub-carriers mixed with data sub-carriers. Furthermore, due to the absence of distributed pilot symbols, the channel predictor may not perform well with high velocity channel conditions such as those encountered in 5G-NR systems.

Turbo equalization is a technique that combines iterative equalization and decoding to mitigate the effects of ISI and ICI in OFDM systems with insufficient CP. The basic idea is to use soft information from the decoder to improve the equalizer output, and vice versa. The equalizer can be implemented using linear or nonlinear methods, such as minimum mean square error (MMSE) [99], decision feedback equalization (DFE) [14], or maximum likelihood sequence estimation (MLSE) [100]. The decoder can be based on convolutional codes [101], turbo codes [102], or low-density parity-check (LDPC) codes [103].

The advantage of turbo equalization is that it can significantly improve the bit error rate (BER) performance of OFDM systems with insufficient CP, especially in highly dispersive channels. The disadvantage is that it requires high computational complexity and latency due to the iterative process and the feedback loop.

## 5.4 Conclusion

Advanced receivers can employ techniques such as time-domain equalization (TEQ), frequency-domain equalization (FEQ), or iterative methods for joint ICI and ISI cancellation. These techniques aim to restore the orthogonality among sub-carriers and reduce the error probability. TEQ operates on the received signal before FFT and tries to shorten the effective channel impulse response within the CP length. FEQ operates on the frequency-domain samples after FFT and tries to invert the channel frequency response on each sub-carrier. Iterative methods exploit soft information from the decoder and feedback it to the equalizer to improve the performance.

The choice of the best technique depends on several factors, such as the channel characteristics, the system parameters, and the computational complexity. In general, iterative methods can achieve better performance than TEQ or FEQ, but at a higher complexity cost. Therefore, a trade-off between performance and complexity should

be considered when designing OFDM systems with insufficient CP length over time-varying channels.

Despite the significant progress made in the development of channel estimation and equalization techniques and iterative techniques for OFDM systems with insufficient cyclic prefix, there are still some challenges that remain unresolved. In particular, the literature currently lacks research on scenarios where the RMS delay spread is much larger than an OFDM symbol. Additionally, there is a lack of research on the application of these techniques to single frequency network broadcasting with short OFDM symbol length. These gaps in the literature call for further investigation and development of novel techniques to address these challenges.

# Chapter 6

## 5G-NR SFN broadcasting with channel shortening

Enabling 5G-NR single frequency network terrestrial broadcasting involves considering two main options. The first option entails adopting a cyclic prefix of sufficient length, while the second option involves designing an advanced receiver. The former option, however, comes with a caveat as it necessitates introducing new numerologies that may not be compatible with the standard 5G-NR new numerology.

Our strategy for enabling 5G-NR single frequency network terrestrial broadcasting involved developing an advanced receiver, which we preferred over opting for a sufficiently long cyclic prefix. This method ensured compatibility between the SFN terrestrial broadcasting system and the existing 5G-NR and its standard numerology.

The current state of research on advanced receivers for OFDM systems has not fully tackled the issue of inter-symbol interference across multiple OFDM symbols. While some studies have attempted to mitigate the impact of ISI with an insufficient cyclic prefix length, they often overlook the fact that ISI can extend beyond a single OFDM symbol.

Furthermore, the existing equalization techniques that aim to address ISI within a single OFDM symbol have limitations, and may not be applicable to multiple symbols. Therefore, our approach represents a significant advancement in addressing the challenges of ISI in 5G-NR terrestrial broadcasting systems, particularly in challenging environments with ISI lasting multiple symbols and high levels of interference.

During the second year of our PhD research, we aimed to adapt channel shortening techniques to suit 5G-NR terrestrial broadcasting. Although these techniques had been successfully adopted in other wireless systems like ADSL, they required modifications to be applicable to our scenario.

During our research, as described in [104], we developed a novel receiver design that incorporated a bank of per-tone time/frequency 2D filters. The selection of these filters was carefully considered to ensure that they were appropriate for the 5G-NR system and effectively mitigated any channel distortion that could potentially degrade the transmission of broadcast signals. Our objective was to equalize the ISI/ICI channel in order to achieve optimal performance. To accomplish this, we utilized a 2D-MMSE filter designed specifically for per tone time/frequency filtering. This approach is superior to a single tap equalizer, which can only be utilized with sufficient CP overhead.

The optimal design for the 2D-MMSE filter was obtained using the procedure outlined in [105], which is applicable for any linear channel. This procedure is based on the channel shortening principle and enables the optimal design of a receiver where a suitable filter precedes a trellis processor with bounded state complexity. We also provided a general procedure for constructing the ISI/ICI channel matrix corresponding to the equivalent channel that includes OFDM processing at both the transmitter and receiver. This matrix was used within the framework of [105] to derive the optimal receiver structure.

Our research revealed several important findings regarding the use of 2D-MMSE filters with Gaussian inputs and 5G-NR numerologies. Firstly, we determined that a carrier spacing of 15 kHz can achieve information rates that are close to the maximum channel capacity, based on our theoretical analysis of the filter.

Furthermore, we conducted a comparison between single-carrier and multi-carrier systems, where the former utilizes the entire bandwidth for a single carrier and an advanced receiver is used. Our results revealed that the mutual information of the multi-carrier system was higher compared to that of the single-carrier system. These findings suggest that in certain scenarios, employing multi-carrier systems may be more beneficial, and serve as a possible rationale for their adoption.

We also discovered that a low complexity receiver design, which does not require an outer trellis processor, can provide higher throughput efficiency than single carrier and other 5G-NR numerologies. Our theoretical predictions were validated by

practical experiments, which showed that the pragmatic capacity associated with practical modulation aligned with our findings.

In our study, we evaluated the performance of an advanced receiver and compared it with that of a traditional receiver in different SFN scenarios, including LPLT, MPMT, and HPHT. The traditional receiver used long OFDM symbols and sufficient cyclic prefix length, with a cyclic prefix overhead of  $1/9$ . In contrast, our advanced receiver was designed to have a lower overhead of  $1/15$ , which is in line with the 5G-NR standard. Our design is based on the 5G-NR standard numerology and utilizes a normal cyclic prefix. However, it is important to note that our approach can also be applied to scenarios where there is no cyclic prefix, such as in CP free OFDM.

We also conducted simulations with an LDPC encoder to evaluate the practical performance of both receivers in the end-to-end communication system. It is widely known that a traditional receiver with sufficient cyclic prefix length can perform similarly to an optimal receiver. However, our advanced receiver outperformed the traditional receiver in all SFN scenarios, with either similar or better performance.

Although the presented results show promising, they are based on the strong assumption of perfect channel knowledge at the receiver. In practical settings, channel estimation is a critical function for achieving optimal receiver performance, especially in mobile environments.

Future research on advanced but "classical receivers" may focus on developing a low-complexity and adaptive 2D channel equalizer that can acquire and track the ISI/ICI channel even in highly mobile environments. The number and positions of the required active taps in both dimensions will be the crucial parameter considered for complexity, as well as its trade-off with performance.

For more detailed information about the advanced receiver we developed for enabling 5G-NR single frequency network terrestrial broadcasting, please refer to Appendix A.

A radical alternative that researchers are recently investigating is that of employing neural networks to substitute parts or the entirety of the digital baseband receiver. Neural networks have shown promising results in various communication systems, including OFDM, and can potentially address the challenges of the considered SFN scenario with high mobility.

A first approach is to use a deep learning-based receiver that can learn the channel characteristics and equalize the channel without requiring explicit channel estimation. The use of deep learning can also enable the receiver to adapt to changing channel conditions in real-time, making it suitable for mobile environments.

Another approach is to use neural networks for the separate tasks of channel estimation and equalization. In this approach, the receiver can estimate the channel using a neural network and then use another neural network for equalization. This approach can potentially reduce the overhead associated with explicit channel estimation and improve the performance of the receiver.

In the next chapter, we will review the fundamentals of deep learning and how they can be applied to various fields, including wireless communications where deep learning has shown great promise in enhancing the performance of systems such as Orthogonal Frequency Division Multiplexing (OFDM).



# **Appendix A**

## **5G-NR terrestrial broadcasting with channel shortening**

# Single Frequency Network Broadcasting with 5G NR Numerology

Majid Mosavat

Department of Electronics and Telecommunications  
Politecnico di Torino  
Turin, Italy  
majid.mosavat@polito.it

Guido Montorsi

Department of Electronics and Telecommunications  
Politecnico di Torino  
Turin, Italy  
guido.montorsi@polito.it

**Abstract**—This paper investigates the possibility of using 5G New Radio (5G NR) OFDM numerology in the deployment of efficient Single Frequency Networks (SFNs) for delivering TV services to user devices. The straightforward approach in the design of the physical layer for broadcasting application is based on the adoption of OFDM signalling with very long OFDM symbol and very low sub-carrier spacing (SCS). This design choice allows to dimension the Cyclic Prefix length to eliminate ISI and ICI induced by the large delay spread with a consequent overhead reduction. The 5G NR numerology is designed for uni-cast transmission and Cyclic Prefix lengths are not compatible with those required for large SFN networks. In this paper we consider a general receiver based on the channel shortening principle, but in the frequency domain. The receiver consists in a bank of per tone time/frequency 2D filters, possibly followed by Maximum-Likelihood (ML) trellis processing on the shortened channel. We provide promising information theoretic bound showing that the extension of 5G NR numerology to SFN is possible with very small performance loss. Even the simplest detector architecture that does not employ trellis processing provides throughput competitive with those that can be obtained with smaller SCS. We provide end to end simulation results with practical modulation and LDPC encoder confirming that the results predicted by the bounds can be closely matched in practice.

## I. INTRODUCTION

In a Single Frequency Network (SFN), a signal is transmitted simultaneously through multiple stations over the same frequency channel. Several useful signals are available to the receiver either from multi path echoes or from different transmitters. The receiver in SFN must be able to overcome multi path conditions and its performances are strongly affected by the performance of channel equalizer.

In an Orthogonal Frequency Division Multiplexing (OFDM) system by adding a Cyclic Prefix (CP) between the OFDM symbols which is at least the size of the Channel Impulse Response (CIR), the non-constructive combination of signals in the receiver can be prevented and a simple receiver structure can be obtained to equalize the channel with only one complex multiplication for each carrier. The DVB-T2 (2<sup>nd</sup> Generation Digital Video Broadcasting Terrestrial) [1] as well as the ATSC 3.0 (Advanced Television Systems Committee) [2] standards allow for large inter-site distances covering up to hundreds of

kilometers (e.g. 60 km - CP duration of 200  $\mu$ s - or 120 km - CP duration of 400  $\mu$ s).

The Third Generation Partnership Project (3GPP) introduced 5G New Radio (5G NR) air interface from Release 15 [3] offering a more flexible and scalable design than LTE, in order to satisfy a wider range of use cases requirements, frequency bands and deployment options. However, 5G NR only supports user-specific uni-cast transmissions. i.e. transmission modes and core functionality not complying with broadcaster's requirements.

A multi-cast mode is currently under development in 3GPP Rel-17 Multimedia Broadcast Service (MBS), but it is limited to supporting general multi-cast and broadcast communication services (e.g. transparent IPv4/IPv6 multi-cast delivery, IPTV, IoT applications, V2X applications, public safety) relevant for distribution over 5G mobile networks. Indeed, 5G NR air interface standardized up to now, is not suitable for delivering media services over stand-alone broadcast down-link network only, employing large SFN areas in a Free-to-Air reception, and receive-only device [4].

In parallel, the 3GPP Enhancements for Television Services known as LTE-based 5G Terrestrial Broadcast was introduced to support the SFN with 100 km cell size and mobile reception up to 250 km/h. This solution is based on new carrier spacing with long CP length and not compatible with original 5G NR numerologies[5].

It is known that the addition of CP in OFDM broadcasting systems reduces the throughput of the channel as it transports unneeded data. The channel shortening is an alternative solution for OFDM receiver with long CP length to deal with multi paths environment. Channel shortening was first proposed in single carrier systems [6] to reduce complexity of trellis detector in ML receiver. The channel shortening principle was also used in multi carrier system mainly focused on Digital Subscriber Line (DSL) system. In [7] have proposed a time domain equalizer to make the equivalent channel response length smaller than the CP thus allowing single tap equalization in the frequency domain.

Ackerr et al. [8] suggested the usage of per tone equalizer (PTEQ) for ADSL applications. They assigned a specific T-Taps equalizer for each carrier separately to optimize the SNR for each carrier. These technique were based on the minimiza-

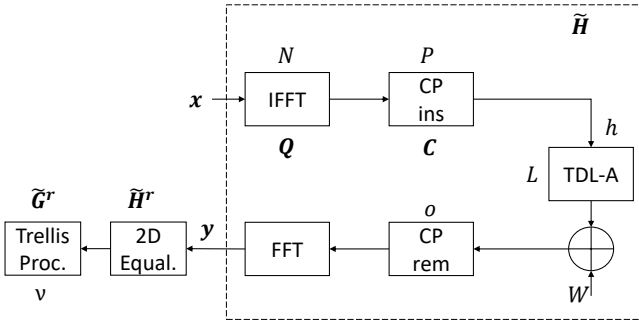


Figure 1. System Model. The complexity of trellis processor exponential with  $\nu$ .

tion of mean square error and this metric does not provide in general the highest throughput. In [9] a general framework for channel shortening for any arbitrary linear channel was proposed. The framework is optimized for Gaussian inputs and generalized mutual information. In this paper we start from the framework developed in [9] to derive optimal receiver structures with channel shortening satisfying broadcast transmission requirements using 5GNR numerologies. We develop a procedure to derive a linear channel which include OFDM modulator with CP insertion, OFDM demodulator and ISI channel. We implement an optimal 2D filter equalizer for an OFDM receiver to equalize received signal in presence of ISI/ICI.

The rest of this paper is organised as follows. In Section II, the complete system model for broadcasting transmission in an SFN network is introduced. In particular, the steps describing the construction of equivalent channel matrix are illustrated. In Section III the channel shortening method in [9] is described and adapted to this scenario. Simulation results are illustrated and discussed in Section IV. Conclusions follow under Section V.

## II. SYSTEM MODEL

The system model is represented in Figure 1.  $N$  parallel inputs  $\mathbf{x}$  are mapped from the frequency domain to the time domain by means of an Inverse Fast Fourier Transform (IFFT) and CP insertion of size  $P$ . The OFDM symbol, of length  $N + P$  is transmitted over the physical channel, modeled as a Tapped Delay Line (TDL) 5G channel model [10].

The TDL channel model can characterize a SFN, where all the transmitters use the same frequency and signals copies can reach user from different transmitters and possibly scatterers at the same time. In this case the ISD characterizing the SFN is modeled with a proper Delay Spread (DS) of the TDL channel model. Two type of channels for TDL model are defined, the TDL-A channel profile with Non Line of Sight (NLOS) for handheld/mobile reception environments, and the TDL-E channel profile with Line Of Sight (LOS) for rooftop reception.

In Table I we report the model parameters of 4 SFN networks scenarios with different ISD and transmitted power. The

Parameter	LPLT	MPMT	HPHT1	HPHT2
ISD [km]	15	50	125	173.2
Transmitted power [dBm]	46	60	70	70
LOS DS [ $\mu$ s]	16	35	45	70
NLOS DS [ $\mu$ s]	20	40	50	75

Table I  
DIFFERENT SFN NETWORKS AND CORRESPONDENT DELAY SPREAD (DS) IN LOS (TDL-E) AND NLOS (TDL-A) CHANNEL MODELS.

4 scenarios cover some possible configurations for terrestrial networks: High Power High Tower (HPHT) and Medium Power Medium Tower (MPMT) typically based on a limited number of transmitters with large antenna heights and Effective Radiated Power (ERP) values in the range of some kW to many tens of kW. Low Power Low Tower (LPLT) architecture is characterized by a dense network of transmitters, with rather low power levels and antenna heights. For each SFN network we report the delay spread derived from system level simulation to be used in the two TDL channel profiles [10].

We consider a TDL channel with channel impulse response ( $h$ ) with length  $L$ , which is known to the receiver. In our setting the length of the impulse response of the channel  $L$  can be much larger than an OFDM symbol. So we derive a matrix representation of the system shown in Figure 1 as follows.

First define the following matrices, representing the block processing at TX and RX side:

- **IFFT:**  $\mathbf{Q}_{ij}^* = \frac{1}{\sqrt{N}} e^{j2\pi \frac{i \cdot j}{N}} \quad \forall i, j \in [0, N - 1]$
- **CP prefix insertion:**  $\mathbf{C}_I = \begin{bmatrix} \mathbf{0}_{N-P} & \mathbf{I}_P \\ & \mathbf{I}_N \end{bmatrix}$ , where  $\mathbf{I}_N$  is the identity matrix of size  $N$ , and  $\mathbf{0}_{N-P}$  is a zero matrix with  $P$  rows and  $N - P$  columns.
- **CP removal:**  $\mathbf{C}_R^{(o)} = \text{cshift}_o \left[ \begin{bmatrix} \mathbf{I}_N & \mathbf{0}_P \end{bmatrix} \right]$ , where “cshift<sub>o</sub>” accounts for a possible circular shift of the columns of the matrix, controlled the parameter  $o$ .
- **FFT:**  $\mathbf{Q}_{ij} = \frac{1}{\sqrt{N}} e^{-j2\pi \frac{i \cdot j}{N}}$ .

We then use the conventional infinite Toeplitz matrix,

$$\tilde{\mathbf{H}}' = \text{Toep}_{\infty}[h_{L-1}, h_{L-2}, h_0],$$

to represent the effect of the channel linear convolution, and introduce the following block diagonal infinite matrices

$$\begin{aligned} \tilde{\mathbf{Q}}^* &\triangleq \text{Toep}_{\infty}[\mathbf{C}_I \mathbf{Q}^*] \\ \tilde{\mathbf{Q}} &\triangleq \text{Toep}_{\infty}[\mathbf{Q} \mathbf{C}_R^{(o)}], \end{aligned}$$

to represent TX and RX OFDM block processing. The notation  $\text{Toep}_{\infty}(\mathbf{M}_1, \dots, \mathbf{M}_N)$  represents the infinite (block) Toeplitz matrix with (block) diagonals  $\mathbf{M}_1, \dots, \mathbf{M}_N$ . The output sequence  $\mathbf{y}$  can now be written as

$$\mathbf{y} = \overbrace{\tilde{\mathbf{Q}} \mathbf{H}' \tilde{\mathbf{Q}}^*}^{\tilde{\mathbf{H}}} \mathbf{x} + \mathbf{w}'.$$

The OFDM processing then transforms the stationary channel in the time domain into a cyclo-stationary channel in the Finite

Fourier Transform domain. The structure of channel matrix  $\tilde{\mathbf{H}}$  becomes

$$\tilde{\mathbf{H}} = \text{Toep}_{\infty}(\mathbf{H}_{J-1}, \dots, \mathbf{H}_0)$$

where  $J = \lceil \frac{L}{N+P} \rceil$ , and  $\mathbf{H}_i$  are  $N \times N$  matrices, substituting the original samples of the time domain impulse response  $h_i$  in  $\mathbf{H}'$ . Notice that this representation depends on the choice of the position of the CP removal offset  $o$ .

The introduced notation allows to represent OFDM systems in the general case where the length of the impulse response of the channel  $L$  take any value, even larger than  $P$  and  $N$ . In the special case, where  $L < P$ , corresponding to the usual setting for OFDM systems, the input-output relationship boils down to

$$\tilde{\mathbf{H}} = \text{Toep}_{\infty}(\mathbf{D}_0),$$

where  $\mathbf{D}_0$  is a diagonal matrix carrying the FFT of the channel impulse response.

The derived input-output relationships can be now casted in the general model introduced in [9] to derive the optimal receiver based on channel shortening.

### III. OPTIMAL CHANNEL SHORTENING

In an OFDM system, as described in the previous section, the received signal can be represented as a complex-valued discrete-time model as follows:

$$\mathbf{y} = \tilde{\mathbf{H}}\mathbf{x} + \mathbf{w}', \quad (1)$$

where  $\mathbf{y}$  is the received signal,  $\tilde{\mathbf{H}}$  is ISI/ICI channel matrix of dimension  $T \times T$  which is perfectly known to receiver,  $\mathbf{x}$  is the input data which is circularly-symmetric complex Gaussian distributed and  $\mathbf{w}'$  Additive Gaussian Noise with variance  $N_0$ . The channel matrix  $\tilde{\mathbf{H}}$  includes IFFT, TDL channel ( $h$ ) and FFT. The absolute limit of achievable rate ( $I_R$ ) over TDL channel ( $h$ ) with length  $L$  is

$$I_R = \log_2 \left( 1 + \frac{\|h\|^2}{N_0} \right), \quad (2)$$

where  $N_0$  is the noise power spectral density. The Equation (2) assumes uniform power allocation over all carrier.

Based on the approach in [9], the optimal channel shortening receiver of Figure 1, for a fixed value of  $\nu$ , is characterized by an optimal  $\tilde{\mathbf{H}}^r$  filter given by:

$$\tilde{\mathbf{H}}^r = \left[ \tilde{\mathbf{H}}\tilde{\mathbf{H}}^\dagger + N_0\mathbf{I} \right]^{-1} \tilde{\mathbf{H}}^\dagger (\tilde{\mathbf{G}}^r + \mathbf{I}), \quad (3)$$

which is a standard MMSE/Wiener filter compensated by trellis processor represented by matrix  $\tilde{\mathbf{G}}^r$ . The  $\tilde{\mathbf{G}}^r$  is a suitably designed matrix that satisfy the following property:

$$(G^r)_{mn} = 0 \quad \text{if} \quad |m - n| > \nu,$$

where  $(G^r)_{mn}$  define elements of matrix  $\tilde{\mathbf{G}}^r$  and  $\nu$  denotes memory of reduced trellis memory.

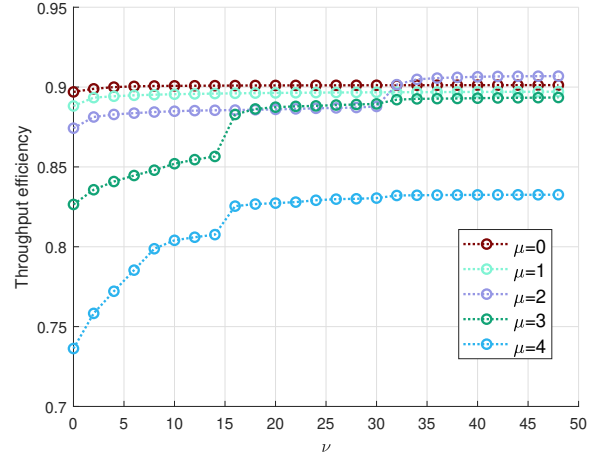


Figure 2. Throughput efficiency versus  $\nu$  for 5GNR numerologies with fixed SNR=5dB and  $SCS = 2^\mu \times 15\text{kHz}$

According to [9], the optimal receiver maximizes, assuming Gaussian inputs, the lower bound to the theoretical achievable rate:

$$I_{LB}(\nu) = \log \left( \det \left( \mathbf{I} + \tilde{\mathbf{G}}^r \right) \right) + \text{Tr} \left\{ \left[ \tilde{\mathbf{G}}^r + \mathbf{I} \right] \tilde{\mathbf{H}}^r \left[ \tilde{\mathbf{H}}\tilde{\mathbf{H}}^\dagger + N_0\mathbf{I} \right]^{-1} \tilde{\mathbf{H}} \right\} - \text{Tr} \left\{ \tilde{\mathbf{G}}^r \right\}, \quad (4)$$

where  $I_{LB}(\nu) < I_R$ .

The goal of the design is then to make the throughput of the OFDM receiver  $I_{LB}$  as close as possible to  $I_R$ . The complexity of system is controlled by the parameter  $\nu$ . We then define the following throughput efficiency metric as performance metric of channel shortening receiver:

$$T_E(\nu) = \frac{I_{LB}(\nu)}{I_R} \times \frac{N}{N+P}, \quad (5)$$

with  $0 < T_E \leq 1$ . Notice that we included in the definition the correction coefficient  $\frac{N}{N+P}$  due to CP insertion.

In Figure 2 we report the  $T_E(\nu)$  versus  $\nu$  for different 5GNR numerologies and HPHT1 NLOS channel scenario of Table I. All plots show as expected performances increasing with  $\nu$ . In particular for  $\mu = 0$  (15 kHz) we notice that the improvement obtained by increasing  $\nu$  is actually marginal and the system reach rapidly the ultimate limit corresponding to CP overhead, that is 6% of 5GNR. So the solution with  $\nu = \mu = 0$ , corresponding to absence of trellis processor is very promising. This receiver can be constructed by simple 2D-MMSE equalizer without adding complexity of trellis processor.

On the other hand a full complexity detector can be obtained by setting  $\nu = T-1$  and the optimal theoretical achievable rate becomes  $I_{LB}(\nu) = I_R$ . As previously mentioned the design of optimal delay offset is crucial for the final performance as it affects the structure of  $\tilde{\mathbf{H}}^r$ . In all reported performance

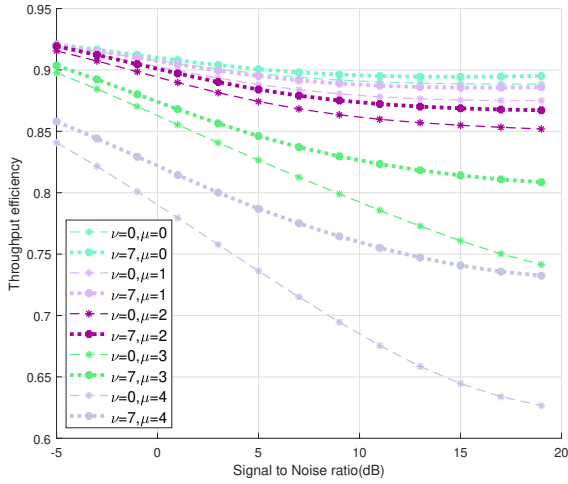


Figure 3. Throughput efficiency  $T_E$  versus receiver complexity ( $\nu$ ) for 5G NR numerologies: TDL-A DS=50 $\mu$ s (HPHT1, NLOS, 125km ISD)

this parameter was preliminary optimised by maximising the energy of received signal after cyclic prefix removal.

#### IV. SIMULATION AND RESULTS

In this section, the performance of optimal  $\tilde{\mathbf{H}}^*$  filter is presented. The TDL-A channel profile with delay spreads in table I is used for evaluating SFNs networks. The bandwidth used in all tests is 9.6 MHz. The velocity of receiver is equal to zero. The channel is assumed to be known at the receiver. The time synchronization and computation of optimal offset is performed as described in the previous section.

##### A. Theoretical and Pragmatic achievable rate by channel shortening

In Figure 3 we report the throughput efficiency (5) of channel shortening receiver for  $\nu = 0, 7$  and Gaussian inputs with 50 $\mu$ s delay spread. The standard 5G NR numerologies with normal CPs length (1/15 of useful signal) is used. These numerologies are given by:

$$SCS(\mu) = 15 \times 2^\mu \text{ kHz} \quad \mu = 0, \dots, 4,$$

For each of these numerologies and the DS=50 $\mu$ s, the maximum value for  $J$  is 7, 14, 28, 55 and 109 OFDM symbols, respectively. The case  $\mu = 0$  shows the higher throughput efficiency for any signal to noise ratio, while the throughput efficiency decreases using larger 5G NR numerologies (e.g.  $\mu = 4$ ). The cases with  $\nu = 0$  (no trellis processor) and  $\nu = 7$  provide similar  $T_E$  for small 5G NR numerologies ( $\mu = 0, 1, 2$ ). On the other hand using trellis processing ( $\nu = 7$ ) can provide significant gains for higher numerologies, especially at high signal to noise ratio. In Figure 4 we fixed the SNR to 5dB and reported the throughput efficiencies versus the sub-carrier spacing for the five 5G NR numerologies, two non-standard smaller carrier spacing (0.37, 2.5 kHz) and the single carrier case (9600 kHz), with  $\nu = 0, 7$ . The CP overhead of the

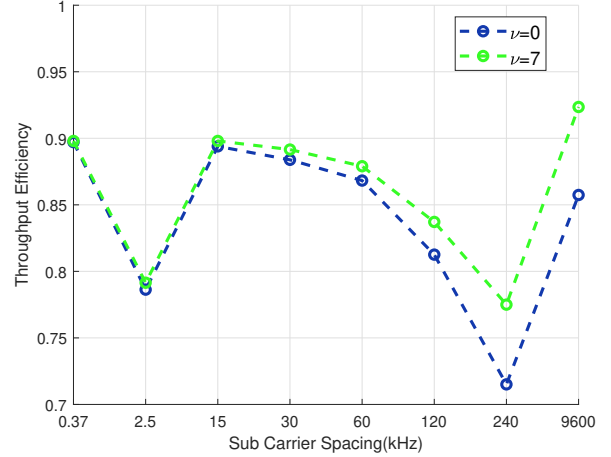


Figure 4. Throughput efficiency versus the sub-carrier spacing for 5G broadcasting, 5G NR numerologies and single carrier spacing with SNR=5dB; TDL-A DS=50 $\mu$ s (HPHT1, NLOS, 125km ISD)

first two non-standard cases is the one specifically designed to allow to deal with large delay spread and with a single tap equalization. The CP overhead is  $\frac{1}{9}$  for 0.37 kHz and  $\frac{1}{4}$  for 2.5 kHz. On the other hand no CP overhead is associated to the single carrier case.

For  $\nu = 0$  (blue line), the best solution is with 15 kHz and provide almost 90% of  $T_E$ . For 5G NR carrier spacing around 6% of  $T_E$  loss is due to insertion of CP overhead and the remaining is associated to receiver loss. Smaller carrier spacing (0.37, 0.25 kHz) provide around 90% and 79%  $T_E$ . This loss is almost totally associated to the larger CP overhead associated to them. Notice that with  $\nu = 0$  the 15 kHz also outperforms the single carrier case. This can be a motivation for using multi carrier OFDM system with 2D-MMSE  $\tilde{\mathbf{H}}^*$  filter for broadcasting in a SFN network.

The single carrier on the other hand performs better by increasing receiver complexity ( $\nu = 7$ ). In fact we can expect that by increasing  $\nu$ , the  $T_E$  converge to the CP correction term in Equation (5) (see Figure 3), which is 1 in this case.

Based on results in Figure 4, 5G NR numerology with 15 kHz with a properly designed 2D-MMSE equalizer ( $\nu = 0$ ) can be a competitive alternative to the 0.37 kHz carrier spacing (3000 $\mu$ s OFDM symbol length) and the need to use trellis processor ( $\nu > 0$ ) is not required.

Previous bounds were obtained assuming an optimal Gaussian input distribution. A more accurate prediction of the system performance can be obtained by computing the mutual information associated to the typical BICM receiver structure. This performance metric, usually referred to as the “pragmatic” capacity, includes the losses due the adoption of a particular constellation and those due to the marginalization to the bit LLR that is performed in the receiver before the channel decoder.

The pragmatic capacities for the practical modulations QPSK (nbits=2), 16QAM (nbits=4) and 64QAM (nbits=6) us-

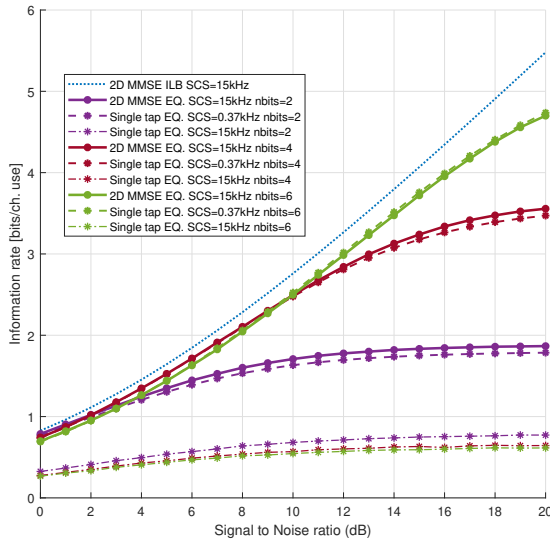


Figure 5. Pragmatic capacity of QPSK, 16QAM and 64QAM inputs for single tap and 2D-MMSE equalizer

ing 15 kHz and 0.37 kHz carrier spacing are shown in Figure 5. For 15 kHz, we considered both the 2D-MMSE (solid line) and the single tap equalizer (dash-dotted line) receiver, for 0.37 kHz we considered only the single tap receiver (dashed line). As a reference, we reported the theoretical information lower bound ( $I_{LB}$ ) using 15 kHz carrier spacing with Gaussian inputs.

The 2D-MMSE equalizer with 15 kHz carrier spacing and single tap equalizer with 0.37 kHz carrier spacing, provide similar pragmatic capacities, with the first slightly better. Increasing the signal to noise ratio the pragmatic capacity of 2D-MMSE and single tap equalizer (0.37 kHz) converges as expected to the modulation efficiency (2, 4 and 6 bits). In low signal to noise ratio the pragmatic capacity provided by 2D-MMSE is close to the theoretical limit with Gaussian inputs ( $I_{LB}$ ). The single tap equalizer with 15 kHz carrier spacing on the other hand can not compensate ISI/ICI interference and increasing the signal to noise ratio can not improve achievable information rate above one. Base on result in Figure 5 the 15 kHz with 2D-MMSE equalizer has similar or even better performance w.r.t. single tap equalizer with long CP length (0.37 kHz carrier spacing).

### B. Performances of realistic system

In this section we present our results of practical full link which comprises of a standard 5GNR LDPC encoder with code rate 0.53, a Mapper to 4QAM, 16QAM or 64QAM modulation, an OFDM modulator and the TDL-A channel. The considered target spectral efficiencies are then 1.06, 2.12, 3.18 bit/s/Hz, respectively.

The Bit Error Rate (BER) for the three considered receiver schemes is reported in Figure 6 with the same convention used

in Figure 5. The realistic link results confirm the pragmatic capacity results in Figure 5. The performance of 2D-MMSE equalizer with 15 kHz carrier spacing is similar to that of single tap equalizer with 0.37 kHz carrier spacing and with long CP length. On the other hand single tap equalizer with 15 kHz carrier spacing and short CP length (less than  $5\mu s$ ) can not compensate channel effect. Since the achievable information rate in this case is below one and target spectral efficiency equal to 1.06 bit/s/Hz, increasing signal to noise ratio can not improve BER.

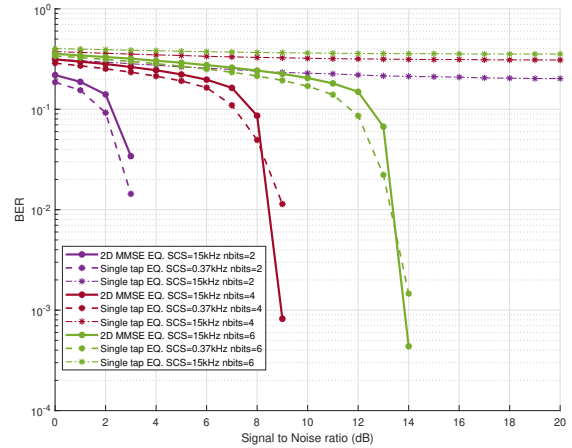


Figure 6. Simulated BER of the three considered realistic systems over TDL-A DS=50 $\mu s$  (HPHT1, NLOS, 125km ISD)

The SNR thresholds at 1% Block Error Rate (BLER) for LPLT, MPMT and HPHT SFNs networks are shown in Figure 7 for the 2D-MMSE and single tap receiver system with 15 and 0.37 kHz carrier spacing, respectively. In all SFN network scenarios, the 2D-MMSE equalizer outperforms single tap equalizer with long CP length (300 $\mu s$ ). The 2D-MMSE performance is uniform in the considered delay spread range and doesn't degrade significantly by increasing the delay spread, so that it may be used also in more challenging scenarios HPHT2 with 75 $\mu s$  delay spread. The 2D-MMSE thus provides an attractive and simple single solution for all SFN network using 5GNR numerologies.

### V. CONCLUSIONS AND FUTURE WORK

In this paper we demonstrated the feasibility of using 5GNR numerologies in the deployment of efficient SFN networks for delivering TV broadcasting services.

In order to achieve this goal, We equalized the ISI/ICI channel using a properly designed 2D-MMSE filter (per tone time/frequency filter) instead of typical single tap equalizer that can be used only with long CP overhead.

The design of the optimal 2D-MMSE filter has been obtained along the procedure outlined in [9], which is valid for any linear channel. The procedure is based on the channel shortening principle and allows to optimally design, assuming Gaussian inputs, a receiver where a suitable filter precedes a



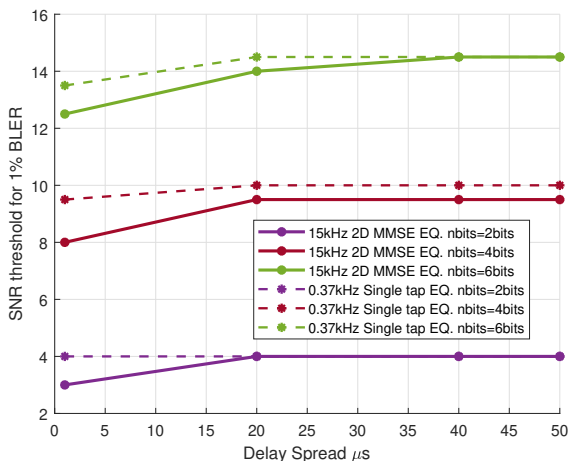


Figure 7. SNR thresholds (dB) at 1% BLER versus Delay spread of TDL-A channel model. Single Tap EQ. vs 2D-MMSE EQ. Code rate 0.53.

trellis processor with bounded state complexity. We provided a general procedure for building the ISI/ICI channel matrix correspondent to the equivalent channel that includes OFDM processing at both TX and RX and use it in the framework of [9] to derive the optimal receiver structure.

The theoretical result of 2D-MMSE filter with Gaussian inputs showed that with 15 kHz carrier spacing the information rate get close to maximum channel capacity even with the simplest low complexity receiver that does not require the adoption of an outer trellis processor. The low complexity 2D-MMSE with 15 kHz carrier spacing provided higher throughput efficiency versus single carrier and the other 5G NR numerologies. The pragmatic capacity associated to practical modulation confirmed the theoretical results.

For the considered SFN network scenarios, single tap equalization with 5G NR numerologies provides very poor performances due to the unacceptable ISI/ICI conditions. On the other hand the adoption of 2D-MMSE filter allows to completely recover the performance losses and provides performances even better than those that can be obtained with OFDM parameters specifically designed for SFN networks [10], requiring much lower carrier spacing and longer CP length.

The presented result are promising but based on the very strong assumption of perfect channel knowledge at the receiver. In practice is well known that channel estimation is a very crucial function for the receiver performances, especially in mobile environment.

Notice that the adoption of the shorter OFDM symbol associated to 5G NR numerologies is also expected to be more suitable in mobile scenario, where the coherence time of channel may becomes too short wrt the OFDM symbol length.

Our future work will then be devoted to the design of a low complexity and adaptive 2D channel equalizer which can acquire and track the ISI/ICI channel also in highly mobile environments. The crucial parameter that will be considered

for complexity will be the number and positions of the required active taps in both dimensions and its trade off with performance.

#### ACKNOWLEDGEMENT

This research was supported by RAI Centre for Research. We would like to acknowledge Assunta De Vita and Vittoria Mignone, whose technical insight and suggestions improved the quality of work.

#### REFERENCES

- [1] D Vargas and D Mi. "LTE-Advanced pro broadcast radio access network benchmark". In: *Deliverable D3 1* (2017), pp. 197–203.
- [2] Inaki Eizemendi et al. "DVB-T2: The second generation of terrestrial digital video broadcasting system". In: *IEEE transactions on broadcasting* 60.2 (2014), pp. 258–271.
- [3] Ayan Sengupta et al. "Cellular terrestrial broadcast—Physical layer evolution from 3GPP release 9 to release 16". In: *IEEE Transactions on Broadcasting* 66.2 (2020), pp. 459–470.
- [4] Jordi Joan Gimenez et al. "5G new radio for terrestrial broadcast: A forward-looking approach for NR-MBMS". In: *IEEE Transactions on Broadcasting* 65.2 (2019), pp. 356–368.
- [5] David Gomez-Barquero, Jordi Joan Gimenez, and Roland Beutler. "3GPP enhancements for television services: LTE-based 5G terrestrial broadcast". In: *Wiley Encyclopedia of Electrical and Electronics Engineering* (2020).
- [6] David D Falconer and FR Magee Jr. "Adaptive channel memory truncation for maximum likelihood sequence estimation". In: *Bell System Technical Journal* 52.9 (1973), pp. 1541–1562.
- [7] Jacky S. Chow, Jerry C. Tu, and John M. Cioffi. "A discrete multitone transceiver system for HDSL applications". In: *IEEE journal on selected areas in communications* 9.6 (1991), pp. 895–908.
- [8] Kathleen Van Acker et al. "Per tone equalization for DMT-based systems". In: *IEEE transactions on communications* 49.1 (2001), pp. 109–119.
- [9] Fredrik Rusek and Adnan Prlja. "Optimal channel shortening for MIMO and ISI channels". In: *IEEE transactions on wireless communications* 11.2 (2011), pp. 810–818.
- [10] 3GPP TS 36.776. "Study on LTE-based 5G terrestrial broadcast. Technical Specification (TS). Version 16.0.0. 3rd Generation Partnership Project (3GPP), Mar. 2019.

# Chapter 7

## An introduction to Deep learning

Deep learning is a type of machine learning that is used to learn complex patterns and representations from data. It is a powerful technique that has gained popularity in recent years due to its ability to automatically learn features from data without the need for human expertise. A neural network is a fundamental component of deep learning and is inspired by the structure and function of the human brain.

A neural network is a computational model that consists of interconnected nodes or neurons. Each neuron receives inputs, performs computations on those inputs, and then produces an output. The output from one neuron can then be used as an input to another neuron, allowing the network to learn complex functions and relationships between input and output data.

The network learns by adjusting the weights of the connections between neurons based on the input and output data. During training, the network is presented with a set of input/output pairs and adjusts the weights to minimize the difference between the predicted output and the true output according to some cost function. Once trained, the network can be used to make predictions on new, unseen data.

In wireless communication, deep learning has shown promising results in various applications such as channel estimation, modulation classification, and signal detection. It is capable of handling large amounts of data and can adapt to changing wireless environments, making it highly adaptable to various scenarios.



In this chapter, we will introduce the fundamental aspects of deep learning, including neural networks, convolutional neural networks, and recurrent neural networks, and their use in wireless communication applications.

## 7.1 Neural network

A neural network, also known as an artificial neural network (ANN) or simulated neural network (SNN), is a computational learning system that uses a network of neurons to understand and translate a data input of one form into a desired output, usually in another form. A neuron, also known as a node, is the basic building block of a neural network. It takes in one or more inputs, performs a computation on these inputs, and produces an output. A neuron in a neural network can be mathematically represented by the equation:

$$y = f \left( \sum_{i=1}^n w_i x_i + b \right), \quad (7.1)$$

where  $x_1, x_2, \dots, x_n$  are the inputs to the neuron,  $w_1, w_2, \dots, w_n$  are the corresponding weights,  $b$  is the bias, and  $f$  is the activation function. The weighted sum of the inputs and the bias is often referred to as the neuron's activation. An illustration of a neuron is provided in Figure 7.1. A feed-forward neural network is a type of neural network consisting of multiple layers of interconnected neurons. The layers are linked by synapses, and each neuron in a layer receives input from the previous layer and produces output for the next layer. The input and output layers, which are responsible for interacting with external data, are situated at the beginning and end of the network, respectively. The layers in between are referred to as hidden layers because they cannot be observed directly from outside. The number of neurons in each layer may vary depending on the complexity of the problem being addressed. An example of a feed-forward neural network with one hidden layer consisting of three neurons is shown in Figure 7.2. The input layer contains two features,  $x_1$  and  $x_2$ , while the output layer has one output. The hidden layer performs computations on the input data and passes the results to the output layer. In a feed-forward neural network, data flows in one direction only, from the input to the output, and there are no loops or cycles in the connections.

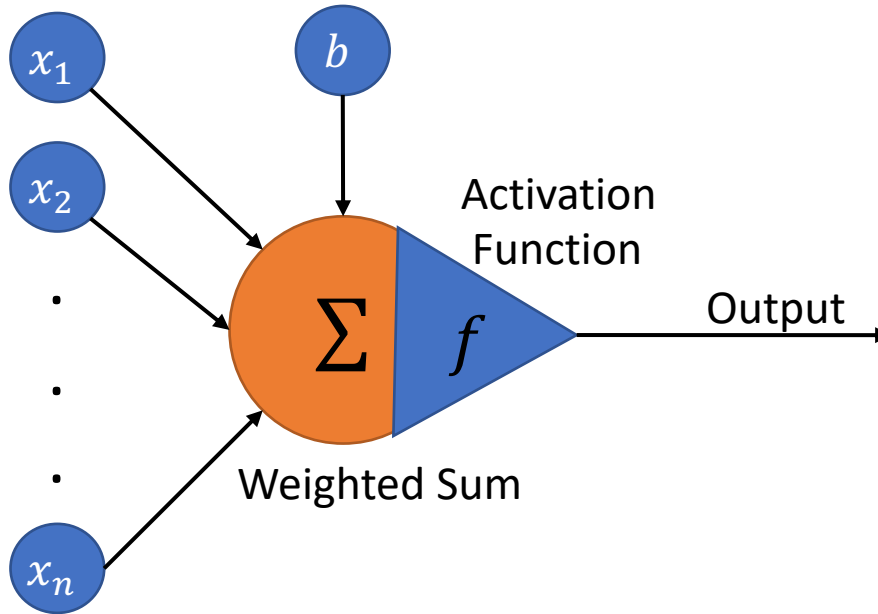


Fig. 7.1 An illustration of a neuron, the basic building block of a neural network, which receives input, applies a weighted sum, and outputs an activation signal.

In a feed-forward neural network with  $L$  layers, the weight matrix for the  $l$ -th layer is represented by  $W_l$ , where  $W_l \in \mathbb{R}^{n_l \times n_{l-1}}$ . The weight matrix defines the weights between the  $l-1$  and  $l$  layers. The bias vector for the  $l$ -th layer is represented by  $b_l$ , where  $b_l \in \mathbb{R}^{n_l}$ . The bias vector defines the bias for layer  $l$ . The activation function for the  $l$ -th layer is represented by  $f_l(\cdot)$ . It is applied element-wise to the output of the weighted sum. The output of the first hidden layer, denoted as  $z_1$ , can be calculated as follows:

$$z_1 = f_1(W_1x + b_1), \quad (7.2)$$

where  $x$  is the input to the network. The output of the  $l$ -th layer, denoted as  $z_l$ , can be calculated as follows:

$$z_l = f_l(W_lz_{l-1} + b_l), \quad (7.3)$$

where  $z_{l-1}$  is the output of the  $(l-1)$ -th layer. The output of the output layer, denoted as  $y$ , can be calculated as follows:

$$y = f_L(W_Lz_{L-1} + b_L), \quad (7.4)$$

where  $z_{L-1}$  is the output of the final hidden layer. The computation carried out by a feed-forward neural network is described by these equations.

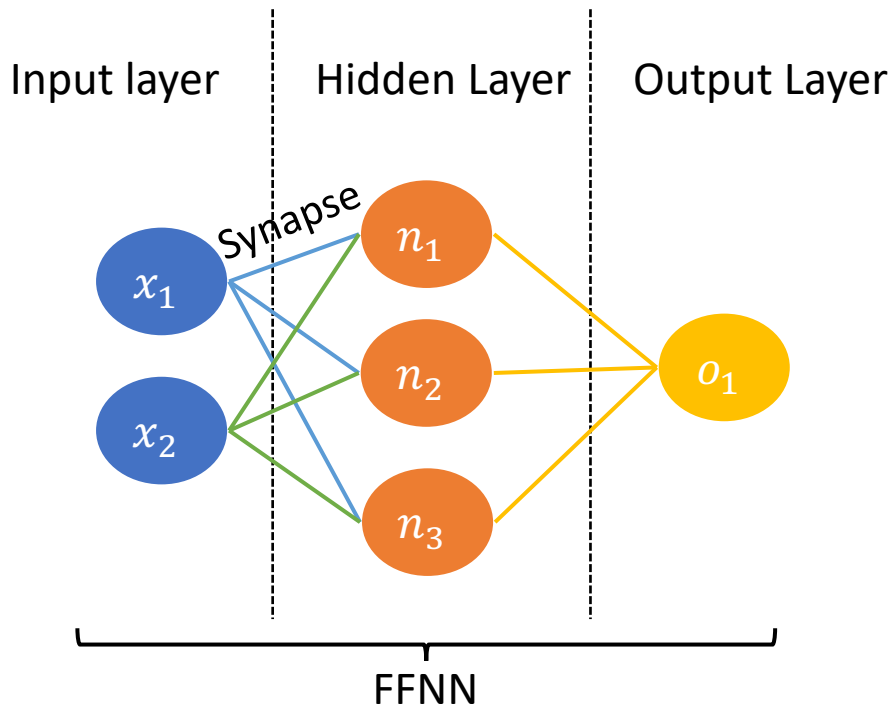


Fig. 7.2 An illustration of a Feed-forward neural network with one hidden layer consisting of three neurons. The input layer receives the input data with two features,  $x_1$  and  $x_2$ , and the output layer produces a single output.

## 7.2 Activation functions

Activation functions are typically applied element-wise to the output of a neuron or a layer, and they introduce non-linearities that allow the neural network to model complex relationships between the input and output.

The sigmoid function is a mathematical function that is commonly used in binary classification problems. The function takes any real input value and maps it to a value between 0 and 1. This property of the sigmoid function is useful in binary classification because it allows the output of a model to be interpreted as a probability. The sigmoid function is defined as the formula:

$$\sigma(x) = \frac{1}{1 + e^{-x}}. \quad (7.5)$$

The ReLU (Rectified Linear Unit) function is another popular activation function used in neural networks. The ReLU function maps any negative input value to 0, and leaves positive input values unchanged. This makes it a popular choice for neural

networks as it can introduce non-linearity into the model while also speeding up computation. The ReLU function is defined as:

$$\text{ReLU}(x) = \max(0, x). \quad (7.6)$$

The tanh function is similar to the sigmoid function in that it is used to introduce non-linearity into a neural network. The difference is that the tanh function maps input values to a range between -1 and 1. The tanh function is defined as:

$$\tanh(x) = \frac{e^x - e^{-x}}{e^x + e^{-x}}. \quad (7.7)$$

The softargmax function is commonly used in the output layer of neural networks for producing a probability distribution over possible classes. This function takes a vector of real numbers as input and returns a vector of the same length, where each value falls between 0 and 1 and the sum of all values equals 1. The equation for softargmax function is given by:

$$\text{softargmax}(z_i) = \frac{e^{z_i}}{\sum_{j=1}^K e^{z_j}}, \quad \text{for } i = 1, \dots, K, \quad (7.8)$$

where  $K$  represents the number of possible classes, and  $z_i$  denotes the output of the  $i$ -th neuron in the output layer. Softargmax is particularly useful in multi-class classification problems where the neural network needs to predict the probability of each class.

The computational cost of each function is different, with the ReLU function being the most computationally efficient due to its simple calculation of just returning the input value if it is positive, while the sigmoid and tanh functions are more computationally expensive due to their exponential calculations. The softargmax function can also be computationally expensive due to the calculation of the exponential function in the denominator.

In summary, ReLU is a simple and efficient activation function that is often used as a default. Tanh is a symmetric activation function that can work well for certain types of problems. Softargmax is used in multi-class classification problems to obtain a probability distribution over the classes. Sigmoid is widely used for binary classification problems and can also be used in the hidden layers of neural networks.

The choice of activation function often depends on the specific problem at hand and can be tuned through experimentation.

## 7.3 Loss Functions

A loss function is a crucial part of machine learning models, as it measures the difference between the predicted output of the NN and the desired output, which is also known as the target value. The loss function is a mathematical function that takes the predicted output of the model and the target value as input and produces a scalar value as output. The scalar value represents the "loss" or "error" of the model on a specific example.

The goal of training a machine learning model is to minimize the value of the loss function over the entire training dataset. To achieve this, the weights and biases of the model are iteratively adjusted during the training process to reduce the value of the loss function.

There are two main types of machine learning problems: classification and regression. In classification problems, the goal is to predict an element in discrete category or class label for a given input. In regression problems, the goal is to predict a continuous numerical value for a given input.

The choice of loss function depends on the type of problem being solved by the machine learning model. For instance, in a binary classification problem, the binary cross-entropy loss is a common choice. It measures the difference between the predicted probability of the positive class and the target value. On the other hand, in a regression problem, a common loss function is the mean squared error (MSE), which measures the difference between the predicted and target values.

MSE measures the average squared difference between the predicted and output values. The mathematical formula for MSE is:

$$\text{MSE} = \frac{1}{n} \sum_{i=1}^n (y_i - \hat{y}_i)^2 \quad (7.9)$$

where  $n$  is the number of samples,  $y_i$  is the target output, and  $\hat{y}_i$  is the predicted output.

Binary cross-entropy, also known as log loss, is a loss function that measures the difference between the predicted probabilities and the true labels in binary classification problems. It is commonly used in machine learning and deep learning algorithms to optimize the performance of the model. The binary cross-entropy loss function for  $n$  samples is given by the formula:

$$L = -\frac{1}{n} \sum_{i=1}^n [y_i \log(p_i) + (1 - y_i) \log(1 - p_i)], \quad (7.10)$$

where  $y_i$  is the true label (0 or 1) for sample  $i$ , and  $p_i$  is the predicted probability (between 0 and 1) for sample  $i$ .

Categorical cross-entropy, also known as softmax loss, is a generalization of binary cross-entropy for multi-class classification problems. It measures the difference between the predicted probabilities and the true labels in multi-class classification problems. The categorical cross-entropy loss function for  $n$  samples can be mathematically defined as:

$$L = -\frac{1}{n} \sum_{i=1}^n \sum_{j=1}^m y_{ij} \log(p_{ij}), \quad (7.11)$$

where  $y_{ij}$  is 1 if sample  $i$  belongs to class  $j$  and 0 otherwise, and  $p_{ij}$  is the predicted probability (between 0 and 1) for sample  $i$  to belong to class  $j$ .

## 7.4 Training Neural Network

Training a neural network refers to the process of iteratively adjusting the parameters (weights and biases) of the network to minimize the difference between its predicted output and the desired output. This is typically done using a dataset of labeled examples, where the inputs and corresponding outputs are known.

During training, the neural network learns to recognize patterns and relationships in the input data, and adjusts its parameters in order to improve its ability to make accurate predictions on new, unseen data. This process involves feeding the input data through the network, calculating the difference between the predicted output and the target output (the loss or cost function), and then using an optimization algorithm (such as stochastic gradient descent) to update the parameters of the network to reduce the loss.

The training process typically involves repeating this process over many iterations (epochs), with the network gradually improving its ability to make accurate predictions as it learns from the training data. Once training is complete, the network can be used to make predictions on new, unseen data.

Suppose we have a training dataset consisting of input vectors  $x_1, x_2, \dots, x_n$  and corresponding binary labels  $y_1, y_2, \dots, y_n$ , where  $y_i$  indicates the true label of  $x_i$  (either 0 or 1). Our objective is to train a feedforward neural network (FFNN) with one hidden layer and one output layer to predict the binary label  $y_i$  of a given input vector  $x_i$ .

The set of weights in the FFNN is denoted as  $w$ . To compute the output of the FFNN, an input vector  $x$  is first multiplied by a weight matrix  $W$ , and the resulting vector is passed through the sigmoid activation function  $\sigma(z) = \frac{1}{1+e^{-z}}$ . The activation values of the hidden layer neurons are then obtained by applying the sigmoid function to the product of the input vector and weight matrix  $W$ , which can be represented as  $h = \sigma(Wx)$ . To obtain the final output of the network for a given input vector  $x$ , the activation values of the hidden layer are multiplied by another weight matrix  $V$ , and the sigmoid function is applied again, resulting in  $\hat{y} = \sigma(Vh)$ .

To train the FFNN, we define the binary cross-entropy loss function. Our aim is to minimize the average loss over the entire training set, which can be expressed as:

$$J(w) = \frac{1}{n} \sum_{i=1}^n L(y_i, \hat{y}_i) \quad (7.12)$$

Here,  $L(y_i, \hat{y}_i)$  represents the binary cross-entropy loss between the true label  $y_i$  and the predicted output  $\hat{y}_i$  for input vector  $x_i$ . We optimize the weights  $w$  of the FFNN by minimizing this loss function.

To minimize the loss function  $J(w)$ , we can use gradient descent optimization algorithm. The goal of gradient descent is to iteratively update the weights  $w$  in the direction of the negative gradient of the loss function with respect to the weights. The update rule for the weights can be expressed as:

$$w^{(t+1)} = w^{(t)} - \alpha \frac{\delta J(w)}{\delta w} \Big|_{w=w^{(t)}} \quad (7.13)$$

Here,  $w^{(t)}$  represents the weights at iteration  $t$ ,  $\alpha$  is the learning rate which controls the step size of the weight update, and  $\left. \frac{\delta J(w)}{\delta w} \right|_{w=w^{(t)}}$  is the gradient of the loss function with respect to the weights at the current iteration.

To compute the gradient of the loss function with respect to the weights, we can use backpropagation algorithm. The backpropagation algorithm computes the gradients of the loss function with respect to the weights in a layer-by-layer manner, starting from the output layer and moving backwards towards the input layer.

To compute the gradient of the loss function with respect to the weights  $W$  connecting the input layer to the hidden layer, we can use the chain rule:

$$\frac{\delta J(w)}{\delta W} = \frac{\delta J(w)}{\delta \hat{y}} \frac{\delta \hat{y}}{\delta h} \frac{\delta h}{\delta W} \quad (7.14)$$

where  $\frac{\delta J(w)}{\delta \hat{y}}$  and  $\frac{\delta \hat{y}}{\delta h}$  can be obtained as:

$$\frac{\delta J(w)}{\delta \hat{y}} = \frac{1}{n} \sum_{i=1}^n \frac{\delta L(y_i, \hat{y}_i)}{\delta \hat{y}_i} = -\frac{1}{n} \sum_{i=1}^n \left( \frac{y_i}{\hat{y}_i} - \frac{1-y_i}{1-\hat{y}_i} \right) \quad (7.15)$$

and

$$\frac{\delta \hat{y}}{\delta h} = V^T \text{diag}(\hat{y} \odot (1 - \hat{y})) \quad (7.16)$$

where  $\odot$  denotes element-wise multiplication and  $\text{diag}(v)$  denotes a diagonal matrix with the elements of vector  $v$  on the diagonal.

To compute the gradient of the loss function with respect to the weights  $W$ , we need to compute the derivative of the sigmoid function  $\sigma(z)$  with respect to  $z$  as:

$$\frac{d\sigma(z)}{dz} = \sigma(z)(1 - \sigma(z)) \quad (7.17)$$

Using this derivative, we can compute the derivative of the hidden layer activation values with respect to the weights  $W$  as:

$$\frac{\delta h}{\delta W} = X^T \text{diag}(h \odot (1 - h)) \quad (7.18)$$

where  $X$  is the input matrix with each row being an input vector. Finally, we can update the weights  $W$  and  $V$  using the gradient descent update rule mentioned earlier. We can repeat this process for multiple epochs until convergence.



The "stochastic" in SGD refers to the fact that the gradient is computed on a single sample at a time, as opposed to using the entire training set. This makes the algorithm faster and more memory-efficient, but also more prone to noise and fluctuations in the loss function. To mitigate these effects, mini-batch SGD can be used, where the gradient is computed on a small batch of samples at a time.

To further optimize the update rule for SGD, other techniques like momentum and adaptive learning rates can be used. Momentum introduces a "velocity" term that helps to smooth out the updates and speed up convergence. Meanwhile, adaptive learning rates adjust the learning rate on a per-parameter basis to improve convergence. Using these techniques can improve the performance of SGD and speed up the training of neural networks.

### 7.4.1 Optimization of gradient

SGD is a simple and effective optimization algorithm for neural networks, but it has a few limitations. One is that it can get stuck in local minima, which are not the global minimum of the loss function. To overcome this, more advanced optimization algorithms such as Adagrad, RMSProp, Adam and their variations have been developed. These algorithms use adaptive learning rates and momentum terms to accelerate the convergence and avoid oscillations. They also require less tuning of hyperparameters than SGD. Therefore, these algorithms are often preferred over SGD for training complex neural networks with large datasets.

#### Momentum

A method that accelerates SGD by adding a fraction of the previous parameter update to the current one, creating a momentum effect that helps escape local minima. The momentum method [106] is a technique to improve the convergence of gradient descent algorithms by using past updates as an additional term in the current update. For each layer  $l$ , we can define two variables  $V_{\delta W_l}$  and  $V_{\delta b_l}$  that represent the velocity (or momentum) of the weight updates. These variables are initialized to zero and updated at each iteration as follows:

$$V_{\delta W_l} = \beta V_{\delta W_l} + (1 - \beta) \delta W_l, \quad (7.19)$$

where  $W_l$  represents the weight matrix of the  $l$ -th layer in a neural network and  $\beta$  is a hyperparameter that controls how much of the previous velocity is retained. Typically,  $\beta$  is set to a value close to 1, such as 0.9 or 0.99. The weight and bias parameters are then updated using these velocity terms instead of directly using the gradients:

$$W_l = W_l - \alpha V_{\delta W_l}, \quad (7.20)$$

The intuition behind this method is that it adds a smoothing effect to the gradient descent updates, preventing oscillations and overshooting, and allowing faster convergence. The momentum term acts like a ball rolling down a hill, accumulating speed and direction as it goes along.

### Adagrad

A method that adapts the learning rate for each parameter based on how frequently it has been updated, giving more weight to rare features. Adagrad [107] is a stochastic optimization method that adapts the learning rate to the parameters. It performs smaller updates for parameters associated with frequently occurring features, and larger updates for parameters associated with infrequently occurring features. Mathematically, Adagrad updates the parameters  $W_l$  of layer  $l$  as follows:

$$W_l = W_l - \alpha \frac{\delta W_l}{\sqrt{G_{W_l} + \epsilon}}, \quad (7.21)$$

The term  $G_{W_l}$  is a sum of the squared gradients of  $\delta W_l$  over time. The term  $\epsilon$  is a small constant added for numerical stability. The effect of this update rule is that each parameter has its own effective learning rate that decreases over time as more gradients are accumulated.

### RMSprop

A method that divides the learning rate for each parameter by an exponentially decaying average of its squared gradients, preventing it from becoming too small or too large. RMSProp [108], which stands for Root Mean Square Propagation. The

motivation behind RMSProp is to overcome the shortcomings of AdaGrad, which decays the learning rate too quickly and prevents convergence .

Mathematically, RMSProp works as follows. Let  $S_{dW_l}$  and  $S_{db_l}$  be exponentially weighted averages of squares of these gradients. Then RMSProp updates these averages using a decay parameter  $\beta$  as follows:

$$S_{dW_l} = \beta S_{dW_l} + (1 - \beta) \delta W_l^2, \quad (7.22)$$

Then RMSProp updates the weights using a small constant  $\epsilon$  to avoid division by zero as follows:

$$W_l = W_l - \alpha \frac{\delta W_l}{\sqrt{S_{dW_l} + \epsilon}}, \quad (7.23)$$

The intuition behind RMSProp is that it adapts the learning rate for each parameter by dividing it by an estimate of its recent magnitude. This way, parameters with large gradients will have smaller effective learning rates, and parameters with small gradients will have larger effective learning rates. This can help speed up convergence and avoid oscillations or divergence .

### Adam

A method that combines RMSProp and momentum by using both adaptive learning rates and moving averages of past gradients. Adam [109] is a popular optimization algorithm for deep learning models that adapts the learning rate for each parameter based on estimates of the first and second moments of the gradient. Mathematically, Adam can be described as follows:

- Initialize the first moment vector  $m_t$  and the second moment vector  $v_t$  to zero vectors.
- For each iteration  $t$ , compute:
  - The first moment estimate:  $m_t = \beta_1 m_{t-1} + (1 - \beta_1) \delta W_l$
  - The second moment estimate:  $v_t = \beta_2 v_{t-1} + (1 - \beta_2) \delta W_l^2$
  - The bias-corrected first moment estimate:  $\hat{m}_t = m_t / (1 - \beta_1^t)$
  - The bias-corrected second moment estimate:  $\hat{v}_t = v_t / (1 - \beta_2^t)$
  - The updated parameter:  $W_l = W_l - \alpha \hat{m}_t / (\sqrt{\hat{v}_t} + \epsilon)$ .

In the Adam optimization algorithm,  $\beta_1$  and  $\beta_2$  are hyperparameters that control the exponential decay rates of the first moment estimate ( $m_t$ ) and the second moment estimate ( $v_t$ ), respectively. Specifically, they control the weight given to the previous estimates of  $m$  and  $v$  relative to the current update. The terms  $\beta_1^t$  and  $\beta_2^t$  in the bias-corrected estimates ( $\hat{m}_t$  and  $\hat{v}_t$ ) correct the bias of the estimates towards zero, especially during the initial iterations when the estimates are still very noisy. By dividing the estimates by  $(1 - \beta_1^t)$  and  $(1 - \beta_2^t)$ , respectively, the estimates are scaled by a factor that increases over time, allowing them to converge towards unbiased estimates. Both  $\beta_1^t$  and  $\beta_2^t$  increase over time, making the estimates less biased towards zero as more iterations are performed. Additionally,  $\epsilon$  is a small constant to prevent division by zero. Adam has several advantages over other optimization methods, such as being computationally efficient, having low memory requirements, being invariant to diagonal rescaling of gradients, and being well suited for problems with sparse gradients or noisy data. The same steps are applied to update  $b_l$  using  $\delta b_l$ .

## 7.4.2 Preprocessing data and hyperparameters

Preprocessing data is an important step in preparing input data for neural networks to ensure accurate predictions. It involves tasks such as data cleaning to correct errors and inconsistencies, data normalization to scale input features to a similar range, and data augmentation to create new training examples. Other techniques such as feature selection, dimensionality reduction, and data encoding may also be used. The specific preprocessing steps used depend on the data set and the requirements of the neural network being trained.

When we train a model, we usually specify two parameters: batch size, epochs. These parameters control how the model updates its weights and how many times it sees the whole dataset. Batch size is the number of samples that are processed by the model in one iteration. A batch is a subset of the dataset that fits into memory and can be fed to the model at once. The model computes the loss and gradients for each batch and updates its weights accordingly. Number of Epochs is the number of times that the model sees the entire dataset during training. One epoch consists of multiple iterations, depending on how many batches are needed to cover all samples in the dataset. The model learns from each epoch and improves its performance over time. Steps per epoch is the number of batches that are performed in one epoch. This

parameter can be calculated by dividing the total number of samples by the batch size, or it can be specified manually. For example, if we have 1000 samples and a batch size of 100, then we need 10 steps per epoch to complete one epoch. These parameters can be adjusted according to our data size, memory capacity and training objective. Generally speaking, smaller batches require more epochs to converge, but they may also prevent overfitting and improve generalization. Larger batches may speed up training but they may also cause gradient issues and reduce accuracy.

### 7.4.3 Regularisation techniques

Overfitting occurs when a neural network becomes too complex and starts to memorize the training data rather than learning to generalize to new, unseen data. This can result in the neural network performing very well on the training data but poorly on the test data. Overfitting can be caused by having too many neurons or layers in the network, or by training for too many epochs.

Underfitting, on the other hand, occurs when a neural network is not complex enough to capture the underlying patterns in the data. This can result in the neural network performing poorly on both the training and test data. Underfitting can be caused by having too few neurons or layers in the network, or by not training for long enough.

Regularization techniques are methods that can prevent overfitting in deep learning models and improve their generalization performance on new data. Regularization techniques aim to reduce the variance of the model without increasing the bias too much.

Some of the common regularization techniques in deep learning are:

- L1 regularization: This technique adds a penalty term to the loss function that is proportional to the absolute value of the weights. This encourages the model to learn sparse weights and perform feature selection.
- L2 regularization: This technique adds a penalty term to the loss function that is proportional to the square of the weights. This encourages the model to learn small weights and reduce their influence on the output.

- **Dropout:** This technique randomly drops out some units and their connections during training, creating a thinned network. This reduces co-adaptation of features and forces the model to learn more robust representations.
- **Batch normalization:** This technique normalizes the inputs of each layer by subtracting the mean and dividing by the standard deviation of each mini-batch. This reduces internal covariate shift and allows for faster training and higher learning rates.
- **Early stopping:** This technique stops training when a validation metric stops improving for a certain number of epochs. This prevents overfitting by avoiding training for too long.

## 7.5 Environment and Hardware for Neural Network Training

There are several popular environments for neural network training, including TensorFlow, PyTorch, and Keras. TensorFlow, an open-source platform developed by Google, is popular for deep learning tasks and provides good support for distributed training across multiple GPUs. However, it can be complex to use, particularly for beginners, and debugging and error handling can be challenging. PyTorch, an open-source machine learning library developed by Facebook, is known for its flexibility and ease of use, particularly in the research community. It provides good support for dynamic computational graphs but distributed training can be challenging. Keras, an open-source neural network library written in Python, provides a high-level API that is easy to use but may not be suitable for complex models.

When it comes to hardware, the choice will depend on the model's size and complexity, as well as the budget. GPUs are well-suited for training deep neural networks, as they can perform many calculations in parallel, significantly speeding up training time compared to using a CPU. However, GPUs can be expensive and may require additional setup and configuration. TPUs are Google's custom-built hardware for accelerating machine learning workloads and are particularly well-suited for training large neural networks. They can provide significant speedups but may not be as widely available as GPUs and may require additional setup and configuration compared to CPUs.

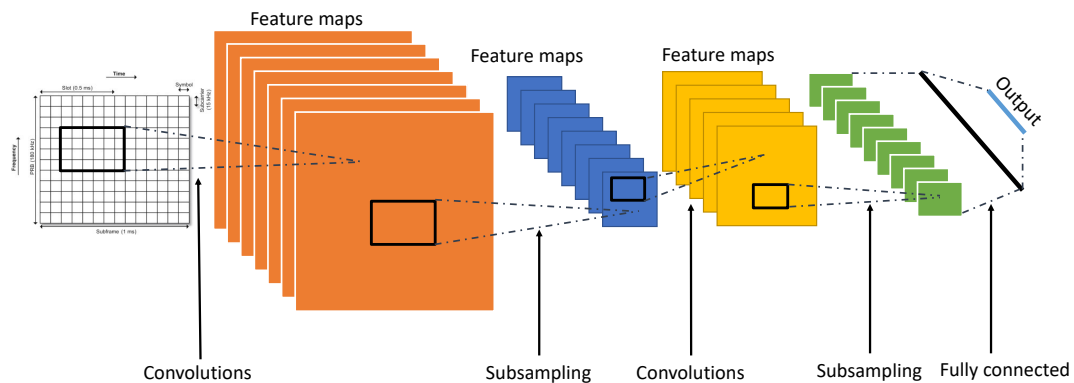


Fig. 7.3 Convolutional Neural Network

## 7.6 Convolutional Neural Network

A convolutional neural network (CNN) is a type of neural network that is designed to process pixel data such as images, speech or signals. A CNN differs from a traditional neural network by using a mathematical operation called convolution instead of general matrix multiplication in at least one of its layers. Convolution allows a CNN to learn local features from small regions of the input data, which can then be combined to form higher-level features. As shown in the figure 7.3, a typical CNN is composed of three main types of layers: convolutional layers, pooling (subsampling) layers, and fully-connected layers. The convolutional layer uses a set of filters or kernels to extract features from the input data, resulting in a set of feature maps that capture different aspects of the data. The pooling layer then applies a downsampling operation, such as max-pooling or average-pooling, to reduce the size and complexity of the feature maps. Finally, the fully-connected layer connects all nodes from the previous layer to every node in the next layer, allowing the network to perform classification or regression tasks.

A convolutional layer operates by sliding filters across the input data, computing element-wise products between them, and summing up the results to generate a single value for each position on the feature map. Filters can be visualized as small windows that extract local information from the input data. By being shared across all positions on the feature map, filters reduce the number of parameters and enable translation-invariant learning.

In a convolutional neural network, a kernel or filter is a matrix of weights that moves over the input data, performs element-wise multiplication, and sums up the

results to generate an output value. The kernel acts as a feature detector that extracts pertinent information from the input data. A convolutional layer can have multiple kernels that produce different output values for the same input region.

The kernel/filter size determines the output of a convolutional layer by controlling the number of input values involved in generating a single output value. A larger kernel captures more global features but reduces spatial resolution. In contrast, a smaller kernel captures more local features but increases computational cost and the risk of overfitting.

Stride is a parameter that controls how much the kernel/filter moves across the input data in each step. A larger stride means that the kernel/filter skips some input regions, which can reduce the output size and speed up computation but also lose some information and features. A smaller stride means that the kernel/filter covers more input regions, which can increase the output size and accuracy but also slow down computation and increase memory usage. Padding is a technique of adding extra pixels around the input data before applying a convolutional layer. The purpose of padding is to preserve the original size of an image when applying a convolutional filter and enable the filter to perform full convolutions on the edge pixels. Padding can also help avoid information loss and improve performance by allowing more flexibility in choosing the kernel/filter size and stride.

A subsampling layer works by dividing each feature map into non-overlapping regions and applying an aggregation function such as max or average to each region. This reduces the spatial dimensions and noise level of the feature maps, while preserving their most important information. Pooling also introduces some degree of invariance to small translations, rotations or scalings in the input data.

The CNN in the Figure 7.3 includes a convolutional layer that generates feature maps and a subsampling layer that reduces the dimensionality of the output. Additionally, there is a fully connected layer that connects every node from the previous layer to every node in the next layer, forming a standard neural network layer that performs classification or regression tasks.

The output of the CNN depends on the specific application, but it typically provides predictions or classifications based on the input data. The architecture of the CNN can be adapted to different data types and applications by modifying the number and type of layers, the kernel/filter size, and the stride. CNNs can also be trained using SGD, as they are also differentiable with respect to their weights.



However, SGD may not be optimal for CNNs, as they have many more parameters than FFNNs and may suffer from slow convergence or local minima. Therefore, other variants of SGD or other optimization algorithms may be preferred for CNNs, such as momentum, adaptive gradient algorithm, RMSProp, Adam, etc.

## 7.7 Recurrent Neural Network

Recurrent neural networks (RNNs) are specialized neural networks that are designed to handle sequential data such as time-series data, natural language text, and speech or audio signals. Unlike feedforward neural networks, RNNs contain loops that allow information to be retained and passed on from one step of the sequence to the next, making them ideal for processing data with temporal dependencies. Recurrent neural networks (RNNs) address this issue by incorporating a hidden state or memory that holds the essence of what has been seen so far. The value of the hidden state at any point in time  $t$  is a function of the value of the hidden state at the previous time step  $t - 1$ , and the value of the input at the current time step  $x_t$ :

$$h_t = \phi(h_{t-1}, x_t). \quad (7.24)$$

Here,  $h_t$  and  $h_{t-1}$  are the values of the hidden states at time  $t$  and  $t - 1$ , respectively, and  $x_t$  is the value of the input at time  $t$ . This equation is recursive, which means  $h_{t-1}$  can be represented in terms of  $h_{t-2}$  and  $x_{t-1}$ , and so on, until the beginning of the sequence. This is how RNNs encode and incorporate information from arbitrarily long sequences. Figure 7.4 shows a graphical representation of an RNN cell.

At time  $t$ , the cell has an input  $x_t$  and output  $y_t$ . Part of the output  $y_t$  (represented by the hidden state  $h_t$ ) is fed back into the cell for use at a later time step  $t + 1$ .

Just as in a feed-forward neural network, where the learned parameters are stored as weight matrices, the RNN's parameters are defined by the three weight matrices  $U$ ,  $V$ , and  $W$ , corresponding to the weights of the input, output, and hidden states, respectively. Figure 7.5 shows the same RNN in an "unrolled view". Unrolling means that we draw the network out for the complete sequence. The network shown here has three time steps, suitable for processing three-element sequences. Note that the weight matrices  $U$ ,  $V$ , and  $W$  are shared between each of the time steps because we are applying the same operation to different inputs at each time step. Sharing

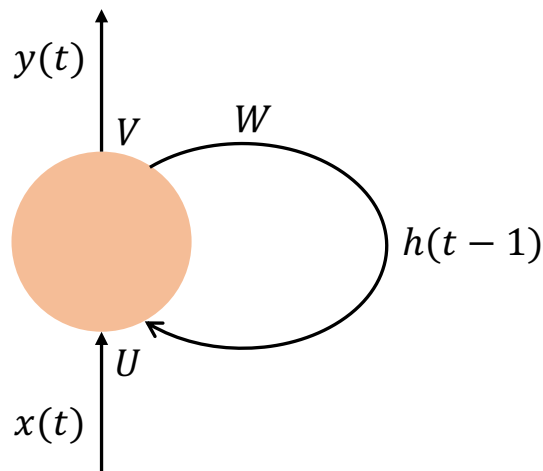


Fig. 7.4 Graphical representation of an RNN cell.

these weights across all the time steps greatly reduces the number of parameters that the RNN needs to learn.

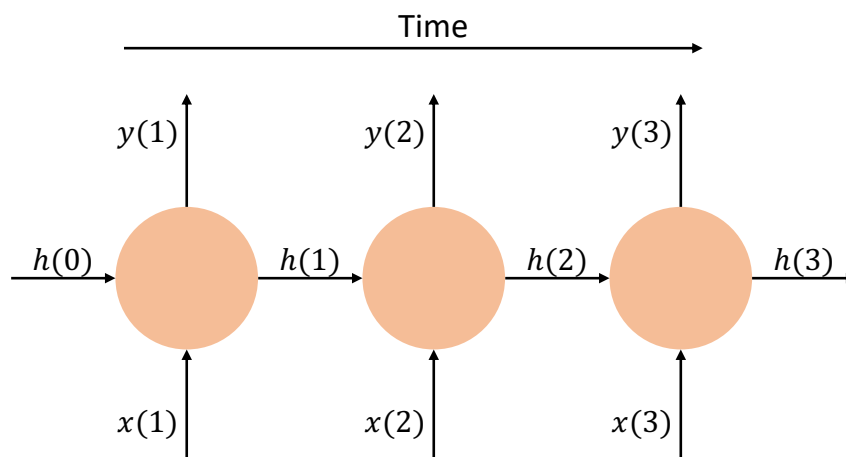


Fig. 7.5 Unrolled view of the same RNN. The weight matrices  $U$ ,  $V$ , and  $W$  are shared across all time steps.

### 7.7.1 Training RNN and vanishing gradient problem

To train an RNN, we typically use backpropagation through time (BPTT), which is a variant of backpropagation that takes into account the recursive nature of the RNN. Specifically, BPTT involves computing the gradients of the loss with respect to the RNN's parameters at each time step, and then accumulating those gradients over the entire sequence before updating the parameters. Mathematically, we can express this

as follows: Let  $L_t$  be the loss at time  $t$ ,  $W^l$  and  $b^l$  be the weight and bias parameters of layer  $l$ , and  $h_t$  be the hidden state at time  $t$ . Then, we can compute the gradients of the loss with respect to the RNN's parameters as:

$$\frac{\delta L_t}{\delta W^l} = \sum_{k=1}^t \frac{\delta L_t}{\delta h_t} \frac{\delta h_t}{\delta h_k} \frac{\delta h_k}{\delta W^l}, \quad (7.25)$$

$$\frac{\delta L_t}{\delta b^l} = \sum_{k=1}^t \frac{\delta L_t}{\delta h_t} \frac{\delta h_t}{\delta h_k} \frac{\delta h_k}{\delta b^l}, \quad (7.26)$$

where the partial derivatives are computed using the chain rule. These equations show that the gradients at time  $t$  depend on the gradients at all previous times, which is a consequence of the recursive nature of the RNN. The vanishing gradient problem arises when the gradients computed during BPTT become very small as they are propagated through time, making it difficult for the RNN to learn long-term dependencies. Mathematically, this can be seen by analyzing the partial derivatives in Equations 7.25 and 7.26. Specifically, if the partial derivative  $\frac{\delta h_t}{\delta h_k}$  is less than 1 for all  $k < t$ , then the gradients at time  $t$  will be multiplied by this term  $t - k$  times as they are backpropagated through time. This can cause the gradients to shrink exponentially as  $t$  increases, leading to the vanishing gradient problem.

One common solution to the vanishing gradient problem is to use a variant of the RNN called a long short-term memory (LSTM) network, which uses specialized memory cells and gating mechanisms to control the flow of information through the network. Another solution is to use a variant called a gated recurrent unit (GRU), which also uses gating mechanisms but with fewer parameters than an LSTM.

### 7.7.2 Long Short-Term Memory

LSTM stands for Long Short-Term Memory, which is a type of recurrent neural network (RNN) architecture. It was designed to address the limitations of traditional RNNs, which tend to struggle with capturing long-term dependencies in sequential data [110].

LSTMs introduce a more complex computational unit called a "memory cell". The memory cell allows the network to selectively "remember" or "forget" information from previous time steps, which makes it better suited for capturing long-term dependencies. The LSTM cell has three gates, namely, the input gate, forget gate,

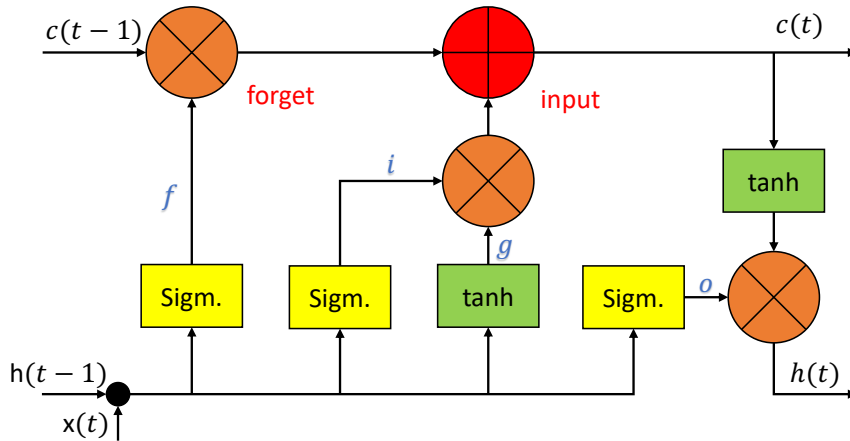


Fig. 7.6 A diagram of the Long Short-Term Memory (LSTM) cell.

and output gate, which control the flow of information (Figure 7.6). The input gate regulates how much of the current input to allow into the memory cell, the forget gate controls how much of the previous memory to discard, and the output gate controls how much of the current memory to output.

Furthermore, LSTMs have a set of learned parameters that allow them to adapt to the specific task at hand. During training, these parameters are updated using backpropagation through time, which enables the network to learn to selectively remember or forget information from previous time steps to optimize the loss function. Figure 7.6 illustrates the diagram of the Long Short-Term Memory (LSTM) cell. The set of equations representing an LSTM are shown as follows:

$$i = \sigma(W_i x_t + U_i h_{t-1} + b_i), \quad (7.27)$$

$$f = \sigma(W_f x_t + U_f h_{t-1} + b_f), \quad (7.28)$$

$$o = \sigma(W_o x_t + U_o h_{t-1} + b_o), \quad (7.29)$$

$$g = \tanh(W_g x_t + U_g h_{t-1} + b_g), \quad (7.30)$$

$$c_t = (f \cdot c_{t-1}) + (g \cdot i), \quad (7.31)$$

$$h_t = \tanh(c_t) \cdot o. \quad (7.32)$$

The input, forget, and output gates, denoted as  $i$ ,  $f$ , and  $o$  respectively, are computed using the same equations but with different parameter matrices  $W_i$ ,  $U_i$ ,  $W_f$ ,  $U_f$ ,  $W_o$ , and  $U_o$ . The sigmoid function ( $\sigma$ ) modulates the output of these gates between 0 and

1, allowing the output vectors produced to be multiplied element-wise with another vector to determine how much of the second vector can pass through the first one. The forget gate determines how much of the previous state  $h_{t-1}$  should be allowed to pass through, while the input gate determines how much of the newly computed state for the current input  $x_t$  should be let through. Similarly, the output gate determines how much of the internal state should be exposed to the next layer. The internal hidden state  $g$  is computed based on the current input  $x_t$  and the previous hidden state  $h_{t-1}$ .

Using the values of input gate ( $i$ ), forget gate ( $f$ ), output gate ( $o$ ), and internal hidden state ( $g$ ), the cell state  $c_t$  at time  $t$  can be computed. This is achieved by multiplying the previous memory stored in the cell state  $c_{t-1}$  by the forget gate value  $f$ , and adding the internal hidden state  $g$  multiplied by the input gate value  $i$ . This operation combines the information from the previous memory with the new input, where setting the forget gate to 0 ignores the old memory and setting the input gate to 0 ignores the newly computed state.

### 7.7.3 Bi-directional Long Short Term Mermory

Bi-LSTM is a type of recurrent neural network (RNN) that can process sequential data in both forward and backward directions. Bi-LSTM consists of two LSTM layers: one that takes the input from left to right (forward LSTM), and one that takes the input from right to left (backward LSTM). The outputs of both LSTM layers are then concatenated or summed to form the final output. Bi-LSTM can capture both past and future contexts of a sequence, which can improve the performance of tasks such as natural language processing, speech recognition, and signal classification.

The main benefit of using a bidirectional LSTM (BiLSTM) is that it allows the model to capture both past and future context information in a time series problem, which can be helpful for making accurate predictions. In a standard unidirectional LSTM, the model processes the input sequence only in one direction, either past or future. However, a BiLSTM processes the input sequence in both directions simultaneously, using two separate hidden states. This enables the model to capture both past and future context information and make more accurate predictions for future time steps.

However, using Bi-LSTM for signal processing also poses some challenges. The bidirectional nature of Bi-LSTM makes it difficult to process signals in real time, as it requires the entire sequence to be available before generating outputs. This may limit its applicability for online or streaming scenarios. The performance of Bi-LSTM depends on various hyperparameters such as the number of hidden units, layers, dropout rate, learning rate, etc. These hyperparameters need to be carefully tuned to optimize the model for different signal processing tasks and datasets. The complexity and computational cost of Bi-LSTM may be high compared to other simpler or more efficient models such as convolutional neural networks (CNNs) or transformers. This may affect its scalability and feasibility for large-scale or resource-constrained applications.

To enable real-time processing with Bi-LSTM, some techniques such as teacher forcing [111], scheduled sampling [112], beam search [113], etc. can be used to generate outputs without waiting for the entire sequence. To optimize the hyperparameters of Bi-LSTM automatically or efficiently, some methods such as grid search [114], random search [115], Bayesian optimization [116], etc. can be applied to explore the parameter space intelligently. To reduce the complexity and computational cost of Bi-LSTM without compromising its performance significantly, some strategies such as pruning [117], distillation [118], etc. can be employed to compress or simplify the model structure or parameters.

There are some similarities between Bi-LSTM and communication algorithms like BCJR. BCJR (Bahl, Cocke, Jelinek, and Raviv) algorithm is a classic algorithm used in communication systems for decoding error-correcting codes. It is a maximum likelihood decoder that uses the Viterbi algorithm to find the most likely sequence of transmitted symbols given the received symbols.

The similarity between Bi-LSTM and BCJR lies in the fact that both use the concept of forward and backward propagation. In Bi-LSTM, the forward and backward LSTMs process the input sequence in opposite directions to capture past and future dependencies, while in BCJR, the forward and backward passes are used to compute the posterior probabilities of the transmitted symbols given the received symbols.

Additionally, both Bi-LSTM and BCJR involve some form of probability calculations. Bi-LSTM uses a softmax layer to predict the probability distribution over

possible output classes, while BCJR uses a metric called the log-likelihood ratio to compute the posterior probabilities of the transmitted symbols.

## 7.8 Neural Networks improves OFDM systems

Neural Networks has been successfully applied to various domains, such as computer vision, natural language processing and speech recognition. Recently, there has been a growing interest in applying deep learning to the physical layer of wireless networks, especially OFDM systems. However, most of the existing works focus on the upper layers of wireless networks, such as routing, resource allocation and security. In this section, we want to provide a comprehensive survey of the deep learning techniques that have been proposed for the physical layer of OFDM systems. We will classify them into different categories based on their objectives and architectures, and compare their advantages and disadvantages. We will also discuss some open challenges and future directions for this emerging research area.

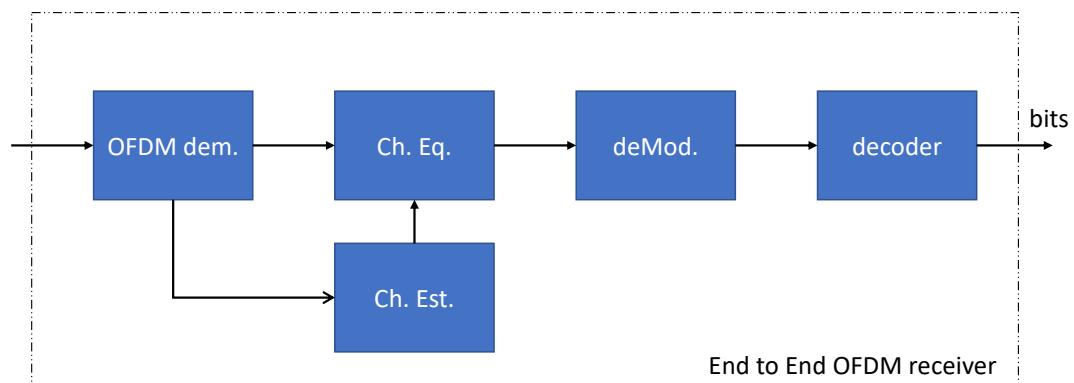


Fig. 7.7 An illustration of an end-to-end deep learning receiver for an OFDM system. The received OFDM signal is directly fed into a neural network that performs all the functions of the OFDM receiver, including demodulation, channel estimation, channel equalization, demodulation providing soft information, and channel decoding, resulting in bits.

One possible way to substitute the receiver block with a neural network is to use an end-to-end [119] deep learning approach (Figure 7.7). This approach involves designing a single neural network that takes in the received OFDM signal and directly outputs the bits without explicitly performing the individual steps of the OFDM receiver. The neural network is trained on a large data-set of OFDM signals with known payloads and their corresponding bits. The advantage of this approach is

that it can potentially improve its performance since the neural network can learn to compensate for the channel effects and other impairments in the OFDM signal. However, this approach requires a large amount of training data and significant computational resources to train and run the neural network.

Another possible option is to use a neural network to replace specific blocks in the OFDM receiver, such as channel estimation [120–123], signal detection [124–128], and interference mitigation [129].

Neural networks can offer several potential benefits for OFDM systems compared to traditional techniques. For example, neural networks can adapt to different channel conditions and modulation schemes without requiring explicit knowledge of the channel model or the cyclic prefix length [130]. Furthermore, neural networks can improve the performance of OFDM systems in terms of bit error rate (BER) [123, 131], spectral efficiency [122, 132] and energy efficiency [133] by exploiting deep features of the received signals and optimizing the system parameters.

The best practices for implementing neural networks in OFDM systems depend on several factors, such as the available computational resources, the amount and quality of training data, and the desired performance metrics. Some general guidelines are:

- Choose an appropriate type and architecture of neural network for each stage of an OFDM system based on its characteristics and requirements.
- Use lightweight neural networks with fewer layers and parameters to reduce computational complexity and power consumption.
- Use modular neural networks that can be trained separately for each stage of an OFDM system to improve flexibility and scalability.
- Use adaptive learning algorithms that can update the neural network parameters online based on feedback signals or changing channel conditions.
- Use regularization techniques such as dropout or batch normalization to prevent overfitting and improve generalization.

However, there are also some limitations and drawbacks of using neural networks in OFDM systems. One limitation is that neural networks require a large amount of



training data to achieve good performance, which may not be available or feasible in some scenarios. Another limitation is that neural networks may suffer from overfitting or underfitting problems if the network architecture or hyperparameters are not properly chosen or tuned. A drawback is that neural networks introduce additional complexity and computational requirements to the OFDM system design and implementation. For example, neural networks may require more memory and processing power than conventional OFDM techniques such as pilot-based channel estimation or FFT-based data detection. Moreover, neural networks may have higher latency and energy consumption than traditional OFDM methods due to their iterative nature.

### 7.8.1 Channel estimation with neural network

Recently, neural network (NN) based channel estimation has emerged as a promising alternative that can exploit the nonlinear relationship between the received signal and the channel state information (CSI) without relying on explicit channel models. NN based channel estimation can be broadly classified into two categories: pilot-based [134, 135] and blind-based [136] approaches. Pilot-based approaches use pilot symbols as inputs to train and test the NN, while blind-based approaches use only data symbols as inputs and exploit some inherent features of OFDM signals such as cyclostationarity or sparsity. Both approaches have shown superior performance over conventional methods in various scenarios such as underwater acoustic OFDM, massive MIMO-OFDM and time-varying OFDM [134–136].

Several studies have proposed FFNN-based channel estimation methods for OFDM systems with different architectures, settings and performance metrics. For example, [137] proposed a fuzzy logic-based neural fuzzy network (FLNFN) algorithm that combines fuzzy logic rules with an FFNN to enhance the accuracy and robustness of channel estimation in various OFDM channel environments.

CNNs offer several advantages for channel estimation in OFDM systems compared to FFNNs [138–140]. First, CNNs can exploit the local correlation and sparsity of the channel in different domains, such as angle-delay, spatial-frequency, or time-frequency domains. By using appropriate convolutional filters and pooling layers, CNNs can reduce the complexity and enhance the denoising ability of channel estimation. Second, CNNs can leverage the Transformer architecture [141] to capture

the long-range dependencies and attention mechanisms of the channel. This can improve the accuracy and robustness of channel estimation for OFDM systems with pilots. Third, CNNs can be combined with RNNs or long short-term memory (LSTM) networks to model the temporal dynamics of the channel [138]. This can further improve the performance of channel estimation for time-varying scenarios.

RNNs can be used for channel estimation in an OFDM system by taking advantage of the temporal correlation of the channel coefficients across different OFDM symbols [142, 143]. However, RNNs also has limitation compared to other types of neural networks for channel estimation in an OFDM system. RNNs may have higher computational complexity and latency than feed-forward neural networks (FFNs) or CNNs due to their sequential processing nature.

Recent research has explored the use of LSTM for channel estimation in OFDM systems. For example, Wang et al. [144] proposed an online channel estimation method that uses an LSTM network to estimate channel coefficients from received pilot symbols. The LSTM network is trained using a recursive least squares (RLS) algorithm that updates the network weights as new pilot symbols are received. Gizzini et al. A temporal-domain channel estimation method proposed in [145], that also uses an LSTM network. Their method exploits the temporal correlation of the channel coefficients across multiple sub-carriers and multiple OFDM symbols to improve channel estimation accuracy.

One of the main advantages of using LSTM-based methods for channel estimation is that they do not rely on any prior knowledge or assumptions about the channel statistics or structure. Moreover, they do not require any matrix inversion or interpolation operations that are commonly used in conventional methods such as LS or MMSE estimations. Another advantage of LSTM-based methods is their ability to adapt to different scenarios such as different signal-to-noise ratios (SNRs), modulation schemes, pilot patterns, and channel models by adjusting their network parameters during training.

Although the use of LSTM-based methods for channel estimation in OFDM systems is a relatively new area of research, these methods have shown promising results and are expected to receive more attention in the future.

Although using variations of LSTM-based methods for channel estimation in OFDM systems, such as using CNNs [146] or FFNNs as feature extractors and using attention mechanisms or GANs to improve performance, appears to be an attractive

approach, there is limited research exploring the practical implementation of these methods. While some initial studies have shown promising results, further research is needed to fully understand their potential and practicality in real-world scenarios.

Compared to other types of neural networks, such as feedforward neural networks (FFN), convolutional neural networks (CNN), and unidirectional LSTM, Bi-LSTM offers several advantages for channel estimation in OFDM systems [147]. Bi-LSTM can capture both long-term and short-term dependencies among the channel coefficients, which are essential for dealing with time-varying channels. FFNN and CNN have limited memory capacity and cannot model long-term dependencies effectively. Unidirectional LSTM can only exploit past information but not future information, which may result in suboptimal performance loss. Bi-LSTM can adapt to different scenarios with different pilot patterns or modulation schemes by adjusting its parameters during training.

### **7.8.2 Data Detection with neural network**

In an OFDM system, the choice of neural network approach for detection depends on various factors, including the desired accuracy, available training data, and computational complexity. One of the popular methods is end-to-end learning [148, 119], where the neural network is trained to map the received OFDM symbols directly to the corresponding transmitted symbols (Figure 7.7). This approach doesn't require explicit feature extraction and can lead to better performance in cases where there are complex dependencies between the transmitted and received symbols. Another method is feature-based learning, where the neural network is trained to extract useful features from the received symbols, which are then used for detection [149]. This method can be useful when there are fewer training data available, and feature engineering can provide a better representation of the signal. A third method is joint detection and decoding [150, 151], where the neural network performs both detection and decoding. This method can achieve better performance in systems with a high degree of channel noise and interference. Finally, a hybrid approach to data detection in OFDM systems that incorporates neural networks involves using a combination of traditional signal processing techniques and neural networks to improve the accuracy and efficiency of detecting data symbols from the received signal. [152].

FFNNs have been used for data detection, with good results in terms of accuracy and computational complexity [153]. However, they may not be able to capture the temporal dependencies between the symbols, which is important in OFDM signal detection. CNNs have also been used for data detection [125], with the advantage of being able to capture spatial dependencies between the symbols. However, they may require more training data and computational resources compared to FFNNs.

RNNs have been used for data detection, as they are able to capture the temporal dependencies between the symbols. LSTMs and Bi-LSTMs have also been used for data detection [154–156, 147], with the advantage of being able to capture long-term dependencies and bidirectional information, respectively. However, they may require more computational resources compared to FFNNs and CNNs.

### 7.8.3 Hybrid model

A hybrid model for OFDM systems combines traditional techniques and neural network techniques to improve OFDM system performance. This approach provides several advantages, including exploiting the strengths of both techniques, overcoming limitations and drawbacks of each technique, and achieving better trade-offs between conflicting objectives [157].

The benefits of a hybrid model depend on the specific application and scenario. For example, using a hybrid model based on deep learning can improve spectral efficiency and lower BER in aerial massive MIMO-OFDM systems with implicit CSI. Alternatively, a hybrid model based on alternating optimization can reduce transmit power consumption and enhance coverage performance in mmWave OFDM distributed antenna systems [158].

Design considerations for a hybrid model include neural network architecture and parameters, training data and objective function, optimization algorithm and convergence criterion, complexity-performance trade-offs, robustness against noise and interference, and compatibility with existing standards and protocols.

The performance of a hybrid model can be optimized for a given application by tuning factors such as antenna configuration, sub-carrier allocation, modulation scheme, coding rate, pilot pattern and power allocation, beamforming weights and directions, and neural network hyperparameters.

Limitations of hybrid models include the need for large amounts of training data and computational resources, difficulty interpreting or explaining neural network behavior, sensitivity to overfitting or underfitting problems, and lack of theoretical guarantees or performance bounds.

The complexity of a hybrid model compared to a traditional OFDM system or one that uses only neural network techniques depends on factors such as the type and number of operations, degree of parallelism or pipelining, hardware implementation cost and feasibility, and scalability with respect to system size and parameters.

#### **7.8.4 Insufficient CP and mobility**

Few research studies have focused on using deep learning to address the challenges of insufficient or absent cyclic prefix (CP) in OFDM systems recently. However, these studies have demonstrated promising results and highlighted the potential of neural networks to mitigate the negative effects of CP impairment [159, 160].

For example, [159] proposes DL-OAMP, a deep learning-based approach that addresses channel estimation and signal detection challenges in an OFDM system without CP. The proposed receiver comprises two neural networks: a channel estimation neural network (CE-Net) and an OAMP-Net for signal detection using Orthogonal Approximate Message Passing. The CE-Net uses the least square channel estimation algorithm for initialization, which is then refined using a minimum mean-squared error (MMSE) neural network. The OAMP-Net is constructed by unfolding the iterative OAMP algorithm and adding trainable parameters to enhance detection performance.

Using deep learning to address the challenges of insufficient or absent CP in OFDM systems is a promising approach that has the potential to improve system performance despite the limited number of research studies available.

On the other hand, there has been a significant increase in research studies that aim to address high mobility scenarios in OFDM systems using the capabilities of neural networks [161, 162]. Researchers have explored various approaches that leverage the power of neural networks. For example, some studies have investigated the use of CNNs for channel estimation [146] in high mobility scenarios. Other studies have proposed the use of recurrent neural networks (RNNs) for predicting the channel impulse response and compensating for the Doppler frequency shift [162].

The increasing number of research studies that explore the use of neural networks in addressing the challenges of high mobility scenarios in OFDM systems highlights the potential of this approach in improving the performance and reliability of future mobile communication systems.

While there has been significant research in the field of OFDM receiver based on neural networks, there is a lack of techniques that can effectively address insufficient cyclic prefix and inter-symbol interference over multiple OFDM symbols, especially in the presence of mobility. In the next chapter, we will introduce a technique that we have developed, which is specifically designed for 5G-NR SFN network broadcasting but can serve as a framework for all OFDM systems.

## Chapter 8

# 5G-NR broadcasting with bi-directional Long Short Term Memory Neural Network

In our earlier research on 5G-NR terrestrial broadcasting, we introduced a linear equalizer as outlined in [104]. However, we did not take into account the impact of mobility scenarios and channel estimation on the equalizer's performance. To address these limitations, we designed a radically new receiver that uses bidirectional long short-term memory (Bi-LSTM) to perform channel estimation, equalization, and LLR computation functions simultaneously, as described in [163]. Additionally, we enhanced the system's spectral efficiency by superimposing the data with the pilot signal at the transmitter instead of interspersing them. Our proposed channel estimation technique substantially reduces the overhead associated with pilot-aided methods. These findings demonstrate the effectiveness of our method in improving the performance of 5G-NR terrestrial broadcasting systems, especially in challenging scenarios with high mobility and strong inter-symbol interference (ISI).

Our neural network is designed to take in a sequence of received OFDM symbols,. The sequence includes both past and future OFDM symbols relative to the currently estimated symbol. The RNN output provides log-likelihood ration on the coded bits that are fed to the following channel LDPC decoder. In the paper we provide a detailed explanation of the RNN training process.

The most critical parameters for controlling the system's performance are the length of the OFDM sequences ( $M$ ) and the alpha ( $\alpha$ ) parameter, which determines the energy ratio between the pilot and data signals. We meticulously chose these hyperparameters to optimize the system's performance.

Our proposed approach outperforms the classical system that was specifically designed for the considered SFN scenarios, even in mobile scenarios. Furthermore, we demonstrate the versatility of our scheme in various scenarios by showcasing that a single RNN, trained at a fixed SNR and user speed, can achieve outstanding results in a wide range of SNRs and user speeds.

Our receiver design was primarily intended for 5G-NR terrestrial broadcasting under mobility conditions. However, it can be viewed as a general proposal for any wireless communication system that utilizes orthogonal frequency-division multiplexing (OFDM). By incorporating mobility constraints into the wireless communication system design, it becomes possible to eliminate the requirement for a cyclic prefix and improve spectral efficiency removing the correspondent overhead. However, it is essential to note that the complexity of implementing such a system poses a significant challenge. Nevertheless, our approach provides a valuable foundation for developing wireless communication systems that are more efficient and high-performing.

Possible future investigations pertaining to this problem include:

1. Adopting other advanced but classical receivers, combined with pilot superposition, to increase system efficiency for a mobile SFN with 5G-NR numerology.
2. Reducing the complexity of the RNN. The proposed Bi-LSTM structure is well-suited for the receiver, but may be too large as it was proposed for solving more complex issues. A deeper investigation into the required RNN features may lead to simpler structures and better understanding of the relationship between the RNN and classical advanced receivers based on MMSE and MLSE.
3. Investigating system performance with higher-order modulations that offer higher spectral efficiencies.
4. Scaling the proposed receiver solution to the practical bandwidth used in broadcasting.



5. Testing the flexibility of a single trained RNN for different network infrastructures (e.g., ISD) and, consequently, different delay spreads.

Additionally, we would like to highlight that the detailed information on the system's implementation, including the mathematical derivations of the proposed algorithms, the simulation setup, and the performance metrics used for the evaluation, can be found in the paper (Appendix B).

## **Appendix B**

# **Single-Frequency Network Terrestrial Broadcasting with 5G-NR Numerology Using Recurrent Neural Network**



*electronics*



Communication

---

# Single-Frequency Network Terrestrial Broadcasting with 5G NR Numerology Using Recurrent Neural Network

---

Majid Mosavat and Guido Montorsi

Special Issue

Machine Learning Applications to Signal Processing


Edited by

Dr. Youye Xie, Dr. Kai Liu and Dr. Zihui Zhu



<https://doi.org/10.3390/electronics11193130>

# Single-Frequency Network Terrestrial Broadcasting with 5G NR Numerology Using Recurrent Neural Network

Majid Mosavat \*  and Guido Montorsi \*

Department of Electronics and Telecommunications, Politecnico di Torino, 10129 Turin, Italy

\* Correspondence: majid.mosavat@polito.it (M.M.); guido.montorsi@polito.it (G.M.)

**Abstract:** We explore the feasibility of Terrestrial Broadcasting in a Single-Frequency Network (SFN) with standard 5G New Radio (5G NR) numerology designed for uni-cast transmission. Instead of the classical OFDM symbol-by-symbol detector scheme or a more complex equalization technique, we designed a Recurrent-Neural-Network (RNN)-based detector that replaces the channel estimation and equalization blocks. The RNN is a bidirectional Long Short-Term Memory (bi-LSTM) that computes the log-likelihood ratios delivered to the LDPC decoder starting from the received symbols affected by strong intersymbol/intercarrier interference (ISI/ICI) on time-varying channels. To simplify the RNN receiver and reduce the system overhead, pilot and data signals in our proposed scheme are superimposed instead of interspersed. We describe the parameter optimization of the RNN and provide end-to-end simulation results, comparing them with those of a classical system, where the OFDM waveform is specifically designed for Terrestrial Broadcasting. We show that the system outperforms classical receivers, especially in challenging scenarios associated with large intersite distance and large mobility. We also provide evidence of the robustness of the designed RNN receiver, showing that an RNN receiver trained on a single signal-to-noise ratio and user velocity performs efficiently also in a large range of scenarios with different signal-to-noise ratios and velocities.

**Keywords:** OFDM; channel estimation; channel equalization; data detection; neural network; RNN; LSTM; 5G NR; broadcasting



**Citation:** Mosavat, M.; Montorsi, G. Single-Frequency Network Terrestrial Broadcasting with 5G NR Numerology Using Recurrent Neural Network. *Electronics* **2022**, *11*, 3130. <https://doi.org/10.3390/electronics11193130>

Academic Editor: Cheng-Chi Lee

Received: 24 August 2022

Accepted: 26 September 2022

Published: 29 September 2022

**Publisher's Note:** MDPI stays neutral with regard to jurisdictional claims in published maps and institutional affiliations.



**Copyright:** © 2022 by the authors. Licensee MDPI, Basel, Switzerland. This article is an open access article distributed under the terms and conditions of the Creative Commons Attribution (CC BY) license (<https://creativecommons.org/licenses/by/4.0/>).

## 1. Introduction

In a Single-Frequency Network (SFN) Terrestrial Broadcasting system based on Orthogonal Frequency Division Multiplexing (OFDM), all broadcasting stations simultaneously transmit the same OFDM signal over the same frequency channel. The signal propagates through different paths and reaches the receiver at separate times, creating an “artificial” delay spread. To compensate the different propagation delays and eliminate the ISI between received symbols, a Cyclic Prefix (CP) is appended to the transmitted symbol. The CP length is then designed to be greater than the echoes’ temporal dispersion, which, in turn, is related to the maximum Intersite Distance (ISD) of the considered broadcasting infrastructure. Most recent Terrestrial Broadcasting OFDM standards are based on this solution, such as DVB-T2 [1] and ATSC 3.0 [2].

LTE-based Terrestrial Broadcasting has also introduced two specific carrier spacings [3] to meet the requirements of a dedicated broadcast network. The 2.5 kHz carrier spacing with a 100  $\mu$ s CP length delivers mobile services to portable and handheld receivers with a 15 km ISD and a speed up to 250 km/h. The 0.37 kHz carrier spacing with a 300  $\mu$ s CP length is designed for roof-top reception and up to a 175 km ISD.

In strongly double-selective scenarios, the classical approach to the OFDM design of SFNs becomes progressively inefficient for the two following reasons. On the one hand, to prevent the ISI, the CP must be kept larger than the delay spread associated with the ISD, and at the same time, the symbol duration must be kept much smaller than the channel coherence time to prevent the ICI. The ratio of the CP to the symbol duration, representing

the system energy and throughput overhead, can become unacceptable. Furthermore, the pilot density required to efficiently estimate and interpolate the channel with a small coherence bandwidth and time becomes unacceptably high, introducing a further overhead.

Fifth-Generation New Radio (5G NR) defines OFDM numerologies designed only for uni-cast transmission, with larger carrier spacing (a minimum of 15 kHz) and characterized by a rather short CP (4.7  $\mu$ s). In this case, with a classical OFDM receiver, it is possible to support SFNs with a maximum of only a 5 km ISD [4], not compatible with most broadcaster infrastructures.

To support larger ISDs with 5G NR numerologies, the receiver must then be equipped with an advanced OFDM detector capable of dealing with a large ISI/ICI.

In [5], we proposed a linear 2D filter in the frequency domain for the equalization of the OFDM system in the presence of the ISI spanning several OFDM symbols. The results showed that, by using the channel shortening technique in [6], it is possible to obtain with 5G NR numerologies the same performance of OFDM systems specifically designed for SFN Terrestrial Broadcasting [3]. Those results, however, were based on a static channel and assumed the channel impulse response is known by the receiver.

In this paper, we approach the more realistic and challenging scenario, where on top of a strong ISI and ICI, due to the adoption of 5G NR numerology for SFN scenarios, the considered channel is very rapidly time-varying (mobile speed up to 200 km/h) and unknown to the receiver.

In the literature, the investigation of advanced receiver techniques for the compensation of the ISI/ICI in an OFDM system is broad, but limited to specific scenarios. For ADSL systems, which are characterized by quasi-static channels, the authors of [7] proposed an approach to compensate the effect of the channel within the CP in a static channel condition. In [8,9], the authors proposed low-complexity equalizers for video broadcasting in time- and frequency-selective channels, although the considered CP length was larger than the delay spread. The authors in [10] studied a one-tap decision feedback equalizer for an OFDM system with the ISI and ICI, but in a low-mobility environment. The authors of [11] designed a more complex system for a doubly dispersive multi-carrier system and focused on a large delay spread with an embedded channel encoder. The delay spread was within the OFDM symbol. Notice that most of these papers assumed channel state information is known by the receiver, a very strong assumption, especially in a mobile environment. Furthermore, in the literature on OFDM for the wireless channel, the amount of ISI is typically limited within one symbol period, while, in our problem, statement, it can last several OFDM symbols. While the adoption of advanced equalization techniques may eliminate the CP inefficiency by removing the constraint on the CP and symbol duration, the second source of inefficiency due to the required pilot density for channel estimation cannot be eliminated.

In this paper, we consider a more recent approach, where the totality or part of the receiver structure is substituted by the RNN. RNNs offer an impressive capability of adapting their behavior to solve very complex inference problems, and they have the ability to learn and extract information from time series [12]. In this research, for the first time, we used an RNN, bidirectional Long Short-Term Memory (bi-LSTM), in processing the 5G NR waveform to enable Terrestrial Broadcasting.

bi-LSTM [13] is a special kind of RNN composed of two chains of concatenated LSTM cells to which the data sequence is fed, once forward and once backward, and finally, concatenated. The structure is similar to that of the BCJR algorithm for maximum likelihood detection, where forward and backward recursions are performed to extract information from the past and future observations relevant for the target variable to be estimated. Each LSTM cell is composed of an input gate, forget gate, output gate, and one candidate memory cell [14].

The ability of the RNN to process time sequences was investigated also in the context of signal processing. For instance, the authors of [15] proposed a Sliding Bidirectional Recurrent Neural Network (SBRNN) for single-carrier real-time sequence detection. The

authors of [16] introduced a scheme for joint channel estimation and symbol detection for an OFDM system. The work in [17] proposed a deep-learning-assisted technique for signal detection in the up-link and fast time-varying channel with bi-LSTM. In [18], the authors proposed a neural network architecture named Cascaded Net (CN) for OFDM symbol equalization.

To the best of our knowledge, in the RNNs that have been proposed in the past for OFDM systems, the authors either assumed the channel impulse response length within the CP length (no ISI) or they did not investigate the OFDM symbol affected by the ISI and time-varying channel jointly. Furthermore, the authors used the classical OFDM approach for assigning specific resources for channel estimation, causing a large amount of overhead to be imposed on the system, especially in situations where the speed of the receiver is high and a dense pilot map is required. In most cases, the authors did not consider the presence of an outer forward error correction technique, e.g., Low-Density Parity Check Code (LDPC), and directly reported the bit error rate at the output of the detector as the key performance indicator.

To remove the two sources of inefficiency, due to the excessive CP length and pilot density, we propose a novel approach that embeds two solutions:

1. Replacement of the channel estimator, channel equalization, and LLR computation blocks with a recurrent neural network block;
2. Usage of superimposed pilots instead of interspersed pilots.

In the proposed receiver, the RNN detector is placed after the FFT and before the LDPC decoding. By suitably training it offline, the designed RNN receiver shows the appropriate flexibility to face rapid channel changes and strong ISI/ICI in a wide set of scenarios. The paper presents the detail of the careful optimization procedure of the RNN that led to the final design.

The rest of this paper is organized as follows. In Section 2, we provide the details of the considered channel models for the SFN scenario and the description of the reference classical OFDM system. We then describe our proposed receiver based on the RNN detector and superimposed pilots, discussing its complexity. In Section 3, we optimize the hyperparameters of the proposed RNN detector for two SFN infrastructures. In Section 4, we present end-to-end simulation results comparing and discussing the performance of the proposed approach with that of the reference system. Conclusions follow in Section 5.

## 2. Reference System and Proposed Approach with RNN and Superimposed Pilots

The considered OFDM system for Terrestrial Broadcasting in an SFN is shown in Figure 1. In the following sections, we provide the details on the channel model, the reference classical system, and the proposed approach, which includes the superposition of the pilots and the adoption of the RNN in a part of the receiver (modification highlighted in red in Figure 1).

### 2.1. Channel Model for SFN

The transmitted signal is sent through a Tapped Delay Line (TDL) channel model, which is characterized by its maximum delay spread. The considered TDL channel model (TDL-A) is the standard one defined in [19]. TDL-A is a challenging channel model for a non-line-of-sight environment. It is used also for modeling an SFN by properly scaling its maximum delay spread according to the considered ISD. In Table 1, we report the correspondence between the maximum delay spread in the TDL-A model and the considered ISD in the SFN for Low-Power Low-Tower (LPLT), Medium-Power Medium-Tower (MPMT), and High-Power-High Tower (HPHT) transmission networks.

**Table 1.** Correspondence between maximum delay spread and intersite distance for modeling SFNs.

Parameter	LPLT	MPMT	HPHT
ISD (km)	15	50	125
Delay spread ( $\mu\text{s}$ )	20	40	50

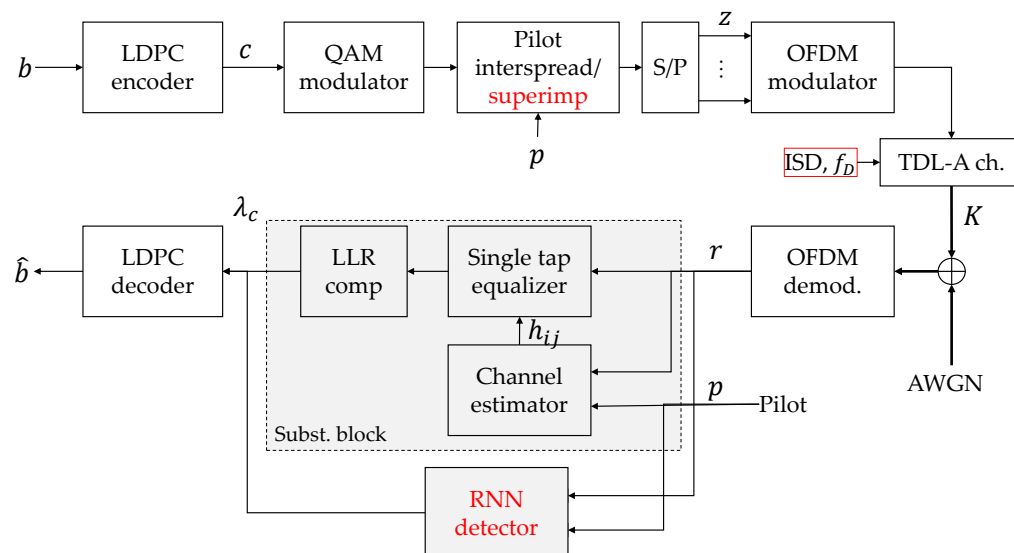


**Figure 1.** The OFDM system and position of the proposed RNN detector.

In all considered scenarios, we fixed the number of receiver antennas to  $K = 2$  and the carrier frequency to  $f_0 = 700$  MHz, a common choice for broadcasting. The considered maximum user speed is  $v = 200$  km/h, corresponding to a maximum Doppler frequency  $f_D = \frac{v}{c} f_0 = 129$  Hz, with Jake’s model for the spectrum of tap coefficients.

2.2. Classical Terrestrial Broadcasting in SFN

The stream of information bits  $b$  generated by the source is encoded by the channel encoder [20], producing the sequence of coded bits  $c$ . The encoded bits are converted to complex signals by the QAM modulator. For channel estimation, a properly designed pilot sequence  $p$  is interspersed with the information signals. The  $N$  parallel frequency domain signals are converted to the time domain via the Inverse Fast Fourier Transform (IFFT), and the CP with a suitable length is inserted to prevent the ISI (OFDM modulator block).

At the receiver side, time domain signals are received by  $K$  antennas. The OFDM demodulators, one for each receiving antenna, convert time domain signals to  $N$  parallel frequency domain signals. A pilot-assisted channel estimation is carried out using the transmitted pilot symbols. The considered channel estimation algorithm in the reference receiver uses least-mean-squares estimation and linear interpolation to obtain the channel gains on data subcarriers. A single tap equalizer is then used to provide the equalized signal. The LLR computation block calculates log-likelihood ratios on coded bits  $\lambda_n$  at time  $n$ , and the LDPC decoder processes the LLR to provide estimated bits  $\hat{b}$ .

It is well known that the performance of this simple receiver scheme is directly connected to the trade-offs between the CP length, channel delay spread, carrier spacing, and user mobility. In the standard design of OFDM numerology, the CP length is kept larger than the delay spread to prevent the ISI and OFDM symbol duration  $1/\Delta f$  is kept much smaller than the channel coherence time to prevent the ICI.

The 5G NR numerology with a short or very short OFDM symbol length makes possible the symbol-by-symbol detection of the OFDM symbol even with a high speed. However, the short CP length ( $4.7 \mu\text{s}$ ) of the 5G OFDM symbol is not compatible with the large ISD of the Terrestrial Broadcasting scenario (see Table 1). The delay spread of SFN environments

makes each transmitted OFDM symbol interfere with *several* contiguous OFDM symbols. The ISI between OFDM symbols destroys the orthogonality of carrier spacing, and the ICI occurs. Terrestrial Broadcasting with 5G NR numerology becomes impossible with the classical data detection scheme.

### 2.3. The Proposed Approach

The blocks highlighted in red in Figure 1 summarize the proposed modifications to the reference system.

#### 2.3.1. Superimposed Pilots

One major obstacle in adopting the RNN structure is that of properly exploiting the pilot sequence information that is provided as side information at the receiver for performing the required channel estimation task. When using pilot sequences interspersed with data symbols, the classical receiver exploits the knowledge of pilot positions to perform different operations at different time/frequency resources. Channel estimation is performed on pilot resources, while equalization, exploiting the channel estimation results, is performed on data resources. This non-stationary behavior of the classical receiver is incompatible with the RNN structure, which is intrinsically stationary, and information about the pilot position is difficult to embed in such structures. For this reason, at the transmitter side, instead of using the typical interspersing pilot technique, pilot and data signals are **superimposed**. The superimposed pilot approach has been already proposed and studied in advanced receivers [21]. At the price of introducing cross-interference between the data and pilots, it offers several advantages. No bandwidth overhead for channel estimation is introduced as all resources are assigned to data, and at the same time, pilot information is available at all resources for channel estimation. The cross-interference between the data and pilot, on the other hand, can be suitably removed by advanced cancellation techniques. In our case, this approach also circumvents the problem of exploiting the information on the pilot position at the RNN detector.

At the transmitter side, with superimposed pilots, the transmitted symbol at time  $n$  on carrier  $m$  is obtained as:

$$z_{mn} = d_{mn}\sqrt{1-\alpha^2} + p_{mn}\alpha \quad (1)$$

where  $d_{mn}$  is the data symbol and  $p_{mn}$  the pilot symbol. The single parameter  $\alpha$  controls the assigned energy ratio for the pilot and data signal.

#### 2.3.2. A Recurrent Neural Network Detector for SFN Terrestrial Broadcasting

In our proposed receiver in Figure 1, we substituted three blocks of the OFDM detector (channel estimator, channel equalizer, and LLR computation) with one RNN block.

The details of the RNN receiver are shown in Figure 2. The RNN includes two layers of bi-LSTM, two dropout layers, and one output dense SoftMax for delivering the bit log-likelihood vector.

With  $K$  receiving antennas, the demodulated OFDM symbol vector becomes  $r_n = [r_{11}, \dots, r_{1N}, \dots, r_{K1}, \dots, r_{KN}]_n$ , and the vector of reference known pilots is denoted by  $p_n = [p_1, \dots, p_N]_n$ . The available observation vector at time  $n$  at the RNN input is then the real vector  $y_n = [\Re[r_n, p_n], \Im[r_n, p_n]]$  with size  $2(K+1) \cdot N$ .

As transmission is affected by the ISI,  $M$  consecutive OFDM symbols are included for the data estimation, so that the input vector at time  $n$  to the RNNs is given by:

$$\bar{y}_n \triangleq [y_{n-\lfloor \frac{M}{2} \rfloor}, \dots, y_n, \dots, y_{n+\lfloor \frac{M}{2} \rfloor}]. \quad (2)$$

The complexity and representation capability of bi-LSTM is controlled by the number of LSTM cell units ( $U$ ), which also corresponds to the size of the output of each LSTM cell. The dropout layer is one regularization technique that is used only during network training



and prevents overfitting [22]. The dense layer maps the output of the previous layer to the dimensionality of the output space, which consists of  $N \times n_b$  bit log-likelihood ratios:

$$\lambda_i = \ln \left( \frac{q_i}{1 - q_i} \right), \tag{3}$$

where  $q_i$  is the  $i$ -th predicted probability of symbol “1”.

To train the RNN detector, we generated  $S$  pairs of  $\bar{y}_n$  and their target coded bits  $c_n$ . At each stage of one training epoch,  $B$  pairs (a batch) from  $S$  pairs are selected randomly and forwarded to the RNN detector. We calculated the error between the target and actual response of the RNN detector with the binary cross-entropy loss function, which is given by:

$$\delta = -\frac{1}{B} \frac{1}{N \cdot n_b} \sum_{j=1}^B \sum_{i=1}^{N \cdot n_b} [c_{ij} \cdot \log q_{ij} + (1 - c_{ij}) \cdot \log(1 - q_{ij})], \tag{4}$$

where  $B$  is the batch size and  $c_{ij}$  is the target bit value. The error  $\delta$  is then backpropagated along the network, revising the weights via the gradient descent algorithm [23]. This operation is repeated  $\frac{S}{B}$  times, and one epoch ends. In the next epoch, each batch is randomly created again, from the same set of  $S$  pairs, and the operation is repeated until an acceptable level of entropy is achieved at the end of an epoch.

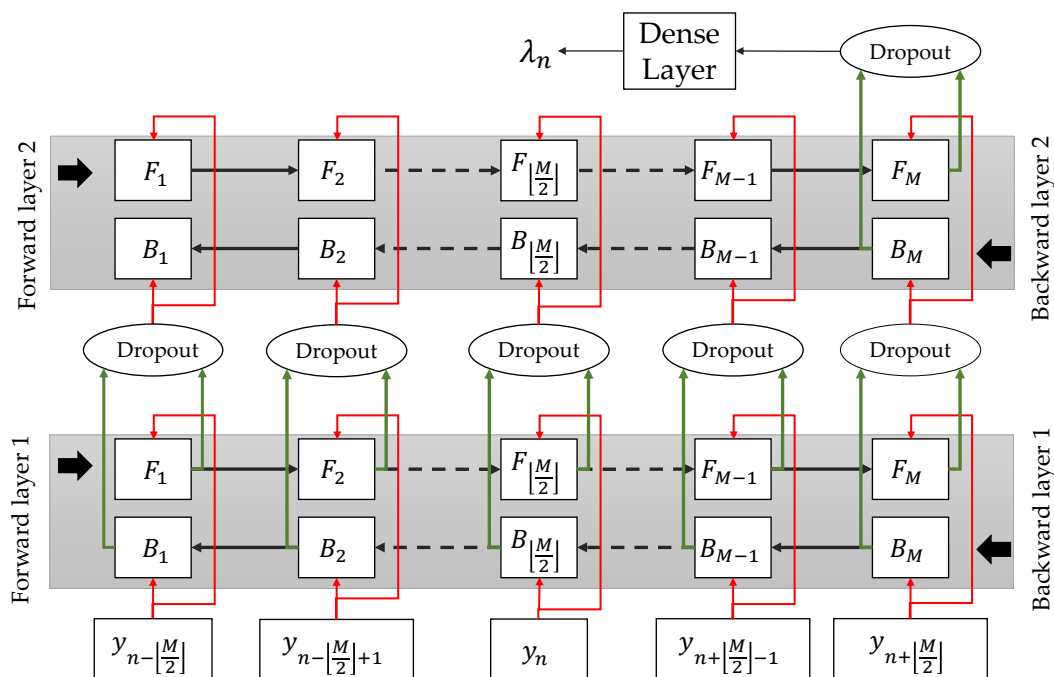


Figure 2. Unrolled RNN detector for an OFDM system ( $M$  is odd).

### 2.3.3. Discussion on RNN Detector Complexity

One of the major issues that prevents the adoption of RNNs as a substitute of the classical receiver structure is their complexity. The number of operations in each of the  $M$  cells in a single layer of bi-LSTM ( $F$ ), corresponding to the number of trainable parameters, is given by:

$$F = 2 \times 4 \times (I \times U + U^2 + U), \tag{5}$$

where  $I$  is the size of the input vector to each bi-LSTM layer. In our RNN in Figure 2,  $I = 2(K + 1) \cdot N$  for the first layer and  $I = 2 \cdot U$  for the second layer. The complexity of the RNN increases then linearly with the increasing size of input vector  $I$  and the sequence length  $M$ , but quadratically with the number of units. The output dense layer complexity amounts to  $n_b \times 2 \times U$  and is negligible. In this study, we fixed the number

of units to  $U = 400$  based on the work of [17]; all optimizations were performed based on this value, but according to further results presented in the final section of Table 2, similar entropy losses were obtained using lower values for the number of units. Using  $U = 100$ , although the training time increased, the performance became slightly better. In this case, the complexity of the system was reduced by a factor 1/16.

### 3. Optimization of RNN

In this section, we define the system parameters of the RNN. Then, the RNN parameters are optimized separately for one LPLT and one HPHT network.

#### 3.1. RNN System Parameters and Preliminary Data Generation for Training

For the RNN, we considered a system with 12 OFDM carriers with a carrier spacing of 15 kHz, yielding a system bandwidth of 180 kHz (one resource element in 5G New Radio) for link-level simulations. This small bandwidth was chosen to facilitate the RNN training process and can be increased to practical values for broadcasting, such as 10 MHz, in which case, the complexity of the receiver increases linearly by replicating the RNN detector for each resource block.

The OFDM symbol length is 71  $\mu$ s, including the normal CP (4.7  $\mu$ s). We used the 4-QAM constellation ( $n_b = 2$ ) corresponding to 24 coded bits transmitted per symbol.

The TDL-A channel model has 20  $\mu$ s and 50  $\mu$ s delay spreads, which are standard values for emulating LPLT and HPHT networks with 15- and 125-kilometer ISDs (see Table 1). We fixed the number of receiver antennas to  $K = 2$  and the carrier frequency to 700 MHz. The receiver speeds used for generating the training pairs were equal to 160 km/h for LPLT and 3 km/h for HPHT, which make the maximum Doppler shift around 103 and 3 Hz, respectively. Ten million pairs  $(y_n, c_n)$  at a fixed SNR = 5 dB were generated for parameter optimization and offline training, one for the LPLT network and one for the HPHT network. The ADAM optimizer [24] was used for training the RNN detector with a learning rate of 0.001. At the end of the training phase, we then generated two RNNs, one trained at 160 km/h for LPLT and one trained at 3 km/h for HPHT. These two RNNs are those used in all results reported in the final section. The Matlab platform was used to generate the input data sequences and output labels of the RNN. The RNN training was performed using Keras, a Python interface for the *Tensorflow* library. The trained RNN was then imported into MATLAB to check the system end-to-end performances.

#### 3.2. RNN Preliminary Hyper-Parameter Optimization for LPLT Network

The target free hyper-parameters for optimizing the proposed RNN system are the value of  $\alpha$  for pilot superposition, the length  $M$  of the input vector to the RNN, and the batch size  $B$  used for training. In the preliminary optimization step, we randomly generated 100 k arrays of  $\bar{y}_n$  with SNR = 5 dB and speed 160 km/h, each with size  $M$ , and corresponding target bits  $c$  from the data pairs created in the previous step. We then trained the network with 90 k arrays of  $\bar{y}_n$ , and the trained RNN detector was tested with the final 10 k of  $\bar{y}_n$ .

Some relevant results of the optimization campaign are reported in Table 2 for the LPLT network. In the second column of the table, we report the minimum binary cross-entropy ( $\delta$ ), and in the third column, the epochs were the minimum reached, to show the amount of time required for optimization.

Fixing  $B = 4096$  and  $M = 15$ , the assignment  $\alpha = 0.5$  provided minimum cross-entropy loss for the test data sequences.

Regarding the optimization of the length of the input observation window  $M$ , since the RNN performs both tasks of channel estimation and equalization,  $M$  is expected in general to be related to both the coherence time of the channel and the delay spread. In our scenario, having fixed  $\alpha = 0.5$  and  $B = 4096$ , the best trade-off was obtained for  $M = 15$ .

We finally examined the effect of batch size  $B$  for the RNN detector, with  $M = 15$  and  $\alpha = 0.5$ . Training the RNN detector with a larger batch size provided a lower binary cross-entropy loss.

Based on this initial parameter optimization, in the final RNN, we set  $\alpha = 0.5$ ,  $B = 4096$ ,  $M = 15$ , dropout to 0.5, and  $U = 400$ . To improve the performance, we increased the training set  $S$  to two million for each epoch, keeping the final 10k pairs for testing (last line in Table 2).

Considering that the RNN complexity is driven by the value of  $U$ , we also checked the network performance by reducing  $U$ . Results are reported in the third part of Table 2. It turned out that, in this case, reducing  $U$  may require a longer training time (third column of the table), but can lead to a network with better performances and lower complexity.

**Table 2.** RNN parameter optimization. Minimum binary cross-entropy loss of the validation data set for the LPLT SFN.

Parameters	Minimum Loss ( $\delta$ )	Minimum Epochs
$\alpha = 0.25$	0.4043	33
$\alpha = 0.5$	<b>0.3774</b>	32
$\alpha = 0.75$	0.442	40
$M = 7$	0.3953	38
$M = 15$	<b>0.3774</b>	32
$M = 21$	0.3972	38
$B = 64$	0.3921	20
$B = 256$	0.3839	15
$B = 4096$	<b>0.3774</b>	20
$U = 400$	0.3774	32
$U = 200$	0.3576	96
$U = 100$	<b>0.3481</b>	271
final LPLT RNN	<b>0.25</b>	56

### 3.3. RNN Hyper-Parameter Optimization for HPHT Network

The described LPLT parameter optimization was repeated for the HPHT network (see Table 3). In this case, the SNR was still fixed to 5 dB and the speed was set to 3 km/h.

We optimized parameter  $\alpha$  with  $M = 9$ ,  $B = 4096$ , and  $U = 400$ . The minimum cross-entropy loss was obtained with  $\alpha=0.5$ , which is the same result obtained for the LPLT network. Then, we optimized  $M$  fixing  $\alpha = 0.5$ . The value  $M = 9$  provided the best performance.

Due to the larger delay spread, as expected, the minimum loss obtained for HPHT was larger than that obtained for the LPLT RNN. For training the final network, setting  $M = 9$ ,  $\alpha = 0.5$ ,  $B = 4096$ , and  $U = 400$ , we increased  $S$  to three million (last line of Table 3).

**Table 3.** RNN parameter optimization. Minimum binary cross-entropy loss of the validation data set for the HPHT SFN.

Parameters	Minimum Loss ( $\delta$ )	Minimum Epochs
$\alpha = 0.25$	0.5057	27
$\alpha = 0.5$	<b>0.3926</b>	32
$\alpha = 0.75$	0.415	37
$M = 7$	0.4067	33
$M = 9$	<b>0.3926</b>	32
$M = 11$	0.3952	30
$M = 13$	0.3939	31
$M = 15$	0.3931	31
$M = 17$	0.3973	30
$M = 19$	0.4009	29
$M = 21$	0.4099	32
final HPHT RNN	<b>0.28</b>	56

#### 4. End-to-End Simulations Compared to a Reference Classical System

In this section, we present the performance of the two RNNs optimized in the previous section against a classical reference system, whose system parameters are described in the next subsection.

##### 4.1. Classical Reference System Numerologies and Pilot Signals

The Third Generation Partnership Project (3GPP) specified two numerologies in Long-Term Evolution (LTE) evolved Multimedia Broadcast Multi-cast Service (eMBMS) to address the requirements of a dedicated broadcast network. The first one, with a carrier spacing of 2.5 kHz with a 100 μs CP length, is designed for the LPLT SFN with a maximum ISD of 15 km. This solution provides high mobility supporting up to 250 km/h for broadcasting scenarios.

The second one, with a carrier spacing of 0.37 kHz and a 300 μs CP length, is designed to support the conventional HPHT SFN up to a 175 km ISD, targeting *fixed* roof-top reception. The performances of these systems in some typical broadcasting scenarios are available in [3,25].

Using the fixed bandwidth of 180 kHz considered for the RNN-based system, the number of carriers for the two systems is  $N = 180/2.5 = 72$  and  $N = 180/0.37 \approx 486$ , respectively.

The suggested pilot pattern in [26] to support the time-varying characteristic of the TDL-A channel requires 1 out of 4 resources allocated for the pilots, with pilot resource frequency spacing  $F_d = 2$  and time spacing  $T_d = 2$ . These values are reduced to 1 out of 6 in the roof-top scenario ( $F_d = 3, T_d = 2$ ).

##### 4.2. End-to-End Simulation for LPLT and HPHT SFN

The transmitted information throughput  $T$  (bits/s) of an OFDM system can be written as

$$T = R_s \times n_b \cdot N \times (\eta \times r_c), \tag{6}$$

where  $R_s$  is the OFDM symbol rate,  $\eta$  is the waveform efficiency, a factor smaller than one that accounts for the system overhead, and  $r_c$  is the code rate. The values of the parameters in Equation (6) differ for the two considered systems due to the different strategies for pilot insertion and different CP overheads. In our RNN system, the overhead is only due to the 5G NR CP insertion, and the efficiency amounts to  $\eta_{RNN} = 15/16 = 0.9375$ ; for the LPLT reference system, it is the product of the CP efficiency (400 μs/500 μs) and the pilot efficiency 3/4, so that, overall, the efficiency is  $\eta_C = 0.6$ .

To have a fair performance comparison, we fixed the same throughput, so that we adjusted the code rate  $r_c$  of the two systems to have a fixed product  $\eta \times r_c$ :

$$r_c^{(C)} \eta_C = r_c^{(RNN)} \eta_{RNN} \rightarrow r_c^{(C)} = 1.5625 \cdot r_c^{(RNN)}.$$

The performance comparison of the two systems (RNN system with 15 kHz 5G NR numerology, classical system with 2.5 kHz), in terms of the BER at the output of the 5G NR LDPC decoder, is shown in Figure 3. For both systems, we used an LDPC encoder with codeword block size 20k and a layered LDPC decoder with 25 iterations.

We report results with two target throughputs  $T1 = 114$  kbit/s and  $T2 = 162$  kbit/s. For  $T1$ , the corresponding code rate for the RNN system is  $r_{c,1}^{(RNN)} = 0.34$  and that required for the reference classical system is  $r_{c,1}^{(C)} = 0.53$ . For  $T2$ ,  $r_{c,2}^{(RNN)} = 0.48$  and  $r_{c,2}^{(C)} = 0.75$ .

The results acquired for the classical system are aligned with the results found in [25] for similar scenario settings. At  $BER = 10^{-3}$ , the RNN provides a gain of 2 dB for  $T1$  and a gain of 4 dB for  $T2$ . Notice that the RNN system with larger throughput  $T2$  (green curve) also outperforms the classical system with lower throughput  $T1$  (blue curve). Although the receiver was trained at  $SNR = 5$  dB, its performance remained excellent at different SNR values.

We also investigated the flexibility of the designed RNN, trained at a fixed speed of 160 km/h and SNR = 5 dB, for other mobile speeds. The results are depicted in Figure 4 for the same throughput of 138 kbit/s, corresponding to  $r_c^{(RNN)} = 0.41$  and  $r_c^{(C)} = 0.64$ .

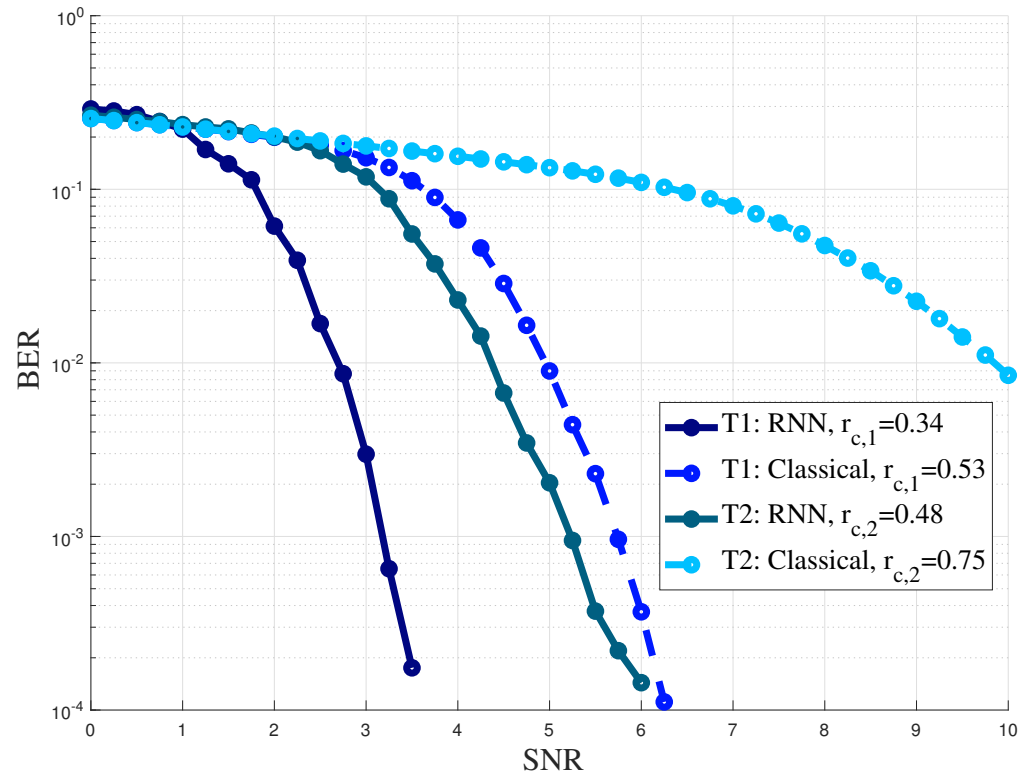


**Figure 3.** LPLT (ISD = 15 km). Performances of the RNN vs. classical Terrestrial Broadcasting system with two throughputs (T1 = 114 kbit/s, T2 = 162 kbit/s) and a fixed speed of 160 km/h.

The RNN receiver performed better than the classic receiver at all speeds. The results showed that the RNN receiver, in addition to flexibility under different SNRs, has also high flexibility with respect to user mobility.

We evaluated the performance of the second trained HPHT RNN and compared it with that of the second classical system designed for the HPHT scenario and a speed of 120 km/h. In this case, the pilot efficiency of the classical system increased to 5/6 and the CP efficiency to 2700/3000, so that its waveform efficiency increased to  $\eta = 0.75$ .

The end-to-end simulation results for throughput systems T1 = 93 kbit/s and T2 = 110 kbit/s are depicted in Figure 5. For the first throughput T1, the RNN code rate was  $r_{c,1}^{(RNN)} = 0.276$  and the classical system code rate was  $r_{c,1}^{(C)} = 0.34$ . For the second throughput T2,  $r_{c,1}^{(RNN)} = 0.34$  and  $r_{c,2}^{(C)} = 0.41$ .

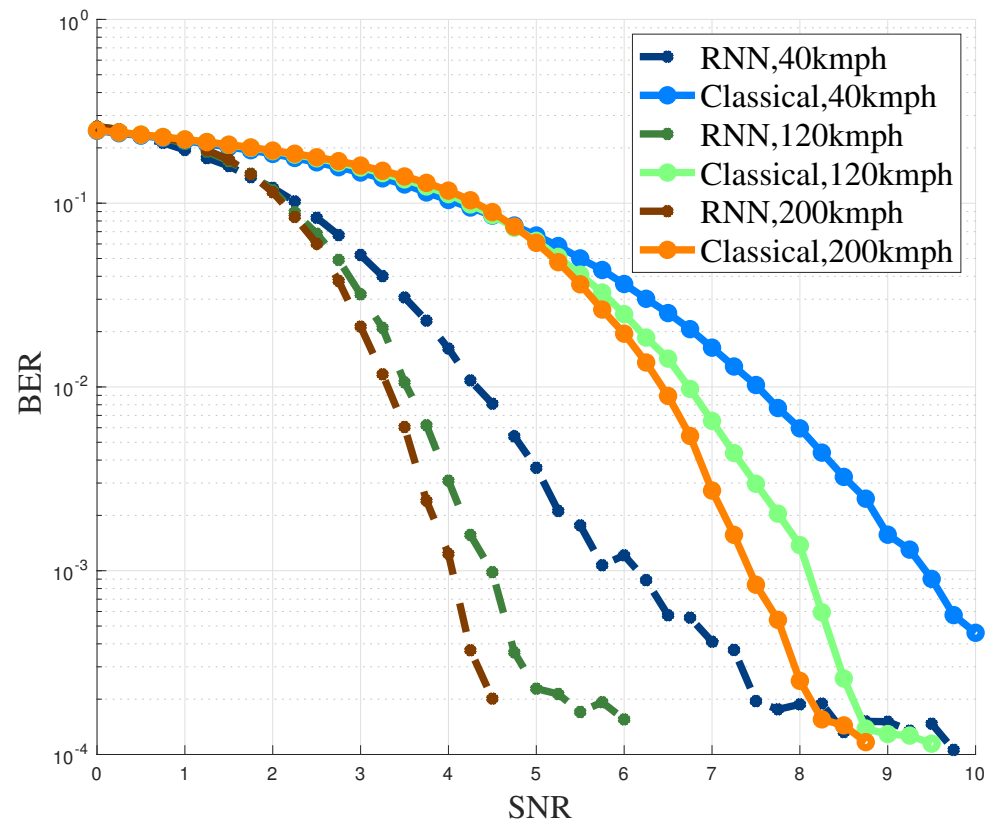


**Figure 4.** LPLT (ISD = 15 km). Performances of the RNN vs. classical Terrestrial Broadcasting system for the same throughput (138 kbit/s) and different user speeds.  $r_c^{(RNN)} = 0.41$  and  $r_c^{(C)} = 0.64$ .

In this case also, the result showed that the RNN system outperformed the classical system, although the gain was reduced because of the increased efficiency of the classical system. At  $BER = 10^{-3}$ , 1.2 dB and 2.3 gains were observed for T1 and T2, respectively.

Although we trained the RNN at a fixed velocity (3 km/h) and a fixed SNR (5 dB), also in this case, the RNN showed robustness at a high speed (120 km/h) and different SNRs. Notice that the classical system in this case was designed for fixed roof-top reception. No numerologies in eMBMS are provided for HPHT and mobile users. Its performances were still reasonable at 120 km/h for low-order modulation. The system however would provide unacceptable losses for higher-order modulation, due to the excessive symbol length (3 ms), incompatible with the time coherence of the channel.

The classic system can provide near-optimal performance for an SFN with a symbol-by-symbol detector by properly adjusting the OFDM length and proper allocation of the CP and pilot signals. In the classical approach, the OFDM numerology is designed to avoid the ISI and ICI and the pilot density is chosen to achieve a satisfactory channel estimation. This approach, however, becomes inefficient in the considered scenarios where the same delay spread is very large (HPHT) and the coherence time is small due to the user mobility.

The simulation results showed that a single trained network has great flexibility with respect to both the SNR and user speed. For HPHT, the network trained at 3 km/h provided excellent results at 120 km/h. For LPLT (see Figure 4), the trained network at 160 km/h provided excellent performance for a large set of speeds.

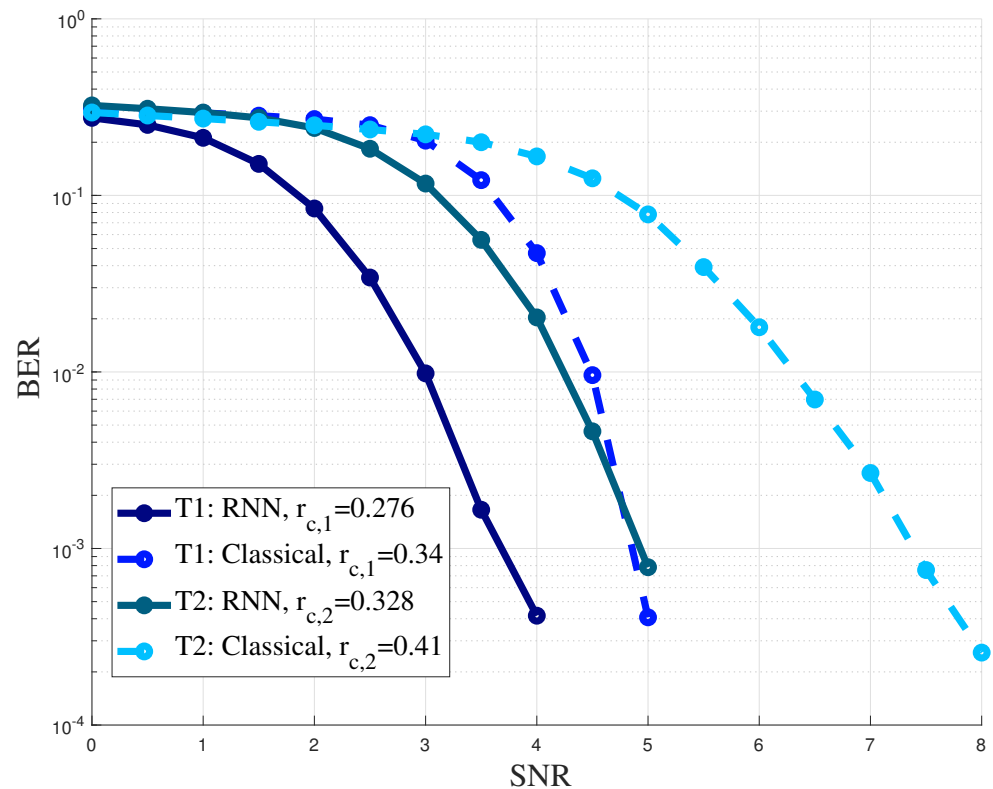


**Figure 5.** The end-to-end simulation for different throughput systems ( $T1 = 93$  kbit/s) and ( $T2 = 110$  kbit/s) at a fixed speed of 120 km/h and a large ISD (125 km ISD). The RNN with 5G NR numerology and trained at 3 km/h and the classical system with a 0.37 kHz carrier spacing with a long cyclic prefix of 300  $\mu$ s.

## 5. Conclusions and Future Work

In this paper, we investigated the use of an RNN-based detector to support SFN Terrestrial Broadcasting. We considered the very challenging scenario where the 5G NR OFDM numerology with a short cyclic prefix (4.7  $\mu$ s) and large carrier spacing (15 kHz) is used in SFN scenarios characterized by a very large delay spread (up to 50  $\mu$ s). Furthermore, we considered high mobility scenarios with an unknown channel at the receiver, so that, also, channel estimation was critical.

The importance of this research comes from the fact that it is not possible to meet the requirements of SFN Terrestrial Broadcasting with the current 5G NR numerology and a classical symbol-by-symbol OFDM receiver. The possibility of using the existing 5G NR numerology for delivering broadcasting services from SFN infrastructures is indeed of great importance for broadcasters.

Previous research on SFNs mostly focused on the design of the classical OFDM system, with an ISI-/ICI-free symbol-by-symbol detection scheme. They designed new numerologies, cyclic prefix lengths, and pilot signals based on new SFN scenarios. Results on advanced, but “classical” techniques for SFNs with 5G NR numerology are not available in the literature, to our knowledge.

We proposed two ingredients for the solution, the superposition of pilots on the data at the transmitter to eliminate the pilot overhead in largely selective channels and the adoption of a suitably trained RNN at the receiver to deal with the large ISI and ICI at the receiver. The superposition of pilots also allowed us to efficiently use and train the RNN. The proposed RNN structure includes two cascaded bi-LSTM networks. In our solution, the RNN substitutes the channel estimation and equalization blocks, while the powerful outer LDPC channel decoder is kept as part of the receiver structure. The RNN thus provides the bit log-likelihood ratio to the following decoder, and the cost function



for training the RNN is changed accordingly. The hyper-parameters of the proposed RNN were optimized for generating two trained RNNs for the LPLT and HPHT SFN scenarios.

While some advanced equalizer solutions and even RNN-based receivers were proposed in past literature for OFDM, no one has considered the full problem related to the SFN as we stated, and no one has investigated the combined approach of the superposition of pilots and an RNN to solve the channel estimation and equalization problem.

We compared the end-to-end performances of the proposed approach with respect to the classical approach, used in OFDM standards such as DVB-T and ATSC. In the classical approach, OFDM numerology is designed to avoid the ISI and ICI and pilot density is chosen to achieve a satisfactory channel estimation. This approach becomes progressively inefficient in the considered scenario, where, at the same time, the delay spread is very large (HPHT) and the coherence time is small due to the user mobility. We used as the key performance indicator the BER after LDPC decoding and, consequently, that delivered to the end user. This KPI is the most relevant one in the evaluation of the physical layer, and the reported gains translate into energy savings and/or a throughput increase for the broadcasters.

The proposed approach largely outperforms the classical system, explicitly designed for the considered SFN scenarios, in all mobile scenarios. We also demonstrated the flexibility of the proposed scheme in different scenarios, as we provided evidence that a single RNN, trained at a fixed SNR and user speed, provides excellent performances in large ranges of SNRs and user speeds.

Possible future investigations related to the considered problem include:

- Adoption for a mobile SFN with 5G NR numerology of other types of advanced, but classical receivers, maybe combined with pilot superposition to increase the system efficiency.
- Reduction of the complexity of the RNN. The proposed structure based on bi-LSTM is well suited for the receiver, but probably oversized, as it was proposed for solving more complex problems. A deeper investigation of the required RNN features would probably lead to simpler structures together with a better understanding of the relationships of the RNN with the classical advanced receivers based on the MMSE and MLSE.
- The investigation of system performance with higher-order modulations, yielding higher spectral efficiencies.
- The scaling of the proposed receiver solution to the practical bandwidth used in broadcasting.
- The flexibility of a single trained RNN also for different network infrastructures (i.e., ISD) and, consequently, different delay spreads.

**Author Contributions:** M.M. designed the experiments and algorithms and wrote the draft of the manuscript. G.M. participated in the revision and discussion of the manuscript. All authors have read and agreed to the published version of the manuscript.

**Funding:** This research received no external funding.

**Data Availability Statement:** Not applicable.

**Acknowledgments:** This work is supported by RAI—Radiotelevisione Italiana Centre for Research. The authors would like to thank Vittoria Mignone and Assunta De Vita at RAI for their suggestions and contributions.

**Conflicts of Interest:** The authors declare no conflict of interest.

## References

1. Jokela, T.; Tupala, M.; Paavola, J. Analysis of physical layer signaling transmission in DVB-T2 systems. *IEEE Trans. Broadcast.* **2010**, *56*, 410–417. [[CrossRef](#)]
2. Fuentes, M.; Mi, D.; Chen, H.; Garro, E.; Carcel, J.L.; Vargas, D.; Mouhouche, B.; Gomez-Barquero, D. Physical layer performance evaluation of LTE-advanced pro broadcast and ATSC 3.0 systems. *IEEE Trans. Broadcast.* **2018**, *65*, 477–488. [[CrossRef](#)]



3. 3GPP TR 36.776. Evolved Universal Terrestrial Radio Access (E-UTRA); Study on LTE-Based 5G Terrestrial Broadcast. Technical Specification (ts), 3rd Generation Partnership Project (3GPP), 2020; p. 11. Version 16.0.0. Available online: [https://www.etsi.org/deliver/etsi\\_tr/136700\\_136799/136776/16.00.00\\_60/tr\\_136776v160000p.pdf](https://www.etsi.org/deliver/etsi_tr/136700_136799/136776/16.00.00_60/tr_136776v160000p.pdf) (accessed on 23 September 2022).
4. Gimenez, J.J.; Carcel, J.L.; Fuentes, M.; Garro, E.; Elliott, S.; Vargas, D.; Menzel, C.; Gomez-Barquero, D. 5G new radio for terrestrial broadcast: A forward-looking approach for NR-MBMS. *IEEE Trans. Broadcast.* **2019**, *65*, 356–368. [[CrossRef](#)]
5. Mosavat, M.; Montorsi, G. Single Frequency Network Broadcasting with 5G NR Numerology. In Proceedings of the 2021 IEEE Latin-American Conference on Communications (LATINCOM), Santo Domingo, Dominican Republic, 17–19 November 2021; pp. 1–6.
6. Rusek, F.; Prlja, A. Optimal channel shortening for MIMO and ISI channels. *IEEE Trans. Wirel. Commun.* **2011**, *11*, 810–818. [[CrossRef](#)]
7. Fatima, B. The Channel Shortening comparison between OFDM & MC-CDMA System over an ADSL Channel using a Water-filling. *Int. J. Electr. Comput. Eng.* **2019**, *9*, 3695.
8. Attar, H.H.; Solyman, A.A.; Mohamed, A.E.F.; Khosravi, M.R.; Menon, V.G.; Bashir, A.K.; Tavallali, P. Efficient equalisers for OFDM and DFrFT-OCDM multicarrier systems in mobile E-health video broadcasting with machine learning perspectives. *Phys. Commun.* **2020**, *42*, 101173. [[CrossRef](#)]
9. Solyman, A.A.; Attar, H.; Khosravi, M.R.; Menon, V.G.; Jolfaei, A.; Balasubramanian, V.; Selvaraj, B.; Tavallali, P. A low-complexity equalizer for video broadcasting in cyber-physical social systems through handheld mobile devices. *IEEE Access* **2020**, *8*, 67591–67602. [[CrossRef](#)]
10. Sun, Y.; Tong, L. Channel equalization for wireless OFDM systems with ICI and ISI. In Proceedings of the 1999 IEEE International Conference on Communications (Cat. No. 99CH36311), Vancouver, BC, Canada, 6–10 June 1999; Volume 1, pp. 182–186. [[CrossRef](#)]
11. Taubock, G.; Hampejs, M.; Svac, P.; Matz, G.; Hlawatsch, F.; Grochenig, K. Low-complexity ICI/ISI equalization in doubly dispersive multicarrier systems using a decision-feedback LSQR algorithm. *IEEE Trans. Signal Process.* **2011**, *59*, 2432–2436. [[CrossRef](#)]
12. Sherstinsky, A. Fundamentals of recurrent neural network (RNN) and long short-term memory (LSTM) network. *Phys. D Nonlinear Phenom.* **2020**, *404*, 132306. [[CrossRef](#)]
13. Hochreiter, S.; Schmidhuber, J. Long short-term memory. *Neural Comput.* **1997**, *9*, 1735–1780. [[CrossRef](#)]
14. Yu, Y.; Si, X.; Hu, C.; Zhang, J. A review of recurrent neural networks: LSTM cells and network architectures. *Neural Comput.* **2019**, *31*, 1235–1270. [[CrossRef](#)] [[PubMed](#)]
15. Farsad, N.; Goldsmith, A. Neural network detection of data sequences in communication systems. *IEEE Trans. Signal Process.* **2018**, *66*, 5663–5678. [[CrossRef](#)]
16. Ye, H.; Li, G.Y.; Juang, B.H. Power of deep learning for channel estimation and signal detection in OFDM systems. *IEEE Wirel. Commun. Lett.* **2017**, *7*, 114–117. [[CrossRef](#)]
17. Wang, S.; Yao, R.; Tsiftsis, T.A.; Miridakis, N.I.; Qi, N. Signal detection in uplink time-varying OFDM systems using RNN with bidirectional LSTM. *IEEE Wirel. Commun. Lett.* **2020**, *9*, 1947–1951. [[CrossRef](#)]
18. Huang, Q.; Zhao, C.; Jiang, M.; Li, X.; Liang, J. A novel OFDM equalizer for large doppler shift channel through deep learning. In Proceedings of the 2019 IEEE 90th Vehicular Technology Conference (VTC2019-Fall), Honolulu, HI, USA, 22–25 September 2019; pp. 1–5.
19. 3GPP TR 38.901. Study on Channel Model for Frequencies from 0.5 to 100 GHz. Technical Specification (ts), 3rd Generation Partnership Project (3GPP), 2020; p. 11. Version 16.1.0. Available online: [https://www.etsi.org/deliver/etsi\\_tr/138900\\_138999/138901/16.01.00\\_60/tr\\_138901v160100p.pdf](https://www.etsi.org/deliver/etsi_tr/138900_138999/138901/16.01.00_60/tr_138901v160100p.pdf) (accessed on 23 September 2022).
20. 3GPP TS 38.212. 5G NR Multiplexing and Channel Coding. Technical Specification (ts), 3rd Generation Partnership Project (3GPP), 2018; p. 7. Version 15.2.0. Available online: [https://www.etsi.org/deliver/etsi\\_ts/138200\\_138299/138212/15.02.00\\_60/ts\\_138212v150200p.pdf](https://www.etsi.org/deliver/etsi_ts/138200_138299/138212/15.02.00_60/ts_138212v150200p.pdf) (accessed on 23 September 2022).
21. Cui, T.; Tellambura, C. OFDM channel estimation and data detection with superimposed pilots. *Eur. Trans. Telecommun.* **2011**, *22*, 125–136. [[CrossRef](#)]
22. Baldi, P.; Sadowski, P.J. Understanding dropout. *Adv. Neural Inf. Process. Syst.* **2013**, *26*. Available online: <https://proceedings.neurips.cc/paper/2013/hash/71f6278d140af599e06ad9bf1ba03cb0-Abstract.html> (accessed on 23 September 2022).
23. Werbos, P.J. Backpropagation through time: What it does and how to do it. *Proc. IEEE* **1990**, *78*, 1550–1560. [[CrossRef](#)]
24. Zhang, Z. Improved adam optimizer for deep neural networks. In Proceedings of the 2018 IEEE/ACM 26th International Symposium on Quality of Service (IWQoS), Banff, AB, Canada, 4–6 June 2018; pp. 1–2.
25. Vargas, D.; Elliott, S.; Haffenden, O.; McCartney, R.; Murphy, A.; Jimenez, J.J. Performance of 5G Broadcast and Benefits of Proposed Time-Interleaving Enhancements. IBC Technical Paper; 14 September 2020. Available online: <https://www.ibt.org/technical-papers/performance-of-5g-broadcast-and-benefits-of-proposed-time-interleaving-enhancements/6745.article> (accessed on 23 September 2022).
26. Sengupta, A.; Alvarino, A.R.; Catovic, A.; Casaccia, L. Cellular Terrestrial Broadcasting—Physical layer evolution from 3GPP release 9 to release 16. *IEEE Trans. Broadcast.* **2020**, *66*, 459–470. [[CrossRef](#)]

# Chapter 9

## Conclusion and future works

Although the physical layer of 5G New Radio (NR) in Release 15 was originally intended for uni-cast transmission, several attempts have been made to enable SFN terrestrial broadcasting in 5G technology. Researchers have tried to optimize the cyclic prefix length in relation to the artificial delay spread of the channel, but this proved challenging due to the 1 millisecond sub-frame limit of the 5G-NR frame structure. Specifically, SFN scenarios with large inter-site distances, such as high-power, high-tower scenarios, were difficult to accommodate within the 5G-NR framework. Furthermore, designing an optimal cyclic prefix for fixed scenarios does not guarantee the same level of performance in mobility scenarios. Ultimately, it became necessary to develop a distinct frame structure from the 5G-NR to enable single frequency network terrestrial broadcasting.

We attempted to investigate a different approach by implementing an advanced techniques at the receiver side to address the challenge of insufficient cyclic prefix length in the presence of mobility. We developed an advanced channel equalizer using the channel shortening technique. This equalizer was designed to receive a sequence of demodulated OFDM symbols affected by ISI and ICI, and provide a linearly equalized signal. To evaluate the effectiveness of this approach, we conducted link level simulations that included the 5G LDPC encoder. Our results demonstrate that this receiver was highly effective, performing on par with numerology designed specifically for terrestrial broadcasting that includes a sufficient cyclic prefix. These promising findings suggest that our advance channel equalizer could be a valuable tool in enabling 5G-NR terrestrial SFN broadcasting.

---

Initially, our approach assumed a static and known channel. However, we recognized that this assumption may not be realistic in real-world scenarios, where factors such as mobility and channel estimation can significantly impact the channel. To address these challenges, we adopted a novel approach based on recurrent neural network neural networks.

We developed an end-to-end OFDM receiver based on Bi-LSTM that can perform channel estimation, channel equalization, and provide soft decisions for the following channel decoder, without any prior knowledge of the channel. To eliminate the overhead for pilot signals, we have superimposed data with the pilot signal. One key advantage is that superimposed pilot techniques can eliminate the need for dedicated pilot signals, which can increase the overall spectral efficiency of the system.

We trained an LSTM-based receiver using a fixed speed and signal-to-noise ratio, and subsequently used the trained receiver to perform link simulations. Our findings indicate that the receiver exhibits a high degree of flexibility in various speed and signal-to-noise ratio settings, resembling the functionality of an OFDM receiver that is custom-designed for a particular SFN broadcasting scenario. These results demonstrate that training the network under limited conditions can still enable it to function effectively in vastly different scenarios.

While our design was originally intended for 5G-NR terrestrial broadcasting, it can also be utilized for any OFDM system that is susceptible to inter-symbol interference (ISI) and inter-carrier interference (ICI). The key advantage of this approach is its ability to handle complex and dynamic channel conditions, such as those that arise in mobile communications, and to provide effective data detection even when there is significant ISI and ICI present.

In light of these considerations, there are several compelling directions for future research. Firstly, it would have been very interesting to conduct an additional study on the proposed Recurrent Neural Network (RNN)-based solution while retaining the dedicated pilot sub-carriers in 5G-NR. This investigation would provide insights into the specific impact and effectiveness of the RNN approach in the presence of dedicated pilot sub-carriers. By comparing the results with the existing solution, a more comprehensive understanding of the proposed solution's performance and advantages could be obtained.

Similarly, it would have been valuable to analyze the superposition of pilot signals with the data signal without relying on the recurrent neural network. This alternative

approach could shed light on the effectiveness of other techniques or algorithms for channel equalization in OFDM systems. By examining the performance of this non-RNN-based method and comparing it to the proposed solution, a more comprehensive analysis of the solution's overall impact and potential limitations could be achieved.

Furthermore, while our research has shown encouraging results, the increased complexity of these receivers may hinder their adoption in real-world systems. Thus, further investigation is needed to explore methods for simplifying these receivers while maintaining their effectiveness. Finding ways to reduce their complexity will be crucial for practical deployment in various systems.

Another important area for future research is evaluating the performance of the proposed Recurrent Neural Network (RNN)-based solution in systems employing higher-order modulation schemes. Although our evaluation has concentrated on specific modulation orders, extending it to higher orders is crucial for determining the practicality of these advanced receivers in a broader range of applications.

Furthermore, our current system design does not incorporate time synchronization, even though we operate in a sequence of OFDM symbols. In future research, it is crucial to incorporate synchronization into our system design and evaluate its impact on the performance of the receivers. Time synchronization is essential for ensuring accurate and reliable data transmission in OFDM systems, and its inclusion will contribute to the overall effectiveness of the proposed solution.

Moreover, it would be interesting to explore the potential use of these advanced receivers beyond broadcasting over a SFN. For instance, in satellite communications or cellular networks, there may be additional applications of these advanced receivers in SFN environments.

Conducting these additional studies, including the exploration of simplified receiver designs, evaluating RNN performance with higher-order modulation, incorporating time synchronization, and investigating alternative infrastructures, will contribute to a deeper understanding of the proposed solution's capabilities, limitations, and practical applicability. These investigations will aid in the development of more robust and versatile solutions for real-world implementation in a wide range of scenarios.

# References

- [1] Anders Mattsson. Single frequency networks in dtv. *IEEE transactions on broadcasting*, 51(4):413–422, 2005.
- [2] ETSI (European Telecommunications Standards Institute). ETSI TR 138 912 V15.0.0 (2018-09) 5G; Study on New Radio (NR) access technology (3GPP TR 38.912 version 15.0.0 Release 15). Technical Report 138 912, ETSI, September 2018.
- [3] ETSI (European Telecommunications Standards Institute). ETSI TR 136 976 V17.0.0 (2022-04) LTE; Overall description of LTE-based 5G broadcast (3GPP TR 36.976 version 17.0.0 Release 17). Technical Report 136 976, ETSI, April 2022.
- [4] 3GPP TS 36.776. “Study on LTE-based 5G terrestrial broadcast. Technical specification (ts), 3rd Generation Partnership Project (3GPP), 03 2019. Version 16.0.0.
- [5] Qualcomm Incorporated. Evaluation results and potential enhancements. 3GPP TSG RAN WG1 Meeting #95, Spokane, WA, USA, 12th - 16th November 2018. Agenda item: 6.2.4.1, Document for: Discussion and decision.
- [6] ETSI. Digital video broadcasting (dvb); frame structure channel coding and modulation for a second generation digital terrestrial television broadcasting system (dvb-t2). Technical Specification EN 302 755 V1.4.1, European Telecommunications Standards Institute, 2015.
- [7] Inaki Eizmendi, Manuel Velez, David Gómez-Barquero, Javier Morgade, Vicente Baena-Lecuyer, Mariem Slimani, and Jan Zoellner. Dvb-t2: The second generation of terrestrial digital video broadcasting system. *IEEE transactions on broadcasting*, 60(2):258–271, 2014.
- [8] Luke Fay, Lachlan Michael, David Gómez-Barquero, Nejib Ammar, and M Winston Caldwell. An overview of the atsc 3.0 physical layer specification. *IEEE Transactions on Broadcasting*, 62(1):159–171, 2016.
- [9] Dazhi He, Wanting Wang, Yin Xu, Xiuxuan Huang, Hao Cheng, Xiaohan Duan, Yihang Huang, Hanjiang Hong, Yiwei Zhang, and Wenjun Zhang. Overview of physical layer enhancement for 5g broadcast in release 16. *IEEE Transactions on Broadcasting*, 66(2):471–480, 2020.

- [10] David Vargas, Simon Elliott, Oliver Haffenden, Ryan McCartney, Andrew Murphy, and Jordi Joan Jimenez. Performance of 5g broadcast and benefits of proposed time-interleaving enhancements. *IBC technical paper*, September 2020.
- [11] J.H. Stott. The how and why of COFDM. *EBU Technical Review*, 1(Winter), 1998.
- [12] Stefan Parkvall, Erik Dahlman, Anders Furuskar, and Mattias Frenne. Nr: The new 5g radio access technology. *IEEE Communications Standards Magazine*, 1(4):24–30, 2017.
- [13] Yu-Ngok Ruyue Li, Mengzhu Chen, Jun Xu, Li Tian, and Kaibin Huang. Power saving techniques for 5g and beyond. *IEEE Access*, 8:108675–108690, 2020.
- [14] Imad Barhumi. Decision feedback turbo equalization for ofdm over doubly selective channels. In *2012 IEEE Global Communications Conference (GLOBECOM)*, pages 3801–3806. IEEE, 2012.
- [15] Kazuyuki Shimezawa, Takashi Yoshimoto, Ryota Yamada, Naoki Okamoto, and Kimihiko Imamura. A novel sc/mmse turbo equalization for multicarrier systems with insufficient cyclic prefix. In *2008 IEEE 19th International Symposium on Personal, Indoor and Mobile Radio Communications*, pages 1–5. IEEE, 2008.
- [16] Jie Zhu, Wee Ser, and Arye Nehorai. Channel equalization for dmt with insufficient cyclic prefix. In *Conference Record of the Thirty-Fourth Asilomar Conference on Signals, Systems and Computers (Cat. No. 00CH37154)*, volume 2, pages 951–955. IEEE, 2000.
- [17] Henuchul Lee, Byeongsi Lee, and Inkyu Lee. Iterative detection and decoding with an improved v-blast for mimo-ofdm systems. *IEEE Journal on Selected Areas in Communications*, 24(3):504–513, 2006.
- [18] Yih-Haw Jan. Iterative joint channel estimation and signal detection for ofdm system in double selective channels. *Wireless Personal Communications*, 99(3):1279–1294, 2018.
- [19] Tareq Y Al-Naffouri, Ahmad Bahai, and Arogyaswami Paulraj. Semi-blind channel identification and equalization in ofdm: An expectation-maximization approach. In *Proceedings IEEE 56th Vehicular Technology Conference*, volume 1, pages 13–17. IEEE, 2002.
- [20] European Broadcasting Union (EBU). TR 016: Benefits and Limitations of Single Frequency Networks (SFN) for DTT. <https://tech.ebu.ch/docs/techreports/tr016.pdf>, —.
- [21] Agnes Ligeti. *Single Frequency Network Planning*. Doctoral dissertation, Royal Institute of Technology, September 1999.

- [22] Andrew Viterbi. Convolutional codes and their performance in communication systems. *IEEE Transactions on Communication Technology*, 19(5):751–772, 1971.
- [23] Stephen B Wicker and Vijay K Bhargava. *Reed-Solomon codes and their applications*. John Wiley & Sons, 1999.
- [24] James Massey. Step-by-step decoding of the bose-chaudhuri-hocquenghem codes. *IEEE Transactions on Information Theory*, 11(4):580–585, 1965.
- [25] Branka Vucetic and Jinhong Yuan. *Turbo codes: principles and applications*, volume 559. Springer Science & Business Media, 2012.
- [26] Jeremy Thorpe. Low-density parity-check (ldpc) codes constructed from protographs. *IPN progress report*, 42(154):42–154, 2003.
- [27] Sai-Weng Lei and Vincent KN Lau. Performance analysis of adaptive interleaving for ofdm systems. *IEEE transactions on Vehicular Technology*, 51(3):435–444, 2002.
- [28] SA Hanna. Convolutional interleaving for digital radio communications. In *Proceedings of 2nd IEEE International Conference on Universal Personal Communications*, volume 1, pages 443–447. IEEE, 1993.
- [29] William T Webb and Lajos Hanzo. *Modern Quadrature Amplitude Modulation: Principles and applications for fixed and wireless channels: one*. IEEE Press-John Wiley, 1994.
- [30] Nabil Svenh Loghin, Jan Zöllner, Belkacem Mouhouche, Daniel Ansorregui, Jinwoo Kim, and Sung-Ik Park. Non-uniform constellations for atsc 3.0. *IEEE Transactions on Broadcasting*, 62(1):197–203, 2016.
- [31] Darshan V Adakane and K Vasudevan. An efficient pilot pattern design for channel estimation in ofdm systems. In *2013 IEEE International Conference on Signal Processing, Computing and Control (ISPCC)*, pages 1–5. IEEE, 2013.
- [32] 3GPP TR 38.901. Study on channel model for frequencies from 0.5 to 100 GHz. Technical specification (ts), 3rd Generation Partnership Project (3GPP), 12 2019. Version 16.1.0.
- [33] N Chen, M Tanaka, and R Heaton. Ofdm timing synchronisation under multi-path channels. In *The 57th IEEE Semiannual Vehicular Technology Conference, 2003. VTC 2003-Spring.*, volume 1, pages 378–382. IEEE, 2003.
- [34] Peter Hoeher and Fredrik Tufvesson. Channel estimation with superimposed pilot sequence. In *Seamless Interconnection for Universal Services. Global Telecommunications Conference. GLOBECOM'99.(Cat. No. 99CH37042)*, volume 4, pages 2162–2166. IEEE, 1999.

- [35] Jia-Chin Lin. Least-squares channel estimation for mobile ofdm communication on time-varying frequency-selective fading channels. *IEEE Transactions on Vehicular Technology*, 57(6):3538–3550, 2008.
- [36] Cheran Vithanage and Stojan Denic. Linear minimum mean-squared error channel estimation for per-subcarrier antenna selection. In *2010 IEEE Global Telecommunications Conference GLOBECOM 2010*, pages 1–6. IEEE, 2010.
- [37] Liang Zhang, Yiyang Wu, Wei Li, Zhihong Hong, Khalil Salehian, Heung Mook Kim, Sung-Ik Park, Jae-Young Lee, Pablo Angueira, Jon Montalban, et al. Enhanced dft-based channel estimation for ldm systems over sfn channels. In *2015 IEEE International Symposium on Broadband Multimedia Systems and Broadcasting*, pages 1–6. IEEE, 2015.
- [38] Eran Sharon, Simon Litsyn, and Jacob Goldberger. An efficient message-passing schedule for ldpc decoding. In *2004 23rd IEEE Convention of Electrical and Electronics Engineers in Israel*, pages 223–226. IEEE, 2004.
- [39] ETSI. Digital video broadcasting (dvb); specification for service information (si) in dvb systems. Technical Specification EN 300 468 V1.15.1, European Telecommunications Standards Institute, 2016.
- [40] Thomas J Richardson, Mohammad Amin Shokrollahi, and Rüdiger L Urbanke. Design of capacity-approaching irregular low-density parity-check codes. *IEEE transactions on information theory*, 47(2):619–637, 2001.
- [41] Digital Video Broadcasting. Implementation guidelines for a second generation digital terrestrial television broadcasting system (DVB-T2). Technical Specification TS 102 831 V1.1.1, European Telecommunications Standards Institute (ETSI), October 2010.
- [42] D Perez-Calderón, C Oria, J Garcia, P López, V Baena, and I Lacadena. Rotated constellations for dvb-t2. In *Proc. XXIV Conf. DCIS*, volume 1, pages 128–133, 2009.
- [43] Vittoria Mignone and Alberto Morello. Cd3-ofdm: A novel demodulation scheme for fixed and mobile receivers. *IEEE Transactions on Communications*, 44(9):1144–1151, 1996.
- [44] Digital Video Broadcasting. Frame structure channel coding and modulation for a second generation digital terrestrial television broadcasting system (DVB-T2) DVB Document A182. Technical report, DVB, June 2022.
- [45] Advanced Television Systems Committee. ATSC Standard: Physical Layer Protocol Doc. A/322:2022-11. Technical Report 202-872-9160, Advanced Television Systems Committee, 1300 I Street, N.W., Suite 400E, Washington, D.C. 20005, November 2022.
- [46] George Xylomenos, Vasilis Vogkas, and George Thanos. The multimedia broadcast/multicast service. *Wireless communications and mobile computing*, 8(2):255–265, 2008.



- [47] Jordi Joan Gimenez, Jose Luis Carcel, Manuel Fuentes, Eduardo Garro, Simon Elliott, David Vargas, Christian Menzel, and David Gomez-Barquero. 5g new radio for terrestrial broadcast: A forward-looking approach for nr-mbms. *IEEE Transactions on Broadcasting*, 65(2):356–368, 2019.
- [48] Liang Zhang, Yiyang Wu, Gordon Kent Walker, Wei Li, Khalil Salehian, and Adrian Florea. Improving lte {e} mbms with extended ofdm parameters and layered-division-multiplexing. *IEEE Transactions on Broadcasting*, 63(1):32–47, 2016.
- [49] IRT EBU, BBC. Evaluation results for lte-based 5g terrestrial broadcast. 3GPP TSG RAN WG1 RL1 R1-1903284, Feb./Mar. 2019.
- [50] Qualcomm Incorporat. Support of longer numerologies for rooftop reception, Aug. 2019.
- [51] HiSilicon Huawei. On new numerologies for pmch to support rooftop reception. [Online]. Available: [http://www.3gpp.org/ftp/TSG\\_RAN/WG1\\_RL1/TSGR1\\_98/Docs/R1-1908093.zip](http://www.3gpp.org/ftp/TSG_RAN/WG1_RL1/TSGR1_98/Docs/R1-1908093.zip), August 2019.
- [52] Shanghai Jiao Tong Univ. New numerology for pmch to support rooftop reception. [Online]. Available: [http://www.3gpp.org/ftp/TSG\\_RAN/WG1\\_RL1/TSGR1\\_98/Docs/R1-1908096.zip](http://www.3gpp.org/ftp/TSG_RAN/WG1_RL1/TSGR1_98/Docs/R1-1908096.zip), August 2019.
- [53] Gordon Kent Walker, Xiaoxia Zhang, and Xiao Feng Wang. Extended duration cyclic prefix with low overhead for lte broadcast, April 26 2016. US Patent 9,325,552.
- [54] 3GPP R1-1712879. Forward Compatibility Consideration for ECP Design and NR-MBMS. Technical report (tr), 3rd Generation Partnership Project (3GPP), 08 2017.
- [55] 3GPP TR 38.912. 5G; Study on new radio access technology. Technical report (tr), 3rd Generation Partnership Project (3GPP), 10 2017. v14.1.0.
- [56] Dukhyun Kim and Gordon L Stuber. Residual isi cancellation for ofdm with applications to hdtv broadcasting. *IEEE journal on selected areas in communications*, 16(8):1590–1599, 1998.
- [57] Satoshi Suyama, H Suzuki, and K Fukawa. An ofdm receiver with smoothed fft-window and rls-mlse for fast multipath fading environments with large delay spread. In *IEEE Seventh International Symposium on Spread Spectrum Techniques and Applications*, volume 2, pages 353–357. IEEE, 2002.
- [58] Kazunori Hayashi and Hideaki Sakai. A simple interference elimination scheme for single carrier block transmission with insufficient cyclic prefix. *Proc. of WPMC 2004*, 2:577–581, 2004.

- [59] Muhammad Danish Nisar, Wolfgang Utschick, Hans Nottensteiner, and Thomas Hindelang. On channel estimation and equalization of ofdm systems with insufficient cyclic prefix. In *2007 IEEE 65th Vehicular Technology Conference-VTC2007-Spring*, pages 1445–1449. IEEE, 2007.
- [60] Van-Duc Nguyen, Matthias Patzold, Fumiaki Maehara, Harald Haas, and Minh-Viet Pham. Channel estimation and interference cancellation for mimo-ofdm systems. *IEICE transactions on communications*, 90(2):277–290, 2007.
- [61] Carlos Prieto del Amo, Víctor P Gil Jiménez, and M Julia Fernández-Getino García. Joint channel and frequency offset estimation in mimo-ofdm systems with insufficient cyclic prefix. *Physical communication*, 4(4):254–265, 2011.
- [62] Carlos Prieto del Amo and M Julia Fernandez-Getino Garcia. Suppression of cyclic prefix in down-link lte like systems to increase capacity. In *2013 IEEE 77th Vehicular Technology Conference (VTC Spring)*, pages 1–5. IEEE, 2013.
- [63] Hui-Chul Won, Jin-Ho Jang, and Gi-Hong Im. Iterative cyclic prefix reconstruction and channel estimation for space-time block coded frequency division multiplexing. In *IEEE International Conference on Communications, 2005. ICC 2005. 2005*, volume 4, pages 2611–2615. IEEE, 2005.
- [64] Xianbin Wang, Paul Ho, and Yiyan Wu. Robust channel estimation and isi cancellation for ofdm systems with suppressed features. *IEEE Journal on Selected Areas in Communications*, 23(5):963–972, 2005.
- [65] Jong-Bu Lim, Eung-Sun Kim, Cheol-Jin Park, Hui-Chul Won, Ki-Ho Kim, and Gi-Hong Im. Bandwidth-efficient ofdm transmission with iterative cyclic prefix reconstruction. *Journal of Communications and Networks*, 10(3):239–252, 2008.
- [66] Carlos Prieto del Amo and M Julia Fernández-Getino García. Iterative joint estimation procedure for channel and frequency offset in multi-antenna ofdm systems with an insufficient cyclic prefix. *IEEE Transactions on vehicular technology*, 62(8):3653–3662, 2013.
- [67] Makoto Yoshida, Yasuharu Amezawa, Satoshi Sonobe, and Atsuhiko Sugitani. Laboratory experiment of ofdm transmission using vlp and pre-fft equalizer over isi channels. In *2004 IEEE 59th Vehicular Technology Conference. VTC 2004-Spring (IEEE Cat. No. 04CH37514)*, volume 1, pages 540–544. IEEE, 2004.
- [68] Erik Dahlman, Stefan Parkvall, and Johan Skold. *4G: LTE/LTE-advanced for mobile broadband*. Academic press, 2013.
- [69] Chengyang Li and Sumit Roy. Subspace based blind channel estimation for ofdm by exploiting virtual carrier. In *GLOBECOM'01. IEEE Global Telecommunications Conference (Cat. No. 01CH37270)*, volume 1, pages 295–299. IEEE, 2001.

- [70] Chengyang Li and Sumit Roy. Subspace-based blind channel estimation for ofdm by exploiting virtual carriers. *IEEE Transactions on Wireless Communications*, 2(1):141–150, 2003.
- [71] Changyong Shin and Edward J Powers. Blind channel estimation for mimo-ofdm systems using virtual carriers. In *IEEE Global Telecommunications Conference, 2004. GLOBECOM'04.*, volume 4, pages 2465–2469. IEEE, 2004.
- [72] Changyong Shin, Robert W Heath, and Edward J Powers. Blind channel estimation for mimo-ofdm systems. *IEEE Transactions on Vehicular Technology*, 56(2):670–685, 2007.
- [73] Yuta Sagae, Satoshi Suyama, Hiroshi Suzuki, and Kazuhiko Fukawa. An ofdm turbo equalizer for scattered pilot signals in multipath environments with delay difference greater than guard interval. In *2004 IEEE 59th Vehicular Technology Conference. VTC 2004-Spring (IEEE Cat. No. 04CH37514)*, volume 1, pages 425–429. IEEE, 2004.
- [74] Jin-Goog Kim and Jong-Tae Lim. Map-based channel estimation for mimo-ofdm over fast rayleigh fading channels. *IEEE transactions on vehicular technology*, 57(3):1963–1968, 2008.
- [75] Hung Nguyen-Le, Tho Le-Ngoc, and Chi Chung Ko. Joint channel estimation and synchronization for mimo-ofdm in the presence of carrier and sampling frequency offsets. *IEEE Transactions on Vehicular Technology*, 58(6):3075–3081, 2008.
- [76] Hung Nguyen-Le, Tho Le-Ngoc, and Chi Chung Ko. Turbo processing for joint channel estimation, synchronization, and decoding in coded mimo-ofdm systems. *EURASIP Journal on Wireless Communications and Networking*, 2009:1–12, 2009.
- [77] Hung Nguyen-Le, Tho Le-Ngoc, and Chi Chung Ko. Rls-based joint estimation and tracking of channel response, sampling, and carrier frequency offsets for ofdm. *IEEE Transactions on Broadcasting*, 55(1):84–94, 2009.
- [78] Hung Nguyen-Le, Tho Le-Ngoc, and Nghi H Tran. Iterative receiver design with joint doubly selective channel and cfo estimation for coded mimo-ofdm transmissions. *IEEE transactions on vehicular technology*, 60(8):4052–4057, 2011.
- [79] Eric Pierre Simon, Laurent Ros, Hussein Hijazi, and Mounir Ghogho. Joint carrier frequency offset and channel estimation for ofdm systems via the em algorithm in the presence of very high mobility. *IEEE Transactions on Signal Processing*, 60(2):754–765, 2011.
- [80] Kun-Chien Hung and David W Lin. Pilot-based lmmse channel estimation for ofdm systems with power–delay profile approximation. *IEEE Transactions on Vehicular Technology*, 59(1):150–159, 2009.

- [81] Geert Leus and Marc Moonen. Per-tone equalization for mimo ofdm systems. *IEEE Transactions on Signal Processing*, 51(11):2965–2975, 2003.
- [82] Imad Barhumi, Geert Leus, and Marc Moonen. Equalization for ofdm over doubly selective channels. *IEEE Transactions on Signal Processing*, 54(4):1445–1458, 2006.
- [83] Naofal Al-Dhahir. Fir channel-shortening equalizers for mimo isi channels. *IEEE transactions on communications*, 49(2):213–218, 2001.
- [84] Wei Li, Yue Zhang, Li-Ke Huang, Carsten Maple, and John Cosmas. Implementation and co-simulation of hybrid pilot-aided channel estimation with decision feedback equalizer for ofdm systems. *IEEE Transactions on Broadcasting*, 58(4):590–602, 2012.
- [85] Anastasios Stamoulis, Georgios B Giannakis, and Anna Scaglione. Block fir decision-feedback equalizers for filterbank precoded transmissions with blind channel estimation capabilities. *IEEE Transactions on Communications*, 49(1):69–83, 2001.
- [86] Dirk S Waldhauser, Leonardo G Baltar, and Josef A Nossek. Adaptive decision feedback equalization for filter bank based multicarrier systems. In *2009 IEEE International Symposium on Circuits and Systems*, pages 2794–2797. IEEE, 2009.
- [87] Haris Gacanin and Fumiyuki Adachi. Nonlinear decision-feedback equalization for ofdm in a fast fading channel. In *2009 IEEE 20th International Symposium on Personal, Indoor and Mobile Radio Communications*, pages 2648–2652. IEEE, 2009.
- [88] Shaoping Chen and Cuitao Zhu. Ici and isi analysis and mitigation for ofdm systems with insufficient cyclic prefix in time-varying channels. *IEEE Transactions on Consumer Electronics*, 50(1):78–83, 2004.
- [89] Jong-Bu Lim, Chan-Ho Choi, and Gi-Hong Im. Mimo-ofdm with insufficient cyclic prefix. *IEEE communications letters*, 10(5):356–358, 2006.
- [90] Jong-Bu Lim, Eung-Sun Kim, Cheol-Jin Park, Hui-Chul Won, Ki-Ho Kim, and Gi-Hong Im. Bandwidth-efficient ofdm transmission with iterative cyclic prefix reconstruction. *Journal of Communications and Networks*, 10(3):239–252, 2008.
- [91] Zhe Chen, Chang Yongyu, and Dacheng Yang. Low-complexity turbo equalization for mimo-ofdm system without cyclic prefix. In *2009 IEEE 20th International Symposium on Personal, Indoor and Mobile Radio Communications*, pages 310–314. IEEE, 2009.
- [92] Satoshi Suyama, Yoshitaka Hara, Hiroshi Suzuki, Yukiyoishi Kamio, and Kazuhiko Fukawa. A maximum likelihood ofdm receiver with smoothed

- fft-window for large multipath delay difference over the guard interval. In *Vehicular Technology Conference. IEEE 55th Vehicular Technology Conference. VTC Spring 2002 (Cat. No. 02CH37367)*, volume 3, pages 1247–1251. IEEE, 2002.
- [93] Wei Shi, Chunming Zhao, and Wei Xu. Reduced-state maximum-likelihood detection for ofdm systems with insufficient cyclic prefix. *Physical Communication*, 51:101560, 2022.
- [94] Tri Pham, Tho Le-Ngoc, Graeme K Woodward, and Philippa A Martin. Channel estimation and data detection for insufficient cyclic prefix mimo-ofdm. *IEEE Transactions on Vehicular Technology*, 66(6):4756–4768, 2016.
- [95] Satoshi Suyama, Hiroshi Suzuki, and Kazuhiko Fukawa. An ofdm receiver employing turbo equalization for multipath environments with delay spread greater than the guard interval. In *The 57th IEEE Semiannual Vehicular Technology Conference, 2003. VTC 2003-Spring.*, volume 1, pages 632–636. IEEE, 2003.
- [96] Satoshi Suyama, Hiroshi Suzuki, and Kazuhiko Fukawa. A mimo-ofdm receiver employing the low-complexity turbo equalization in multipath environments with delay difference greater than the guard interval. *IEICE transactions on communications*, 88(1):39–46, 2005.
- [97] Paul Alexander, David Haley, and Alex Grant. Outdoor mobile broadband access with 802.11. *IEEE Communications Magazine*, 45(11):108–114, 2007.
- [98] Brian P Crow, Indra Widjaja, Jeong Geun Kim, and Prescott T Sakai. Ieee 802.11 wireless local area networks. *IEEE Communications magazine*, 35(9):116–126, 1997.
- [99] Kun Fang, Luca Rugini, and Geert Leus. Low-complexity block turbo equalization for ofdm systems in time-varying channels. *IEEE Transactions on Signal Processing*, 56(11):5555–5566, 2008.
- [100] Michael Tüchler and Andrew C Singer. Turbo equalization: An overview. *IEEE Transactions on Information Theory*, 57(2):920–952, 2011.
- [101] Jun Tao and Yahong Rosa Zheng. Turbo detection for mimo-ofdm underwater acoustic communications. *International journal of wireless information networks*, 20:27–38, 2013.
- [102] Dan Raphaeli and Yoram Zorai. Combined turbo equalization and turbo decoding. *IEEE Communications Letters*, 2(4):107–109, 1998.
- [103] Ivan B Djordjevic, Lyubomir L Minkov, and Hussam G Batshon. Mitigation of linear and nonlinear impairments in high-speed optical networks by using ldpc-coded turbo equalization. *IEEE Journal on Selected Areas in Communications*, 26(6):73–83, 2008.

- [104] Majid Mosavat and Guido Montorsi. Single frequency network broadcasting with 5gnr numerology. In *2021 IEEE Latin-American Conference on Communications (LATINCOM)*, pages 1–6. IEEE, 2021.
- [105] Fredrik Rusek and Adnan Prlja. Optimal channel shortening for MIMO and ISI channels. *IEEE transactions on wireless communications*, 11(2):810–818, 2011.
- [106] Ashok Cutkosky and Harsh Mehta. Momentum improves normalized sgd. In *International conference on machine learning*, pages 2260–2268. PMLR, 2020.
- [107] Agnes Lydia and Sagayaraj Francis. Adagrad—an optimizer for stochastic gradient descent. *Int. J. Inf. Comput. Sci*, 6(5):566–568, 2019.
- [108] Shuxia Lu and Zhao Jin. Improved stochastic gradient descent algorithm for svm. *International Journal of Recent Engineering Science (IJRES)*, 4(4):28–31, 2017.
- [109] Diederik P Kingma and Jimmy Ba. Adam: A method for stochastic optimization. *arXiv preprint arXiv:1412.6980*, 2014.
- [110] Sepp Hochreiter and Jürgen Schmidhuber. Long short-term memory. *Neural computation*, 9(8):1735–1780, 1997.
- [111] Shaik Rafi and Ranjita Das. Rnn encoder and decoder with teacher forcing attention mechanism for abstractive summarization. In *2021 IEEE 18th India Council International Conference (INDICON)*, pages 1–7. IEEE, 2021.
- [112] Samy Bengio, Oriol Vinyals, Navdeep Jaitly, and Noam Shazeer. Scheduled sampling for sequence prediction with recurrent neural networks. *Advances in neural information processing systems*, 28, 2015.
- [113] Gábor Szűcs and Dorottya Huszti. Seq2seq deep learning method for summary generation by lstm with two-way encoder and beam search decoder. In *2019 IEEE 17th International Symposium on Intelligent Systems and Informatics (SISY)*, pages 221–226. IEEE, 2019.
- [114] Ishaani Priyadarshini and Chase Cotton. A novel lstm–cnn–grid search-based deep neural network for sentiment analysis. *The Journal of Supercomputing*, 77(12):13911–13932, 2021.
- [115] Klaus Greff, Rupesh K Srivastava, Jan Koutník, Bas R Steunebrink, and Jürgen Schmidhuber. Lstm: A search space odyssey. *IEEE transactions on neural networks and learning systems*, 28(10):2222–2232, 2016.
- [116] Maria Kaselimi, Nikolaos Doulamis, Anastasios Doulamis, Athanasios Voulodimos, and Eftychios Protopapadakis. Bayesian-optimized bidirectional lstm regression model for non-intrusive load monitoring. In *ICASSP 2019-2019 IEEE International Conference on Acoustics, Speech and Signal Processing (ICASSP)*, pages 2747–2751. IEEE, 2019.

- [117] Jing Zhong, Guiguang Ding, Yuchen Guo, Jungong Han, and Bin Wang. Where to prune: Using lstm to guide end-to-end pruning. In *IJCAI*, pages 3205–3211, 2018.
- [118] Gakuto Kurata and Kartik Audhkhasi. Improved knowledge distillation from bi-directional to uni-directional lstm ctc for end-to-end speech recognition. In *2018 IEEE Spoken Language Technology Workshop (SLT)*, pages 411–417. IEEE, 2018.
- [119] Fayçal Ait Aoudia and Jakob Hoydis. End-to-end learning for ofdm: From neural receivers to pilotless communication. *IEEE Transactions on Wireless Communications*, 21(2):1049–1063, 2021.
- [120] Rongkun Jiang, Xuettian Wang, Shan Cao, Jiafei Zhao, and Xiaoran Li. Deep neural networks for channel estimation in underwater acoustic OFDM systems. *IEEE access*, 7:23579–23594, 2019.
- [121] Muhammet Nuri Seyman and Necmi TaşPıNar. Channel estimation based on neural network in space time block coded mimo–ofdm system. *Digital Signal Processing*, 23(1):275–280, 2013.
- [122] Kalpesh Hiray and K Vinoth Babu. A neural network based channel estimation scheme for ofdm system. In *2016 International Conference on Communication and Signal Processing (ICCSP)*, pages 0438–0441. IEEE, 2016.
- [123] Necmi Taşpınar and M Nuri Seyman. Back propagation neural network approach for channel estimation in ofdm system. In *2010 IEEE International Conference on Wireless Communications, Networking and Information Security*, pages 265–268. Ieee, 2010.
- [124] Hao Ye, Geoffrey Ye Li, and Biing-Hwang Juang. Power of deep learning for channel estimation and signal detection in ofdm systems. *IEEE Wireless Communications Letters*, 7(1):114–117, 2017.
- [125] Xiao Chen, Miao Liu, Guan Gui, Bamidele Adebisi, Haris Gacanin, and Hikmet Sari. Complex deep neural network based intelligent signal detection methods for ofdm-im systems. In *2021 Joint European Conference on Networks and Communications & 6G Summit (EuCNC/6G Summit)*, pages 90–94. IEEE, 2021.
- [126] Xin Yan, Fei Long, Jingshuai Wang, Na Fu, Weihua Ou, and Bin Liu. Signal detection of mimo-ofdm system based on auto encoder and extreme learning machine. In *2017 International Joint Conference on Neural Networks (IJCNN)*, pages 1602–1606. IEEE, 2017.
- [127] Yunan Zhu, Biao Wang, Jianghui Li, Youwen Zhang, and Fangtong Xie. Y-shaped net-based signal detection for ofdm-im systems. *IEEE Communications Letters*, 26(11):2661–2664, 2022.

- [128] Fei Li, Min Zhou, and Haibo Li. A novel neural network optimized by quantum genetic algorithm for signal detection in mimo-ofdm systems. In *Computational Intelligence in Control and Automation (CICA)*, pages 170–177. IEEE, 2011.
- [129] Qingyi Quan and Junggon Kim. Intercarrier interference suppression for ofdm systems using hopfield neural network. *IJCSNS*, 6(6):157–162, 2006.
- [130] Fuxin Zhang, Chunbo Luo, Jialang Xu, Yang Luo, and FuChun Zheng. Deep learning based automatic modulation recognition: Models, datasets, and challenges. *Digital Signal Processing*, page 103650, 2022.
- [131] Jing Zhang, Yu Cao, Guangyao Han, and Xiaomei Fu. Deep neural network-based underwater ofdm receiver. *IET communications*, 13(13):1998–2002, 2019.
- [132] Yi Sun. Bandwidth-efficient wireless ofdm. *IEEE Journal on selected areas in communications*, 19(11):2267–2278, 2001.
- [133] DV Soundari, P Tharani, B Savitha, and M Sreegayathre. Improved energy efficiency of massive mimo-ofdm. In *2021 5th International Conference on Intelligent Computing and Control Systems (ICICCS)*, pages 38–42. IEEE, 2021.
- [134] Mahdi Boloursaz Mashhadi and Deniz Gündüz. Pruning the pilots: Deep learning-based pilot design and channel estimation for mimo-ofdm systems. *IEEE Transactions on Wireless Communications*, 20(10):6315–6328, 2021.
- [135] B Nithya, D Brijesh, S Karan Kumar, and J Pathmakarthik. Pilot based channel estimation of ofdm systems using deep learning techniques. *International Journal of Information Technology*, pages 1–13, 2023.
- [136] A Naveed, IM Qureshi, TA Cheema, and A Jalil. Blind equalization and estimation of channel using artificial neural networks. In *8th International Multitopic Conference, 2004. Proceedings of INMIC 2004.*, pages 184–190. IEEE, 2004.
- [137] Chia-Hsin Cheng, Yung-Fa Huang, Hsing-Chung Chen, and Tsung-Yu Yao. Neural network-based estimation for ofdm channels. In *2015 IEEE 29th International Conference on Advanced Information Networking and Applications*, pages 600–604. IEEE, 2015.
- [138] Peiwen Jiang, Chao-Kai Wen, Shi Jin, and Geoffrey Ye Li. Dual cnn-based channel estimation for mimo-ofdm systems. *IEEE Transactions on Communications*, 69(9):5859–5872, 2021.
- [139] Bin Lin, Xudong Wang, Weihao Yuan, and Nan Wu. A novel ofdm autoencoder featuring cnn-based channel estimation for internet of vessels. *IEEE Internet of Things Journal*, 7(8):7601–7611, 2020.



- [140] Annapurna Pradhan, Susmita Das, and Deepak Dayalan. A two-stage cnn based channel estimation for ofdm system. In *2021 Advanced Communication Technologies and Signal Processing (ACTS)*, pages 1–4. IEEE, 2021.
- [141] Jinbao Li and Qi Peng. Lightweight channel estimation networks for ofdm systems. *IEEE Wireless Communications Letters*, 11(10):2066–2070, 2022.
- [142] Shovon Nandi, Arnab Nandi, and Narendra Nath Pathak. Channel estimation of massive mimo-ofdm system using elman recurrent neural network. *Arabian Journal for Science and Engineering*, 47(8):9755–9765, 2022.
- [143] Yong Liao, Yuanxiao Hua, Xuewu Dai, Haimei Yao, and Xinyi Yang. Chanestnet: A deep learning based channel estimation for high-speed scenarios. In *ICC 2019-2019 IEEE international conference on communications (ICC)*, pages 1–6. IEEE, 2019.
- [144] Zhiyong Wang, Fangling Pu, Xiaoshi Yang, Ning Chen, Yongmin Shuai, and Rui Yang. Online lstm-based channel estimation for hf mimo sc-fde system. *IEEE Access*, 8:131005–131020, 2020.
- [145] Abdul Karim Gizzini, Marwa Chaffi, Shahab Ehsanfar, and Raed M Shubair. Temporal averaging lstm-based channel estimation scheme for ieee 802.11 p standard. In *2021 IEEE Global Communications Conference (GLOBECOM)*, pages 01–07. IEEE, 2021.
- [146] Peihao Dong, Hua Zhang, Geoffrey Ye Li, Ivan Simoes Gaspar, and Navid NaderiAlizadeh. Deep cnn-based channel estimation for mmwave massive mimo systems. *IEEE Journal of Selected Topics in Signal Processing*, 13(5):989–1000, 2019.
- [147] D Venkata Ratnam and K Nageswara Rao. Bi-lstm based deep learning method for 5g signal detection and channel estimation. *AIMS Electronics and Electrical Engineering*, 5(4):334–341, 2021.
- [148] Alexander Felix, Sebastian Cammerer, Sebastian Dörner, Jakob Hoydis, and Stephan Ten Brink. Ofdm-autoencoder for end-to-end learning of communications systems. In *2018 IEEE 19th International Workshop on Signal Processing Advances in Wireless Communications (SPAWC)*, pages 1–5. IEEE, 2018.
- [149] Syed Junaid Nawaz, Sajjad Mohsin, and Ataul Aziz Ikaram. Neural network based mimo-ofdm channel equalizer using comb-type pilot arrangement. In *2009 International Conference on Future Computer and Communication*, pages 36–41. IEEE, 2009.
- [150] Xiangyun Deng, Jin Sha, Xiaotian Zhou, Yuxiang Fu, Zaichen Zhang, Xiaohu You, and Chuan Zhang. Joint detection and decoding of polar-coded ofdm-idma systems. *IEEE Transactions on Circuits and Systems I: Regular Papers*, 66(10):4005–4017, 2019.

- [151] Markus A Dangel, Doris Yacoub, Ulrich Marxmeier, Werner G Teich, and Jürgen Lindner. Performance of joint detection techniques for coded mimo-ofdm and mimo-mc-cdm. In *Proc. COST 273 Workshop on Broadband Wireless Local Access*, page 17, 2003.
- [152] Yan Zhang, Dejun Liu, Jialin Liu, Yixuan Xian, and Xu Wang. Improved deep neural network for ofdm signal recognition using hybrid grey wolf optimization. *IEEE Access*, 8:133622–133632, 2020.
- [153] Thien Van Luong, Youngwook Ko, Ngo Anh Vien, Duy HN Nguyen, and Michail Matthaiou. Deep learning-based detector for ofdm-im. *IEEE wireless communications letters*, 8(4):1159–1162, 2019.
- [154] Aswathy K Nair and Vivek Menon. Joint channel estimation and symbol detection in mimo-ofdm systems: A deep learning approach using bi-lstm. In *2022 14th International Conference on Communication Systems & Networks (COMSNETS)*, pages 406–411. IEEE, 2022.
- [155] Shengyao Wang, Rugui Yao, Theodoros A Tsiftsis, Nikolaos I Miridakis, and Nan Qi. Signal detection in uplink time-varying ofdm systems using rnn with bidirectional lstm. *IEEE Wireless Communications Letters*, 9(11):1947–1951, 2020.
- [156] Guangliang Pan, Zitong Liu, Wei Wang, and Minglei Li. A signal detection scheme based on deep learning in ofdm systems. In *2021 IEEE 32nd Annual International Symposium on Personal, Indoor and Mobile Radio Communications (PIMRC)*, pages 1–6. IEEE, 2021.
- [157] Minghui Wu, Zhen Gao, Zhijie Gao, Di Wu, Yang Yang, and Yang Huang. Deep learning-based hybrid precoding for fdd massive mimo-ofdm systems with a limited pilot and feedback overhead. In *2022 IEEE International Conference on Communications Workshops (ICC Workshops)*, pages 318–323. IEEE, 2022.
- [158] Zhen Gao, Minghui Wu, Chun Hu, Feifei Gao, Guanghui Wen, Dezhi Zheng, and Jun Zhang. Data-driven deep learning based hybrid beamforming for aerial massive mimo-ofdm systems with implicit csi. *IEEE Journal on Selected Areas in Communications*, 40(10):2894–2913, 2022.
- [159] Jing Zhang, Hengtao He, Chao-Kai Wen, Shi Jin, and Geoffrey Ye Li. Deep learning based on orthogonal approximate message passing for cp-free ofdm. In *ICASSP 2019-2019 IEEE International Conference on Acoustics, Speech and Signal Processing (ICASSP)*, pages 8414–8418. IEEE, 2019.
- [160] Yan Sun, Chao Wang, Huan Cai, Chunming Zhao, Yiqun Wu, and Yan Chen. Deep learning based equalizer for mimo-ofdm systems with insufficient cyclic prefix. In *2020 IEEE 92nd Vehicular Technology Conference (VTC2020-Fall)*, pages 1–5. IEEE, 2020.

- 
- [161] Yi Sun, Hong Shen, Zhenguo Du, Lan Peng, and Chunming Zhao. Icinet: Ici-aware neural network based channel estimation for rapidly time-varying ofdm systems. *IEEE Communications Letters*, 25(9):2973–2977, 2021.
- [162] Yong Liao, Yuanxiao Hua, and Yunlong Cai. Deep learning based channel estimation algorithm for fast time-varying mimo-ofdm systems. *IEEE Communications Letters*, 24(3):572–576, 2019.
- [163] Majid Mosavat and Guido Montorsi. Single-frequency network terrestrial broadcasting with 5gnr numerology using recurrent neural network. *Electronics*, 11(19):3130, 2022.